MULTIDISCIPLINARY DESIGN TECHNIQUES APPLIED TO CONCEPTUAL AEROSPACE VEHICLE DESIGN

by

JOHN ROBERT OLDS

A dissertation submitted to the Graduate Faculty of
North Carolina State University
in partial fulfillment of the
requirements for the Degree of
Doctor of Philosophy

AEROSPACE ENGINEERING

Raleigh

1993

APPROVED BY:

_____ _____

_____ _____

Chairman of Advisory Committee

ABSTRACT

OLDS, JOHN ROBERT. Multidisciplinary Design Techniques Applied to Conceptual Aerospace Vehicle Design. (Under the direction of Dr. Gerald D. Walberg.)

Multidisciplinary design optimization (MDO) is an emerging discipline within aerospace engineering. Its goal is to bring structure and efficiency to the complex design process associated with advanced aerospace launch vehicles. Aerospace vehicles generally require input from a variety of traditional aerospace disciplines - aerodynamics, structures, performance, etc. As such, traditional optimization methods cannot always be applied. Several multidisciplinary techniques and methods have been proposed as potentially applicable to this class of design problem. Among the candidate options are calculus-based (or gradient-based) optimization schemes and parametric schemes based on design of experiments theory.

A brief overview of several applicable multidisciplinary design optimization methods is included in this dissertation. Methods from the calculus-based class and the parametric class are reviewed, but the research application reported in this work focuses on methods from the parametric class.

A vehicle of current interest was chosen as a test application for this research. The rocket-based combined-cycle (RBCC) single-stage-to-orbit (SSTO) launch vehicle combines elements of rocket and airbreathing

propulsion in an attempt to produce an attractive option for launching medium sized payloads into low earth orbit. The RBCC SSTO presents a particularly difficult problem for traditional one-variable-at-a-time optimization methods because of the lack of an adequate experience base and the highly coupled nature of the design variables. MDO, however, with it's structured approach to design, is well suited to this problem.

This dissertation presents the results of the application of Taguchi methods, central composite designs, and response surface methods to the design optimization of the RBCC SSTO. Attention is given to the aspect of Taguchi methods that attempts to locate a "robust" design - that is, a design that is least sensitive to uncontrollable influences on the design. Near-optimum minimum dry weight solutions are determined for the vehicle.

This dissertation concludes with a summary and evaluation of the various parametric MDO methods employed in this research. Recommendations for additional research are provided.

Biography

John Robert Olds was born on [redacted] in [redacted], [redacted] He attended North Carolina State University under a full academic scholarship and graduated summa cum laude in 1987 with a Bachelor of Science degree in Aerospace Engineering. During the summers of 1985, 1986, and 1987, he worked at NASA - Johnson Space Center, NASA - Langley Research Center, and Lockheed Missiles and Space Company in Sunnyvale, CA.

Mr. Olds earned a National Science Foundation Graduate Fellowship to attend Stanford University. He graduated in 1988 with a Master of Science degree in Aeronautics and Astronautics. After working at General Dynamics Space Systems Division in Huntsville, AL for two years, he returned to graduate school at North Carolina State University. He has spent the last two years as a graduate student researcher in the Vehicle Analysis Branch at the NASA - Langley Research Center in Hampton, VA.

Acknowledgments

I would like to express appreciation to everyone who helped me complete this research and who guided my education in the fields of multidisciplinary design optimization and advanced aerospace vehicle design. There is a long list of people that I have met along the way, but some deserve to be singled out for a special thanks.

I would like to thank my advisor, Dr. Gerald Walberg, whose experience and wisdom were invaluable to me over the course of the last few years. Thanks also to the members of my committee who accepted a relatively new field of research and supported my research efforts.

My parents, Dan and Betty Olds, have always encouraged me to pursue my education and have supported me emotionally and financially throughout the process. Thank you Mom and Dad for providing a wonderful home environment.

The engineers in the Vehicle Analysis Branch at NASA - Langley have contributed significantly to my understanding of the design process – always patiently answering questions pertaining to the workings of a particular analysis code or providing challenging discussions concerning different design methods. In particular, Doug, Resit, Dick, Roger, Larry, Mac, Walt, Kay, Lance, Garry, Chris, and Steve provided valuable data and information that contributed to my research.

Finally, I would like to thank my wife, Melinda, for always standing beside me and being my biggest cheerleader. You have been supportive, understanding, encouraging, and loving. Thank you for always believing in my abilities.

Table of Contents

List of Tables

List of Figures

List of Symbols and Acronyms

A_c ..... engine cowl annular capture area (ft^2)
ACC ..... advanced carbon-carbon thermal protection
AMLS ..... advanced manned launch system
APAS ..... aerodynamic preliminary analysis system
CCD ..... central composite design
C_t ..... airbreathing coef. of thrust, thrust/qAc
DOE ..... design of experiments
ECLSS ..... environmental control and life support sys.
EMA ..... electro-mechanical actuators
GLOW ..... gross lift-off weight (lbs)
GSE ..... global sensitivity equation (for SSA)
HTO ..... horizontal take-off
IOC ..... initial operational capability
I_{sp} ..... specific impulse, thrust/prop flow rate (sec)
L/D ..... lift-to-drag ratio
LH2 ..... liquid hydrogen
LOX ..... liquid oxygen
MDO ..... multidisciplinary design optimization
MECO ..... main engine cut-off
MER ..... mass estimating relationship
MR ..... mass ratio (GLOW/MECO weight)
M_{tr} ..... scramjet to rocket mode transition Mach number
NASP ..... National Aerospace Plane
NASTRAN ..... a structural analysis code
OMS ..... orbital maneuvering system
PEEK ..... polyether-ether ketone thermoset resin
POST ..... program to optimize simulated trajectories
q ..... dynamic pressure ($1/2\rho V^2$)(psf)

RBCC ..... rocket-based combined-cycle
RCS ..... reaction control system
RSM ..... response surface methods
SSA ..... system sensitivity analysis
SSD ..... system sensitivity derivatives
SSTO ..... single-stage-to-orbit
STS ..... space transportation system (shuttle)
TPS ..... thermal protection system
T/Wo ..... take-off vehicle thrust-to-weight ratio
VTO ..... vertical take-off
y ..... experimental responses or objective functions
α (1) ..... angle of attack (deg.)
α (2) ..... optimizer step size
α (3) ..... star point distances in CCD
β ..... coefficients in approximate response models
Θ ..... cone half angle (deg.)
Φ ..... cowl wrap around angle (deg.)
ξ ..... propellant fraction, 1-1/MR

Introduction

The design of advanced space transportation vehicles typically depends heavily on analysis from many of the traditional fields of aerospace engineering - performance, aerodynamics, structures, weights and sizing, propulsion, cost, operations, avionics and power, etc. Design decisions from any single discipline are strongly influenced by decisions made in the other disciplines. Power requirements depend on aerodynamic control requirements which may, in turn, depend on a performance analysis. Such a design process is *multi*-disciplinary, and each of the disciplines is one component of a complicated network of data flows and interactions. These networks are often characterized by iterative loops between several of the disciplines.

Because of the interactive nature of the disciplines, experts in each of the fields involved are generally placed in close proximity – creating a design team. Each discipline typically deals with one or two computer tools for its work, and data is exchanged manually or automatically between disciplines. A project engineer directs the process as data is exchanged and fine tuned between disciplines in order to produce a final, converged design that meets all of the requirements.

As in any design process, the objective is to find the best design from a set of competing alternatives. In launch vehicle design, minimum weight is often a criteria against which designs are judged – partly because of the extremely high cost of launching a pound of material to low earth orbit. The U.S. Space Shuttle delivers payloads for a cost on the order of $6000/lb [1]. The problem of minimizing weight is difficult if only one discipline is involved. For a multidisciplinary problem, the problem is significantly harder. Rather than optimizing a particular part of the overall design, the optimization process must be performed at the systems level. For example, consider the design of a winged launch system. An aerodynamicist may want to minimize the thickness of the wing in order to reduce wave drag (and thus propellant

requirements), but the structures expert may want a thicker wing in order to minimize wing weight [2]. Which is the right answer? Historically, "trade studies" have been employed to locate the best design. Trade studies generally fix most of the design variables at some median initial value, and vary one variable at a time in an attempt to find its best setting. Once a preferred setting has been found for the first variable, it is fixed at that setting for the rest of the study. The next variable is then varied in an attempt to find its best setting. It is easy to imagine a scenario where such an approach may not be able to locate an optimum point design. The best setting of one variable will most likely depend on the settings of all of the other design variables. Changing one variable at a time has little chance of optimizing the entire system. A structured approach to optimizing several variables simultaneously in a multidisciplinary design environment in required. Multidisciplinary design optimization attempts to address this need.

Multidisciplinary design optimization (MDO) is a fledgling field in aerospace engineering that attempts to bring a structured methodology to locating the best possible design in a multidisciplinary environment. In fact, MDO can be considered to be a discipline in and of itself with the goal of acting as an agent to bind the other disciplines together [3]. MDO methods can be either from the gradient-based class of methods (including classical optimization, decomposition methods, and new techniques created specifically for multidisciplinary environments like system sensitivity analysis) or the parametric methods class based on Design of Experiments theory (fig. 1). Each class of methods has it's strengths and weaknesses, and each is suitable for different types of problems [4].

Parametric methods are particularly well suited to the design environment found in aerospace vehicle **conceptual** design (i. e. the very early phase of design). The number of systems level design variables is generally less than ten. Parametric methods are most useful for small numbers of variables. Conceptual vehicle analysis is generally accomplished via time consuming iteration between several existing engineering analysis computer

codes (and engineering experts). Parametric methods retain the existing codes and explore the design space through a series of carefully selected point designs. Each point design is analyzed using the existing methods. No additional gradient or derivative information is required from each discipline. Conceptual design spaces are likely to contain discrete variables because major design configuration decisions are still being made. Several parametric methods are capable of handling discrete variables. Finally, the fact that parametric methods only produce a "near-optimum" result is not considered a particularly serious problem for conceptual design. Parametric methods can be used to locate a region of interest within which a more detailed analysis can take place if required.

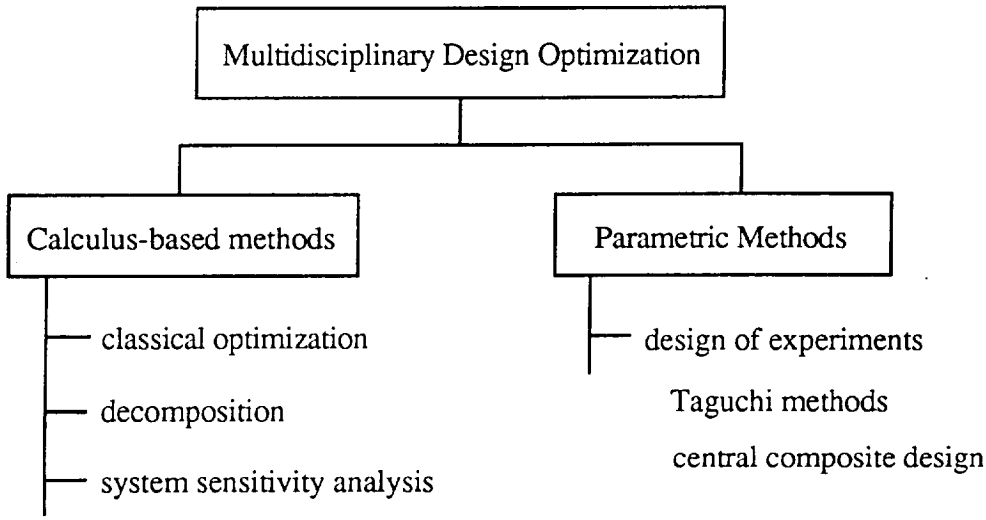

Figure 1 - MDO Hierarchy

Four specific methods from the parametric class of method were selected for additional study within this research – Design of Experiments methods, Taguchi methods, central composite designs, and response surface

methods. An example launch vehicle (RBCC SSTO) was designed and optimized using three of the four parametric techniques. The optimization of the rocket-based combined-cycle (RBCC) SSTO vehicle was a highly multidisciplinary process that would have been difficult, if not impossible, without the aid of multidisciplinary design optimization. It served as an excellent test case for evaluating the strengths and weaknesses of the methods.

It is hoped that the details of this research will help contribute to the state-of-the-art in multidisciplinary design by demonstrating the applicability of parametric methods to conceptual aerospace vehicle design. These methods have been successfully applied in several different manufacturing industries, but literature on aerospace design applications is sparse. Only in the last few years have some aerospace applications begun to be reported [5,6,7,8]. Interest in MDO and parametric design methods is increasing, however. This research will hopefully serve as a pathfinder for research to follow.

Overview of Multidisciplinary Design Optimization Methods

Classical Optimization

Classical optimization techniques can be readily applied to some of the more manageable problems of aerospace vehicle conceptual design. The process first requires that the problem be placed in standard form (discussed below). Given a starting, non-optimum design, the method then steps from one design to the next until an optimum design is found that meets all constraints and minimizes the objective function. The method can take advantage of a variety of available non-linear optimization numerical methods such as variable metric, steepest descent, and several non-gradient techniques like Powell's method and random walk [9]. The multidisciplinary nature of the design problem will usually necessitate an iterative approach - sometimes even within each step.

The standard form of a classical optimization problem has an objective function and a list of constraints. A composite objective function representing a weighted assessment of the goals of each of the disciplines is written in the form:

$$\text{minimize } f(y_1, y_2, \ldots, y_i, \ldots) \tag{1}$$

and the corresponding set of constraints written in the standard form are:

$$g_i\,(y_1, y_2, \ldots, y_i, \ldots) \leq 0 \tag{2}$$

For example, if f was vehicle weight, the y's might be subsystem weights. The overall objective function is a function of the lower level outputs. A typical constraint may be minimum deliverable payload. The analysis outputs, y_i, are functions of the independent design input variables, x_i. Therefore, the goal of the design process is to find the design variables, x_i, which will minimize the

objective function while satisfying all of the constraints. Continuous variables are easily handled by the method. Discrete variables, like number of engines or number of boosters, are more difficult to handle, but techniques exist to accommodate them to some extent.

Figure 2 shows the graphical depiction of a design space with two independent variables. The classical optimization method employs a repetitive convergence method by first assessing the system objective functions and constraints, calculating gradients, updating the design variables, and then reevaluating the new objective function and constraints. Using this stepping technique, an optimum feasible solution is eventually found. Because the method steps from one solution to a better one by changing design variables appropriately, it is not necessary to predetermine a limiting range of each variable as required by parametric methods. The entire design space can be used if needed because there are no artificial limits.

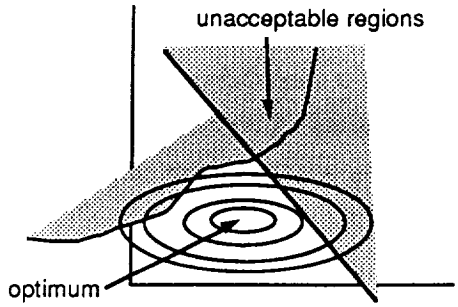

Figure 2 - Design Space with Constraints

The constraints in classical optimization can be treated in a variety of ways. For linear problems, the Simplex method from linear programming can be used [9]. The Simplex method uses the fact that the optimum solution to a linear problem (linear objective and linear constraints) will be at the intersection of two constraints. Those constraints are given the designation

"active", and the "≤" is replaced by "=" in equation 2. For more typical non-linear problems, the constraints can be represented by penalty functions that treat the constraints, not as on-off step functions, but as steeply sloping functions beginning at the point where the constraint is "just satisfied" and increasing as the design moves away from the feasible region. The penalty function is then added (for a minimization problem) to the overall objective function. In this way, the objective is "penalized" for being outside the feasible region, and gradient methods will lead the design away from the penalties and toward a feasible solution. The penalty functions are zero inside the feasible region. Penalty functions are one method of treating constraints in a non-linear problem. Additional methods are discussed in reference 10.

Gradient methods used in classical optimization, as the name implies, use the gradient of the objective function, ∇f, to perform the minimization. They start with a given set of design variables and then numerically, or analytically, determine the derivative of the objective function in each of the design variables directions, i.e. the gradient.

$$\nabla f = \left(\frac{\partial f}{\partial x_1}, \frac{\partial f}{\partial x_2}, \ldots, \frac{\partial f}{\partial x_i}, \ldots\right) \tag{3}$$

The simplest gradient method, steepest descent, then uses the fact that the negative of the gradient lies in the direction that most improves the objective function (for a minimization problem). Therefore, the vector of design variables, represented by $\mathbf{X}$, is changed in that direction.

$$\mathbf{X}_{new} = \mathbf{X}_{old} - \alpha * \nabla f \tag{4}$$

In equation 4, α is a scalar that varies the magnitude of the step. Once the gradient direction is determined, α is started at a small value, an intermediate value of f is determined, and α is systematically increased until the value of the intermediate f is no longer an improvement over the previous step. In other words, the current gradient direction is followed until it is "played out". In practice, maximum move limits are sometimes established to

keep the optimizer from taking too large a step in a non-linear problem. Once a best α is determined for the current gradient direction, the design variables, $\mathbf{X}$, are updated and a new gradient direction is calculated. From here, the process is repeated until the problem converges. Other numerical optimization techniques may use different methods to update the design variables, but almost all use a stepping scheme.

The minimum (or maximum) is found when the derivatives of all the variables are equal to 0,

$$\frac{\partial f}{\partial x_1} = \frac{\partial f}{\partial x_2} = \frac{\partial f}{\partial x_i} = 0 \tag{5}$$

A minimum is, therefore, a point where changing any design variable will result in an increase in the objective function (the increase in the objective function may be the result of a penalty from a violated constraint). It is possible that the optimization process may find a local minimum which is not the global minimum. Techniques exist to solve this problem, but most involve restarting the optimization process from a new initial condition.

Pros and Cons

The classical optimization technique depends heavily on the ability to quickly evaluate the objective function and constraints at each iteration (and several times within each iteration to evaluate the derivatives). The multidisciplinary nature of most aerospace vehicle designs makes this requirement very difficult to achieve. The current design practice of using distributed experts and existing analysis codes would require that each discipline perform an analysis for each iteration of the solution. If the system is coupled, the solution process becomes even more complex and time consuming. Discrete variables are more difficult to accommodate in this method than in parametric studies. Additionally, the objective function and constraints may become very difficult to formulate in a standard form.

Therefore, the classical optimization technique should only be applied to a limited class of conceptual aerospace design problems.

If the design problem can either be limited in scope or approximations can be made to simplify the analysis equations, classical optimization becomes a viable method. A simple objective function and set of constraints must be written in order to allow fast evaluation. While the problem can still be multidisciplinary, complex computer codes for detailed aerodynamics, propulsion, controls, and structures analysis are generally discarded in favor of approximate methods - simple algebraic equations combined into a single monolithic computer code in most cases. Applied to a suitable problem, classical optimization provides a numerically optimum solution (limited only by the accuracy of the model, not the method), a design that meets all constraints, and a method that doesn't require the designer to place predetermined limits on design variable ranges.

Decomposition

If a system consists of several coupled disciplines or tasks, it may be possible to organize the system into a top down hierarchy of smaller subproblems or combinations of subproblems (figure 3). This process of decomposing the coupled system leads to a simpler set of subproblems that can be optimized in a one-at-a-time manner rather than the all-at-once manner employed by classical optimization. In a sense, system decomposition enables the extension of the ideas of classical optimization to larger coupled problems.

Because multi-level decomposition generates a series of subproblems, it lends itself well to the idea of retaining the existing tools of the disciplinary experts and using them to provide the required level of analysis detail in an overall design optimization problem. Once the system is decomposed, the

subproblems of the hierarchical tree can be treated as "design modules" providing outputs to and receiving inputs from other contributing subproblems. Optimization of the overall design is accomplished by top down optimization of the elements of the decomposed structure. Compared to classical optimization, fewer simplifications to the analyses are required because the existing, detailed design programs of the disciplinary experts are retained.

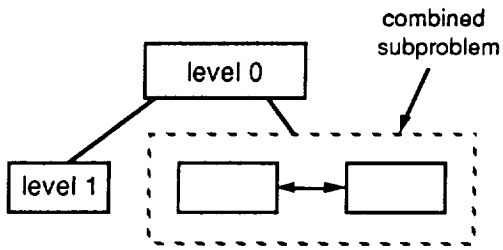

Figure 3 - Complex System as a Hierarchical Structure

The setup of a decomposition problem involves describing the overall system as individual subsystems (modules), their output variables, and their input requirements. For example, thermal protection analysis may be a module. It would provide TPS type, thickness, and weight as outputs and require aerodynamic heat loads and structural backface temperature limits as inputs. Once the entire network is created, the modules are organized in a manner that reduces feedback (iteration) from lower to upper levels and creates a logical hierarchical structure. Some modules may be so coupled that they are impossible to break apart. They may instead be combined into a larger subproblem (circuit) within which iteration may occur. Decomposition may lead to aerodynamic analysis being performed before TPS analysis, and the propulsion and propellant tank analysis may be combined into a new "circuit", for example.

At NASA's - Langley Research Center, a knowledge based tool called DeMaid - Design Manager's Aid for Intelligent Decomposition [11] was created in order to automate the process of decomposition (figure 4). In the simple four module N by N graph example shown, module 2 provides output to modules 1 and 3, and modules 3 and 4 provide outputs to each other. DeMaid can then be applied to transform the coupled, complex design problem into a more manageable hierarchical structure of subproblems. The reorganized system recommends analysis in module 2 first (it depends on input from no other module) and combines modules 3 and 4 into a new circuit. A top down analysis is now possible because no feedback loops exist.

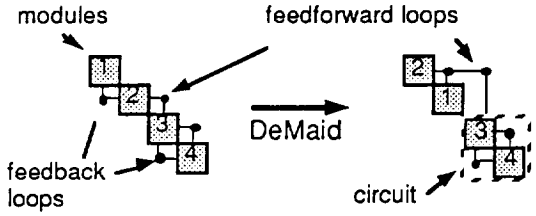

Figure 4 - Decomposition Reduces Feedback

Assuming that the system can be decomposed (some systems may be too highly coupled to create a hierarchical structure), a structured process can be utilized to optimize the individual subproblems so that the optimum solution of the subproblems is the optimum solution of the entire system [12] This process is known as coordination.

As in the case of classical optimization, the overall objective function can be written as a function of the outputs of the individual disciplines (modules).

$$\text{minimize } f(y_1, y_2, \ldots, y_i, \ldots) \tag{6}$$

In the simplest decomposition problem, the outputs of each of the modules enter only into the calculation of the objective function and not into the

outputs of any of the other modules (called a *block diagonal dependency matrix* system). For such a case, the objective function could be split into a series of smaller independent objective functions so that:

$$\Sigma f_i(y_i) = f(y_1, y_2, \ldots, y_i, \ldots) \quad (7)$$

and the objective function of the i-th subproblem will become:

$$\text{minimize } f_i(y_i) \quad (8)$$

The system constraints can also be broken into smaller, subproblem level constraints. In a simplified example, if the system objective function is to minimize vehicle weight, the TPS subproblem objective may be to minimize TPS thickness. Other subproblems would have their own objective functions so that when each is optimized separately, the result will be the lightest overall vehicle.

Having decomposed the system into a hierarchical structure and rewritten the systems level objective function and constraints into subsystem level equations, the design process proceeds from the top of the hierarchical tree to the lower levels. Recall that higher level subproblems are analyzed before lower level subproblems because the higher level outputs (feedforward data) are required as inputs to lower level analyses. The individual optimizations of the subproblems can be solved in a variety of ways, including some of the non-linear, numerical optimization methods like steepest descent discussed in the classical optimization section. For smaller subproblems, designer experience may be sufficient to find an appropriate solution.

Pros and Cons

System decomposition enables a designer to extend the ideas of classical optimization to larger and more coupled problems. However, if a problem is very tightly coupled, it may be impossible to decompose the problem into a simple set of subproblems that can be handled by classical optimization. Simplifications are often made to reduce the system coupling,

that is, some of the weaker dependencies are often neglected. However, in practice many aerospace design problems will be difficult to address by hierarchical decomposition. If the overall design can at least be broken down into 2 or more highly coupled subproblems, the system sensitivity analysis technique (discussed later) can be used on each of the subproblems separately, and then the problems can be recombined using coordination thereby saving time and effort.

When applicable, decomposition can be used to improve the efficiency of the design team. Because of the branching nature of the hierarchical tree, unrelated lower level subproblems can be analyzed at the same time (parallel execution), thereby speeding up the overall analysis process. Also, the performance of the non-linear optimizers is considerably better for the smaller subproblems than it would be for the entire system [12].

The decomposition method allows the computer codes most often used by the individual disciplinary experts to be retained because the subproblems created are often associated with an existing discipline. However, it is not necessary to rely solely on computer based analysis for each subproblem. Some subproblems can be "optimized" using only the experience and judgment of the designer. That is, the decomposed system can consist of automatic and "manual processes". "Manual" optimization of this nature is generally prohibitive in the case of classical optimization where the entire system-level analysis process must be quickly repeated a number of times and is, therefore, usually completely automated.

Because most aerospace designs are difficult to break into smaller subproblems, system decomposition may be best used as a planning and scheduling tool. The ability to visualize the subsystems and structure as related design modules is very beneficial, especially for new or one-of-a-kind designs like those found in conceptual aerospace design. Since the method varies design variables numerically like classical optimization, it has more difficulty handling discrete variables. Other methods, such as system

sensitivity analysis (discussed below) perhaps used in conjunction with decomposition, may be more suitable for the overall optimization process.

System Sensitivity Analysis

System sensitivity analysis (SSA) is a multidisciplinary design and optimization method designed to answer "what if" type questions and perform optimization of an entire system. It replaces system-level gradient calculation with a more efficient, distributed calculation scheme [2]. While classical optimization and system decomposition/coordination are usually limited to smaller sized or less coupled problems, sensitivity analysis is well suited to handle more highly coupled and complex aerospace vehicle design. In fact, it can easily incorporate the techniques of the other two methods. Therefore, system sensitivity analysis may have the widest applicability of any of the numerical techniques discussed in this dissertation.

System sensitivity analysis treats a system as a highly coupled set of subproblems - perhaps determined from a decomposition process that was unable to completely separate all of the subproblems. These subproblems are generally associated with traditional design disciplines that retain their existing, more detailed, design codes. These existing design codes (like NASTRAN or POST) can be treated as individual "design modules" - exchanging inputs and outputs with other "design modules" in the overall system.

To compute the total change in an output variable with respect to a change in an input design variable, the SSA method first analyzes the impacts of the various subproblems on the output, then secondly analyzes the impacts of a change in the input design variable on each of the subproblems while holding other influences constant. For example, an aerodynamics subproblem

would evaluate its own sensitivities to changes in other subproblems. Increased wing weight from the structures subproblem might produce a different trim point with a corresponding increase in induced drag. If wing aspect ratio is a design variable, the aerodynamic discipline could also calculate the change in trim lift coefficient with increased aspect ratio - temporarily disregarding the fact that an increase in aspect ratio may increase wing weight which indirectly will also affect the trim lift coefficient. This second influence is calculated separately. The total change (sensitivity derivative) in wing weight is the sum of these two influences [13]. These system sensitivity derivatives (SSD's) are total derivatives and are essentially *system* level gradients to be used by a designer either intuitively or numerically to iteratively improve the design. The advantage of the method over top level system finite differencing lies in the computational efficiency, ability to perform subproblem tasks in parallel, and the need to only calculate the disciplinary interdependencies once (per iteration) to analyze all design variable influences. A brief discussion of the mathematical basis of SSA is given below.

A complex coupled system can be thought of as a mathematical function that, for a converged solution, generates a set of output values for a given set of input values. For example, for a given sweep, thickness ratio, aspect ratio, Mach number, etc., a wing will have a given coefficient of lift. If **X** is a set of input variables, and **Y** is a set of output variables, then:

$$\mathbf{Y} = f(\mathbf{X}) \tag{9}$$

or written another way:

$$F(\mathbf{X},\mathbf{Y}) = 0 \tag{10}$$

The output variables are generally used in the evaluation of the objective function or the various constraints. Assume that the parts of the system output vector are generated by distinct disciplines so that the system output vector can be partitioned:

$$\mathbf{Y} = (\mathbf{Y}_1, \mathbf{Y}_2, \mathbf{Y}_3)^T \tag{11}$$

where, for simplicity, three disciplines have been assumed. For example, aerodynamic coefficients would be generated by an aerodynamics discipline, engine performance would be generated by a propulsion discipline, and the wing stresses would be generated by a structures discipline. Combining equations (10) and (11) leads to:

$$F(\mathbf{X}, \mathbf{Y}_1, \mathbf{Y}_2, \mathbf{Y}_3) = 0 \tag{12}$$

The implicit function theorem allows the equation to be rewritten such that one variable is expressed as a function of the others (assuming decomposition has been performed so that one discipline is not a function of its own outputs [14]).

$$\mathbf{Y}_1 = f_1(\mathbf{Y}_2, \mathbf{Y}_3, \mathbf{X}) = \mathbf{Y}_1(\mathbf{Y}_2, \mathbf{Y}_3, \mathbf{X}) \tag{13a}$$

$$\mathbf{Y}_2 = f_2(\mathbf{Y}_1, \mathbf{Y}_3, \mathbf{X}) = \mathbf{Y}_2(\mathbf{Y}_1, \mathbf{Y}_3, \mathbf{X}) \tag{13b}$$

$$\mathbf{Y}_3 = f_3(\mathbf{Y}_1, \mathbf{Y}_2, \mathbf{X}) = \mathbf{Y}_3(\mathbf{Y}_1, \mathbf{Y}_2, \mathbf{X}) \tag{13c}$$

This system and its corresponding subproblems are shown graphically in figure 5. **X** represents all the inputs, and **Y** is shown in partitioned form.

Taking equation 13a as a representative example and using the chain rule to write the differential form:

$$d\mathbf{Y}_1 = \frac{\partial \mathbf{Y}_1}{\partial \mathbf{Y}_2} d\mathbf{Y}_2 + \frac{\partial \mathbf{Y}_1}{\partial \mathbf{Y}_3} d\mathbf{Y}_3 + \frac{\partial \mathbf{Y}_1}{\partial \mathbf{X}} d\mathbf{X} \tag{14a}$$

and the total derivative is:

$$\frac{d\mathbf{Y}_1}{d\mathbf{X}} = \frac{\partial \mathbf{Y}_1}{\partial \mathbf{Y}_2}\frac{d\mathbf{Y}_2}{d\mathbf{X}} + \frac{\partial \mathbf{Y}_1}{\partial \mathbf{Y}_3}\frac{d\mathbf{Y}_3}{d\mathbf{X}} + \frac{\partial \mathbf{Y}_1}{\partial \mathbf{X}} \tag{14b}$$

Recall that, due to the coupling of the system, $\mathbf{Y}_1$ is influenced by each of the other subsystems as well as the input variable(s). Equation 14b states that the total change in the output $\mathbf{Y}_1$ with respect to a change in an input

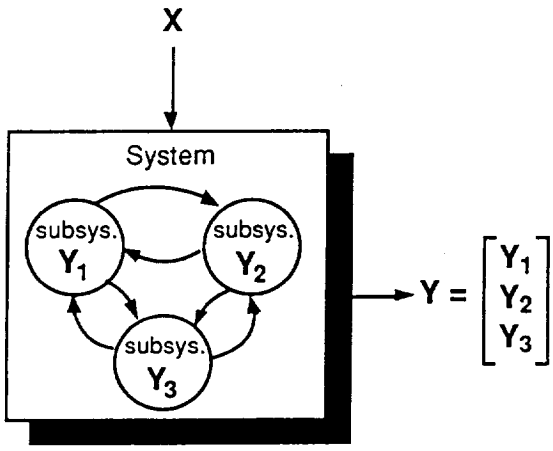

Figure 5 - Coupled System as Three Disciplines

variable is the sum of the changes in each of the other subsystems times their individual effects on $\mathbf{Y}_1$ (these are the partial derivatives) plus the change in $\mathbf{Y}_1$ itself due to a change in the input variable. Performing a similar process on the other two subsystems will lead to the coupled matrix equation known as the Global Sensitivity Equation (GSE).

$$\begin{bmatrix} \mathbf{I} & -\frac{\partial \mathbf{Y}_1}{\partial \mathbf{Y}_2} & -\frac{\partial \mathbf{Y}_1}{\partial \mathbf{Y}_3} \\ -\frac{\partial \mathbf{Y}_2}{\partial \mathbf{Y}_1} & \mathbf{I} & -\frac{\partial \mathbf{Y}_2}{\partial \mathbf{Y}_3} \\ -\frac{\partial \mathbf{Y}_3}{\partial \mathbf{Y}_1} & -\frac{\partial \mathbf{Y}_3}{\partial \mathbf{Y}_2} & \mathbf{I} \end{bmatrix} \begin{bmatrix} \frac{d\mathbf{Y}_1}{d\mathbf{X}} \\ \frac{d\mathbf{Y}_2}{d\mathbf{X}} \\ \frac{d\mathbf{Y}_3}{d\mathbf{X}} \end{bmatrix} = \begin{bmatrix} \frac{\partial \mathbf{Y}_1}{\partial \mathbf{X}} \\ \frac{\partial \mathbf{Y}_2}{\partial \mathbf{X}} \\ \frac{\partial \mathbf{Y}_3}{\partial \mathbf{X}} \end{bmatrix} \tag{15}$$

Note that the partitions of the output vector, $\mathbf{Y}_1$, $\mathbf{Y}_2$, and $\mathbf{Y}_3$ are typically also vectors so the terms of the GSE (e.g. $-\partial \mathbf{Y}_1/\partial \mathbf{Y}_2$) will generally be matrices [14]. The matrix on the left side of the GSE is called the global sensitivity matrix. It contains the sensitivities of each discipline to outputs from other disciplines. The vector on the right side contains the local sensitivity derivatives. It contains the sensitivities of each discipline to changes in the input variables while holding other influences constant. Given values for both of these from discipline level analysis, it is possible to solve

the linear problem for the vector of system sensitivity derivatives (left side unknown vector) using existing matrix techniques [15]. That is, system level *total* derivatives (SSD's) are calculated from discipline level *partial* derivatives. Note that the vector of local sensitivity derivatives is dependent on the particular input variable (e.g. aspect ratio) being evaluated, and therefore, it must be recalculated for each input variable. However, the global sensitivity matrix is dependent only on the discipline interactions and is only calculated once per iteration.

Using the technique described above, a new set of system sensitivity derivatives (SSD's) is generated for each design variable. These SSD's are essentially gradients of the output variables (weight, cost, etc.), and therefore the objective function, with respect to changes in the design variables (aspect ratio, wing sweep, nose radius, etc.). The calculation of the SSD's is the equivalent of performing a finite difference analysis on the entire system for each design variable. The SSD's can be used intuitively by the designer who would then make changes in the inputs in order to improve the objective function. Alternately, the SSD's could be used in a numerical optimization scheme.

Pros and Cons

System sensitivity analysis (SSA) is very well suited to handle large, highly coupled aerospace vehicle design problems. By making use of decomposition/coordination techniques to break a problem down into a set of smaller subproblems, a complex task can be divided among several design teams. If desired, classical optimization methods can be used to optimize a set of design variables based on the system sensitivity derivatives (SSD's) generated by SSA. Because of this ability to incorporate and expand on previously discussed techniques, SSA may have the widest applicability of the numerical techniques discussed here.

Once a system is divided into subproblems, they can be treated as "design modules" providing outputs to and receiving inputs from other "design modules". This capability is of particular interest because it allows certain disciplines to retain their existing detailed deign tools (e.g. NASTRAN) to process inputs and create necessary outputs. Modification of existing codes is usually not necessary - except to perhaps speed data exchange.

SSA, by nature of its distributed network of subproblems, allows the parallel execution of some of the subproblem tasks. For instance, local aerodynamic sensitivities to wing sweep and local structural sensitivities to wing sweep could be performed simultaneously by separate design groups and later combined to form the local sensitivity derivative vector. By taking advantage of parallel execution of design tasks, the iteration time and the overall design time can both be shortened.

On the negative side, a highly non-linear design may necessitate the frequent reevaluation of the global sensitivity matrix. One advantage of the SSA method lies in its ability to save computational time by using the same global sensitivity matrix for several iterations of design variable changes. Non-linear problems may erode some of these time savings.

Like all numerical optimization schemes, SSA prefers to deal with smooth, continuous functions in order to evaluate derivatives. In typical aerospace vehicle design, discrete variables are highly likely to be present (for example, the number of engines or structural material type). Techniques exist within numerical optimization to deal with discrete variables, but the methods work much better with continuous variables.

Finally, the system sensitivity analysis method is highly numerically intensive during the evaluation of the global and local sensitivities. In practice, the method may be difficult to apply to some disciplines that are not used to working with sensitivities to given inputs (e.g. cost sensitivity to wing sweep).

Parametric Methods

Unlike the methods discussed in the previous sections that rely on gradient derived directions to move through a design space toward a progressively improved solution, methods based on design of experiments theory (parametric methods) approach a design problem from a significantly different point of view. Parametric methods establish a fixed set of point locations (i.e. variable combinations) inside the design space at the beginning of the optimization process. The set of points is determined based on a variety of statistical schemes to be discussed in later sections. The points in the set (called the experimental array) provide adequate coverage of the entire design space (see figure 6). In parametric methods, there is no "starting point" and the optimization process does not depend on gradient information gathered at one design point in order to determine the next design point. Rather, information on the location of a desirable region of the design space is extrapolated from the results of the predetermined point designs. Because they do not require derivatives, this class of methods is suitable for problems with discrete and continuous variables [16, 17, 18].

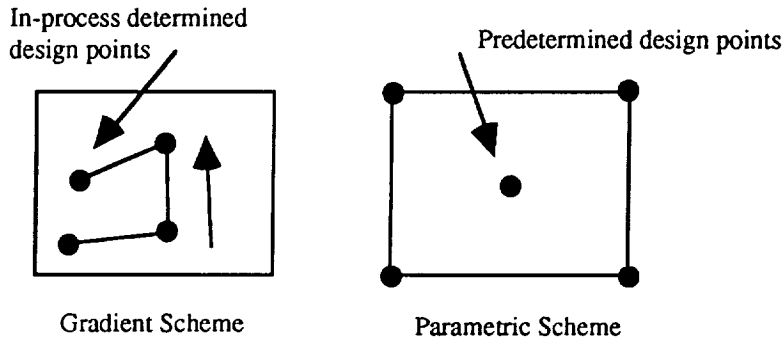

Figure 6 - Gradient Schemes vs. Parametric Schemes

The term *parametric methods* represents an entire class of specific multidisciplinary design optimization methods including Design of Experiments methods, Taguchi methods, central composite designs (with response surface methods), Box and Behnken designs, Box and Draper designs, and many others [16, 19, 20]. Each method has unique characteristics and certain advantages and disadvantages when applied to aerospace vehicle conceptual design. A detailed mathematical discussion of several selected methods is provided in succeeding sections. This section will address some common characteristics of parametric methods – including their applicability to the current class of design problem.

All parametric methods approach a problem by discretizing the design variables over an established range in the design space. That is, all variables are reduced to a few (usually two or three) distinct values within their design range. For example, if wing area ranges from 2500 ft^2 to 3500 ft^2, it may be reduced to only three values - 2500 ft^2, 3000 ft^2, and 3500 ft^2. For variables that are already discrete or integers (e.g. number of engines), parametric methods simply use the established values. Note that the number of levels of discretization will determine the type of response that can be predicted. It takes at least two levels to predict a linear effect. At least three levels are required to predict a curvature effect. Once all of the design variables have been discretized, various combinations of these discretized variables are selected from all possible combinations throughout the design space according to a statistical strategy. These combinations are combined into a set called an experimental array. Table 1 shows a sample experimental array for a problem with two design variables – wing area and tail area. Each variable has been discretized to two levels within its range. In this case, the experimental array contains every combination of the two variables and their two levels.

It is common practice to normalize (or "code") the design variables over their determined range in a manner such that the midpoint of the range is represented by a 0 (zero) and the lower and upper extremes are represented by -1 and +1 respectively. Normalizing the variables over their ranges makes it

easier to compare the effects of changing variables from one end of their range to the other even if they have different magnitudes of associated units. The wing and tail area example is shown in normalized form in table 2 (assuming that the previous points represented extremes of the variables).

Table 1 - Two Variable Experimental Design Array

run	Wing Area (ft^2)	Tail Area (ft^2)
1	2500	300
2	2500	500
3	3500	300
4	3500	500

Table 2 - Normalized Two Variable Experimental Design Array

run	Wing Area (ft^2)	Tail Area (ft^2)
1	-1	-1
2	-1	1
3	1	-1
4	1	1

Objective function values are determined for each row in the experimental array. That is, a point design is performed with the design variables "set" at the levels prescribed by the experimental array. For the example design, four point designs would be performed. The first one would fix wing area at 2500 ft^2 and the tail area at 300 ft^2 and determine the vehicle weight for those settings. The other runs would follow according to the rows in the experimental array. Different experimental methods use different

experimental arrays and the details of the interpretation of the results vary, but in general, parametric methods use the results of this broad exploration of the design space to determine the region that is most likely to contain the optimum. That is, individual point design information is extrapolated throughout the design space.

One benefit of a broad search of the design space is the fact that small localized effects tend to be averaged out, and therefore local minima traps can often be avoided. However, parametric methods often lack local resolution for the same reason. Therefore, they may only be able to identify a near-optimum solution rather than a true optimum.

The details of several individual methods from the parametric design class will be discussed in later sections.

Pros and Cons

Parametric methods are able to avoid some of the short comings of methods based on gradient schemes. By examining the design space broadly, parametric methods avoid falling into local minimums. They are perfectly suited to problems containing discrete variables because they already rely on a built-in discretization process.

Because parametric methods approach the design problem by establishing a set of predetermined runs (the experimental array), they enable parallel execution of some of the elements of the design. For example, once the wing area ranges have been fixed for each point design in an experimental array, an aerodynamicist may be able to perform all of the required aerodynamic analysis without waiting for additional inputs. Gradient-based methods determine the next point design based on information derived from the current point design and therefore must perform most of the multidisciplinary analyses required between iterations in series. The aerodynamicist would be forced to wait for the wing area results of the previous iteration before proceeding with the next design.

Parametric methods place no requirements on the analysis tools to be integrated into a single code. They are very well suited to the "design module" environment typical in conceptual aerospace vehicle design. The design process is ultimately just a relatively small, predetermined set of analysis cycles. The methods are easy to learn and apply (there are no gradients or derivatives to determine).

Parametric methods also have some disadvantages, however. For example, they only provide a near optimum solution to the problem. Most parametric methods can only choose the most promising combination from all of the possible combinations of the discretized variables (including those not included in the experimental array). The resolution of the discretization process limits the process to only a near optimum because there is no built-in interpolation between the variable levels. In some cases, equations can be fit to point design data (response surface methods), but even in those cases, the model is only an approximation of the real design space. However, a near-optimum solution is frequently all that is required for a conceptual design. Additionally, parametric methods have few provisions for treating design constraints. Each point design in the experimental array is assumed to lie within the feasible region of the design space.

In practice, parametric methods could be applied during the early portions of a design process when discrete variables may exist and a very broad search of the design space is required. A near-optimum solution may be sufficient for making broad configuration choices early in the design process. Based on the preliminary results, the design space could be refined by adjusting variables ranges and eliminating variables that may have been proven unimportant. A second parametric study could be used to further refine the design space, or a gradient-method could be used to "home-in" on a numerically optimum answer by starting in the near-optimum region identified in the initial parametric study. That is, parametric methods could easily serve as "front-ends" to gradient methods if applied in a sequential fashion.

Because of the potential of parametric methods for use in conceptual aerospace vehicle design, this research will be focused only on methods from this class of multidisciplinary design optimization methods – specifically, Design of Experiments methods, Taguchi methods, and central composite design (with response surface methods).

Discussion of Selected Parametric Methods

This section will discuss the mathematical basis for four selected techniques from the parametric class of multidisciplinary design optimization methods. The specific methods are Design of Experiments methods, Taguchi methods, central composite designs, and response surface methods. Design of Experiments (DOE) methods are a widely used parametric design scheme. Taguchi methods are a closely related field to DOE. In fact, many of the arrays used in Taguchi methods are subsets of Design of Experiments arrays. One of the goals of Taguchi methods is to reduce the number of point designs (or experiments) in the design array [16]. Central composite designs add additional experiments to two-level arrays in order to capture curvature effects in the design variables. Response surface methods can be used to create a mathematical model (response surface) of the objective function that approximates the design space. The response surface can then be optimized to find the best possible design. Mathematical models of constraints can also be determined.

These four methods were selected for further study from the class of parametric methods because they seem to be well suited to the problems of conceptual aerospace vehicle design. These methods are not new. They have been successfully applied in a variety of fields – mostly manufacturing related industries like automobiles and electronics [21]. While these methods may be relatively well understood by industrial engineers and operations researchers, aerospace engineers have had far less exposure to parametric design methods. Additionally, parametric methods have traditionally been applied later in the design cycle like during the product improvement and process design phases. Conceptual design problems have been addressed less frequently, although this particular set of four methods seems well suited for the early phases of aerospace design. Hopefully, the current research will contribute to the literature in the field and increase the acceptance of these methods as

multidisciplinary design optimization methods for conceptual aerospace design. Each method is discussed in detail in the following sections.

Design of Experiments Methods

Design of Experiments methods (or sometimes simply Designed Experiments) had their origin with Sir R.A. Fisher in England in the 1920's [16]. Fisher was performing agricultural experiments to increase crop yields. Typical variables were field conditions, fertilizer, seed types, etc. His goal was to be able to determine the effect of each input variable on the overall crop yield given that interactions are likely to exist between the variables. That is, the effect of one variable is dependent on the values of the other variables. For example, the crop yield may increase dramatically for a case where one seed type is combined with a particular fertilizer type. Such an interaction (or coupling) could easily be overlooked if a one-variable-at-a-time optimization method was used.

Fisher's design space is analogous to some multi-variable design spaces found in conceptual aerospace design. The number of systems level design variables is typically small – less than 10 in most cases. The variables are most likely coupled, and discrete variables are likely to be present early in the design. For example, a decision to place the engines under the wings or at the aircraft tail is likely to be found during the conceptual, exploratory phases of the design. Design of Experiments methods are ultimately the basis for almost all methods from the parametric class.

DOE methods have been advanced over the years by statistical researchers like Box, Hunter, and Hunter (see reference 22), Box and Draper (see reference 23), and Hicks (see reference 22) [16]. DOE related methods have been successfully applied in a variety of industries – manufacturing,

automotive, and electronics [21]. They are generally easy to apply, only requiring elementary knowledge in statistics to get useful results. Based on preliminary research, DOE methods have considerable potential in the area of conceptual aerospace design.

Design of Experiments methods begin with the identification of a set of design variables and a process that produces a measurable objective function (or response). The design variables could be chosen based on engineering experience, concurrent engineering with inputs from various engineering disciplines, or as the results of preliminary investigations. The number of variables in a DOE application is usually relatively small (less than 10) in order to keep the experimental effort small. Ranges of interest are established for each design variable, and the combination of design variables and ranges forms a *design space*. The design space is a regular sided, multidimensional figure (e.g. a cube for three variables). There are an infinite number of design points within the design space, but the objective of the method (like all parametric methods) is to identify a manageable set of points for which to perform an analysis, and then extrapolate the resulting information throughout the complete design space. The selected set of points is called the *experimental array*.

DOE methods create the experimental array by discretizing the variables across each of their predetermined ranges. That is, each variable is temporarily limited to only a few values over its entire range. The discretized values of the variables are referred to as "levels" or "settings". The levels are generally evenly spaced throughout the design space (although this is not a requirement). For example, a variable discretized to three levels would have one value at each of its extreme settings and one value at its midpoint. In order to make simple comparisons between the effects of variables with different units, the levels are typically normalized to a range of -1 to +1 as shown in table 3. Discrete variable settings are simply assigned to a value on the normalized range. For example, a discrete variable such as "Does the vehicle

have canards - Yes or No?" could assign "Yes" to a value of +1 and "No" to a value of -1 as shown in table 4.

Table 3 - Discretization of a Continuous Thrust Variable

Variable	Range	Discretized	Normalized
engine thrust	100 - 200 Klbs	100 Klb	-1
		150 Klb	0
		200 Klb	+1

Table 4 - Use of a Truly Discrete Design Variable

Variable	Discrete	Normalized
Canards?	Yes	+1
	No	-1

In order to keep the problem manageable, the number of variable levels is limited to three or four. Two-level arrays are the most popular. Arrays containing variables with different numbers of levels among the variables (called mixed level arrays) are possible, but it is more common to have the same number of levels for all of the variables in the array.

Consider a problem with three design variables, A, B, and C. Each of the three variables can be discretized to two levels and normalized to a range of -1 to +1. That is, each variable can be either -1 or +1. For the purposes of this example, it doesn't matter whether the design variables were originally continuous or if they are truly discrete. All eight (2^3) possible combinations of these three variables are represented in table 5. Each combination is represented as a row in the experimental array. Point designs are often referred

to as "runs" or "experiments" because of the method's origin in process analysis where an apparatus may have been tested after an experimental setup.

Table 5 - Example of All Variable Combinations

Run	A	B	C
1	-1	-1	-1
2	-1	-1	1
3	-1	1	-1
4	-1	1	1
5	1	-1	-1
6	1	-1	1
7	1	1	-1
8	1	1	1

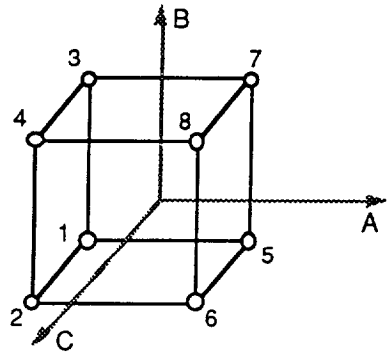

Figure 7 - Graphical 2^3 Full Factorial Array

Such an experimental array that contains all of the combinations of all of the variables is called a *full factorial* array. The information in table 5 is a full factorial array for three two-level design variables. Graphically, the eight design points are shown in figure 7 where each of the eight corner points of the cube represents an experimental run in the array. Note that a full factorial array for four variables at two levels each would require 2^4 =16 runs (or experiments).

Setting up all of the combinations of the design is only one part of the process. The goal of the method is to determine the effects of each variable on the response. For the two-level array shown in table 5, a linear model with interaction terms can be created like

$$y = \beta_0 + \beta_1*A + \beta_2*B + \beta_3*C + \beta_4*AB + \beta_5*AC + \beta_6*BC + \beta_7*ABC \quad (16)$$

where y is the measured response (i.e. the objective function). A, B, and C are the design variables that can take on values of +1 or -1. The eight β values are the unknown coefficients that represent the magnitudes of the effects of each term on the response. For example, if the variable A is placed at its largest level (+1) then a value of β_1 is added to the mean response. If A is placed at its smallest level (-1) then a value of β_1 is subtracted from the mean response. The cross terms like AB represent the interaction between design variables. If A and B are both +1 or both -1, then a value of β_4 is added to the mean response. If either A or B is -1 and the other is +1, then a value of β_4 will be subtracted from the mean response. This model is sometimes called an *additive* model because the effects of each term are "added" or "subtracted" from the average response [16]. The average response is represented by the β_0 coefficient in equation 16. In general, the additive model for a full factorial, two-level array of n design variables is:

$$y = \beta_0 + \sum_{i=1}^{n} \beta_i x_i + \sum_{i=1}^{n} \sum_{j=i+1}^{n} \beta_k x_i x_j + \ldots + \beta_{2^n-1} x_1 x_2 \ldots x_n \quad (17)$$

where,

k= (n+1) to n(n+1)/2 by 1's

In the example in table 5 and equation 16, there are eight experimental runs in the design array and there are eight unknowns in the additive model. The unknowns can be determined exactly by using the following matrix equation

$$\bar{y} = [X]\bar{\beta} \tag{18}$$

where $\bar{y}$ is the vector of the eight experimental responses and $\bar{\beta}$ is the vector of the eight unknown coefficients of the additive model. That is,

$$\bar{y} = (y_1, y_2, y_3, y_4, y_5, y_6, y_7, y_8)^T \tag{19}$$

$$\bar{\beta} = (\beta_0, \beta_1, \beta_2, \beta_3, \beta_4, \beta_5, \beta_6, \beta_7)^T \tag{20}$$

The matrix [X] is called the *design matrix*. For the example experimental design, the design matrix [X] is :

$$[X] = \begin{bmatrix} 1 & -1 & -1 & -1 & 1 & 1 & 1 & -1 \\ 1 & -1 & -1 & 1 & 1 & -1 & -1 & 1 \\ 1 & -1 & 1 & -1 & -1 & 1 & -1 & 1 \\ 1 & -1 & 1 & 1 & -1 & -1 & 1 & -1 \\ 1 & 1 & -1 & -1 & -1 & -1 & 1 & 1 \\ 1 & 1 & -1 & 1 & -1 & 1 & -1 & -1 \\ 1 & 1 & 1 & -1 & 1 & -1 & -1 & -1 \\ 1 & 1 & 1 & 1 & 1 & 1 & 1 & 1 \end{bmatrix} \tag{21}$$

Each term of the additive model is assigned to a column in the design matrix as shown in table 6. The column for the mean is associated with the constant term β_o and is always a column of all +1's. The columns for A, B, and C are taken directly from the experimental array settings. The columns for AB, AC, etc. are determined by multiplying the terms in each of the required

columns together. Each row in the design matrix represents an experimental run (i.e. a point design).

In order for a solution to be possible, the rows of the design matrix must form an independent set of vectors. That is, the determinant |X| cannot equal 0. If the determinant |X|=0, then the matrix is singular and cannot be inverted.

Table 6 - Column Assignments in Design Matrix for Example Array

term	mean	A	B	C	AB	AC	BC	ABC
column	1	2	3	4	5	6	7	8

The vector, $\bar{y}$, in equation 19 contains the responses for each of the experimental runs. The response is the value to be minimized or maximized. Vehicle weight is a typical response to be minimized in aerospace design. Other typical responses are power requirements, aerodynamic drag, or fuel requirements. A simple evaluation of an algebraic model may be all that is required to determine some simple responses, but most aerospace design problems require complicated, iterative, multidisciplinary analysis cycles in order to generate responses. Each entry in the $\bar{y}$ vector could be the result of hours or even weeks of work.

For the example experimental design (equation 18), the vector of unknowns, $\bar{\beta}$, can be determined from the following matrix equation in which the design matrix has been inverted:

$$\bar{\beta} = [X]^{-1}\bar{y} \tag{22}$$

which can be represented by:

$$\begin{bmatrix}\beta_0\\ \beta_1\\ \beta_2\\ \beta_3\\ \beta_4\\ \beta_5\\ \beta_6\\ \beta_7\end{bmatrix} = \frac{1}{8}\begin{bmatrix} 1 & 1 & 1 & 1 & 1 & 1 & 1 & 1\\ -1 & -1 & -1 & -1 & 1 & 1 & 1 & 1\\ -1 & -1 & 1 & 1 & -1 & -1 & 1 & 1\\ -1 & 1 & -1 & 1 & -1 & 1 & -1 & 1\\ 1 & 1 & -1 & -1 & -1 & -1 & 1 & 1\\ 1 & -1 & 1 & -1 & -1 & 1 & -1 & 1\\ 1 & -1 & -1 & 1 & 1 & -1 & -1 & 1\\ -1 & 1 & 1 & -1 & 1 & -1 & -1 & 1\end{bmatrix}\begin{bmatrix}y_1\\ y_2\\ y_3\\ y_4\\ y_5\\ y_6\\ y_7\\ y_8\end{bmatrix} \qquad (23)$$

The resulting β's are inserted into the additive model given in equation 16. Since the variables have been normalized to the same -1 to +1 range, the relative sizes of the β coefficients indicate the magnitude of the influence of each of the variables on the response as each variable is varied over its range. For example, if β_1 is significantly larger than the other coefficients, then variable A would have a larger influence on the response than the other variables. The additive model can be used to find the best settings of the design variables that will optimize the response. Usually this process can be done by simple inspection. For example, if the response is to be minimized, then the largest terms of equation 16 should be made negative by choosing appropriate values of A, B, and C. Since the additive model is linear in all variables, the minimum (or maximum) will lie at one corner of the design space (unless one of the coefficients is zero). That is, each term in the model will either have a positive or negative slope and the minimum will either be at +1 or -1. In cases where the interaction terms are as large as the main effect terms, an optimization routine could be used to determine the proper settings for each variable.

In some cases, the number of experiments required by a full factorial experimental array (every combination) may be too time consuming or too costly to perform. In such cases, it is common to use only a subset of the full factorial array. The subset is called a *fractional factorial* array and the process

of creating the new array is sometimes referred to as "fractionating" the full factorial array [22].

In most cases, the full factorial is reduced by a power of the number of levels in the array. For example, a full factorial array like 2^4 (a 16 run two-level array of four variables) might be reduced to eight runs (divide by 2^1) or to four runs (divide by 2^2). The notation for a fractional two-level array is 2^{n-p} where n is the number of variables in the full array and p is the power of the fraction. A half fraction of a two-level array of four variables would be designated a 2^{4-1} fractional factorial array, and it would require eight runs.

It is obvious that some information must be sacrificed when the size of the array is reduced. In the example design, all eight experimental runs are required to determine the eight coefficients in the additive model. For a half fraction (also called a half-replication), the model can contain no more than four coefficients. The selection of the subset of four runs (from the complete set of eight) depends on the coefficients in the model to be estimated. The problem must always be well posed and the design matrix must be invertible (if the number of equations and unknowns are equal).

Assume that the model for the three variable, two-level design is now written:

$$y = \beta_0 + \beta_1 * A + \beta_2 * B + \beta_3 * C \qquad (24)$$

In this model (one of many possible with four terms), only the main effects are being estimated. The design engineer may know enough about the design to know that the interaction terms will be negligible, and he or she wants to save some experimental effort by only performing four experiments. In practice, it is dangerous to assume that the interactions in an unknown design space will be small because, if they are present but ignored, then their effects will influence the other coefficients in the design. If it is necessary to fractionate a design, a proper selection of the subset of runs will provide some predictable structure to the way the ignored terms could possibly influence the

included terms. The process of selecting the subset of runs for a fractional factorial array is discussed below.

There are many ways to create a 2^{3-1} fractional factorial array for the 2^3 array shown in table 5. If the full factorial array is fractionated by selecting the second, fourth, sixth, and eighth runs, then the following, singular, design matrix would be created.

$$[X] = \begin{bmatrix} 1 & -1 & -1 & 1 \\ 1 & -1 & 1 & 1 \\ 1 & 1 & -1 & 1 \\ 1 & 1 & 1 & 1 \end{bmatrix} \tag{25}$$

Table 7 - Column Assignments for Singular Design Matrix

term	mean	A	B	C
column	1	2	3	4

Note that the first and last columns are identical. This design matrix cannot be inverted. A better selection in this case would be the second, third, fifth, and eighth runs from table 5. The design matrix would then be

$$[X] = \begin{bmatrix} 1 & -1 & -1 & 1 \\ 1 & -1 & 1 & -1 \\ 1 & 1 & -1 & -1 \\ 1 & 1 & 1 & 1 \end{bmatrix} \tag{26}$$

where the column assignments are the same as those shown in table 7. Equation 26 is an invertible matrix that would allow a solution for the main effects model shown in equation 24.

The increased experimental efficiency of a fractional factorial array allows the main effects to be estimated in only four experiments. However, as previously mentioned, fractional factorial arrays have a hidden danger. By ignoring some of the interaction terms, a designer is assuming that they do not exist. In reality, interactions almost always exist in advanced aerospace design, he or she is just hoping that they are small compared to the main effects.

The design matrix in equation 26 is designed to capture three main effects. If an interaction between variables A and B exists (an AB term), it will have the same design vector as the C variable. That is, C=A*B for every row in [X], or put another way, the product of all of the terms in the second and third columns is equal to the terms in the fourth column. The effects are indistinguishable. This situation is called *confounding* [16] and the main effect C is said to be *aliased* with AB. Similarly, A is aliased with BC, and B is aliased with AC in equation 26. If the interaction terms are suspected to be large, then the experimental array should be carefully chosen to keep the desired coefficients free from aliasing interference. Aliasing patterns and methods to select a suitable fractional array are discussed in references [16], [20], and [22]. The designer should be aware of the fact that simplifying the model does not simplify the design space. Just because an interaction does not appear in the model, does not mean it is absent from the true response.

To this point, only arrays that have equal numbers of experiments and unknowns in the additive model have been considered. That is, the design matrices have been square and invertible. Square designs are called *saturated designs* [25]. Saturated designs perform the minimum number of runs required to fit the additive model. It is possible, however, to create an experimental array with more than the minimum number of point designs. Consider the

following equation with more experimental runs than coefficients in the model:

$$\bar{y}_{m,1} = [X]_{m,n}\,\bar{\beta}_{n,1} \qquad \text{where } m>n \tag{27}$$

In this case, [X] is not directly invertible. The vector of coefficients, $\bar{\beta}$, can be estimated, however, using the method of least squares described in reference 19. The method of least squares selects the coefficients that minimize the square of the residual errors between the observed responses and the predicted responses. The solution for $\bar{\beta}$ is determined as follows.

$$[X^T]\bar{y} = [X^T][X]\bar{\beta} \tag{28a}$$

$$[X^TX]^{-1}[X^T]\bar{y} = \bar{\beta} \tag{28b}$$

By using such a regression technique, measurement errors in the responses can be "averaged out" and while the model may no longer pass through every design point, it will probably more accurately represent the overall design space.

Additional statistical tests are possible for experimental arrays with more experiments than coefficients. Phadke [16] gives a discussion of analysis of variance (ANOVA) tests, tests to determine the quality of the regression fit, and tests for statistical significance of each of the coefficients.

Consider the experimental array in table 8. The experimental runs can be used to predict the coefficients in equation 24. This array contains five point designs, but there are only four coefficients in the additive model. Therefore, the design matrix [X] is not square, and the method of least squares must be to be used to solve for the $\bar{\beta}$ vector of coefficients. Note that this particular design array is being used only to demonstrate the concept of least squares. It is not a recommended design because it is not fractionated based on a power of two.

Table 8 - Fractional Factorial Experimental Array

Run	A	B	C
1	-1	-1	-1
2	-1	-1	1
3	-1	1	-1
4	-1	1	1
5	1	-1	-1

The design matrix, [X], associated with table 8 is

$$[X] = \begin{bmatrix} 1 & -1 & -1 & -1 \\ 1 & -1 & -1 & 1 \\ 1 & -1 & 1 & -1 \\ 1 & -1 & 1 & 1 \\ 1 & 1 & -1 & -1 \end{bmatrix} \tag{29}$$

The vector of unknowns, $\overline{\beta}$, can be solved using the method of least squares.

$$\overline{\beta} = [X^T X]^{-1}[X]^T \overline{y} \tag{30a}$$

$$\begin{bmatrix} \beta_0 \\ \beta_1 \\ \beta_2 \\ \beta_3 \end{bmatrix} = \frac{1}{8} \begin{bmatrix} -1 & 1 & 1 & 3 & 4 \\ -3 & -1 & -1 & 1 & 4 \\ -2 & -2 & 2 & 2 & 0 \\ -2 & 2 & -2 & 2 & 0 \end{bmatrix} \begin{bmatrix} y_1 \\ y_2 \\ y_3 \\ y_4 \\ y_5 \end{bmatrix} \tag{30b}$$

Many specialized forms and applications of Design of Experiments have been researched and developed since Fisher's early work. Specialized arrays have been developed that fractionate full factorial arrays in ways that are useful for determining only main variable effects (i.e. Plankett-Burman

designs [20]). Saturated designs have been developed that are able to minimize the variance in the coefficients in the model. Most of these designs are based on the so called "D-optimality" criteria [25]. Other statistically generated minimum variance criteria have also been proposed for evaluating experimental arrays (e.g. "G-optimality") [25]. Genichi Taguchi developed a systematic approach to robust design based on orthogonal experimental arrays [18] that is of particular interest to engineers in conceptual design. In other methods, the simple additive models of two-level experimental arrays are efficiently augmented by runs at additional levels in order to capture curvature in the design space. These second order methods are called central composite designs, and they are closely associated with a curve fitting method called response surface analysis [19, 20]. These last three methods will be discussed in more detail in the following sections.

Taguchi Methods

Taguchi methods are based on Design of Experiments methods, and in some cases, the experimental arrays used by the Taguchi method are simply carefully selected fractions of full DOE arrays. Taguchi methods emphasize *orthogonal* experimental arrays in his method because they exhibit attractive characteristics for solving for the coefficients in an additive model. Because of the use of orthogonal arrays, the effects of the variables are easy to determine.

Taguchi methods are named for the Japanese engineer, Genichi Taguchi, who refined and simplified existing DOE methods through the use of orthogonal arrays [26]. Taguchi applied experimental design techniques to quality improvement issues. He formulated many of his ideas while trying to improve the off-line quality control of the Japanese communications system after World War II [27]. He realized that the quality of a given product must be "designed in" during the *early* stages of the overall design process. If the

product was designed properly off-line (i.e. before it actually went into production), it would be fairly insensitive to the uncontrollable noises it may encounter during the manufacturing process and therefore fewer defects would be produced and money could be saved. Taguchi wanted a technique that could be used by engineers early in the design phase. The existing statistical methods embodied by Fisher's design of experiments theory were available, but they were generally thought to be too complicated or unwieldy for the average engineer to use. Taguchi used simple orthogonal arrays to reduce the complexity and the number of experimental runs involved in solving a problem with a full factorial design. Taguchi published the orthogonal arrays used by his method, and he essentially "cook-booked" the analysis techniques that allow the designer to efficiently analyze the experimental results in order to determine the most important parameters. Since the mid-1960's all Japanese engineers have been trained in the use of Taguchi methods [28]. In the early 1980's, the Taguchi method began to be used by engineers in the United States - primarily in the manufacturing, automotive, and electronics industries [28]. The method has applicability to the early stages of aerospace vehicle design.

Taguchi methods are based on the use of orthogonal experimental arrays. An orthogonal array is one that produces a design matrix, [X], whose columns are all mutually orthogonal. That is, the dot product of any two columns of the design matrix is 0. Taguchi identifies his orthogonal arrays by the letter L followed by a subscript indicating the number of rows in the array. For example, an L_{32} orthogonal array will contain 32 rows. The maximum number of columns in the orthogonal array depends on the number of levels of the design variables. Two-level arrays contain one less column than the number of rows. The L_{32} orthogonal array will contain a maximum of 31 columns. Table 9 shows an L_4 experimental array designed to capture three main variable effects (as in equation 24).

Table 9 - L_4 Orthogonal Array

run	A	B	C
1	-1	-1	1
2	-1	1	-1
3	1	-1	-1
4	1	1	1

The design matrix, [X], associated with table 9 is:

$$[X] = \begin{bmatrix} 1 & -1 & -1 & 1 \\ 1 & -1 & 1 & -1 \\ 1 & 1 & -1 & -1 \\ 1 & 1 & 1 & 1 \end{bmatrix} \tag{31}$$

We can verify that the first two columns of the design matrix are orthogonal by evaluating their dot product.

$$(\text{col } 1)\bullet(\text{col } 2) = (1*-1)+(1*-1)+(1*1)+(1*1) = 0 \tag{32}$$

All other columns in the design matrix are similarly orthogonal. Note that some arrays with three or more levels can also be orthogonal.

Another characteristic of orthogonal arrays is called the *balancing property* [16]. Every column contains an equal number of the variable levels and, for every set of two columns, the pairs of levels -1 and +1 occur in all combinations and an equal number of times. For the L_4 array, the pairs of levels (-1,-1), (-1,+1), (+1,-1), and (+1,+1) each occur once for any two columns. For an L_8 orthogonal array, those combinations would each appear twice. The balancing property has the effect of making the array "unbiased" with respect to any one of the variable levels. As a result, the effects of changing variable levels is distributed evenly between any two columns and the array is not "slanted" toward any one setting of the design variables. The

balancing property is a sufficient condition to prove the orthogonality of an experimental array [16]. Figures 8a, 8b, and 8c show the concept of orthogonality graphically. Figure 8a shows a full factorial array of three variables (A, B, and C) at two levels each and figure 8b shows a selection of four points that is **not** balanced. Figure 8c shows a proper, balanced array (the L_4 array).

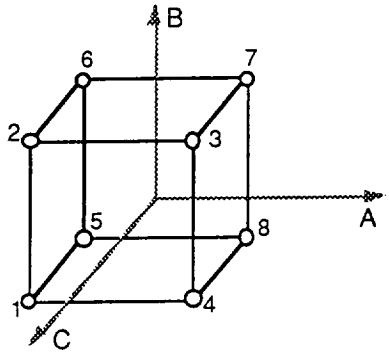

Figure 8a - Full Factorial Array

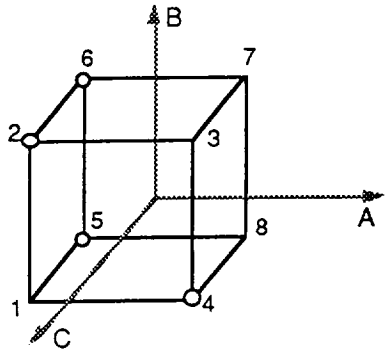

Figure 8b - Unbalanced Array

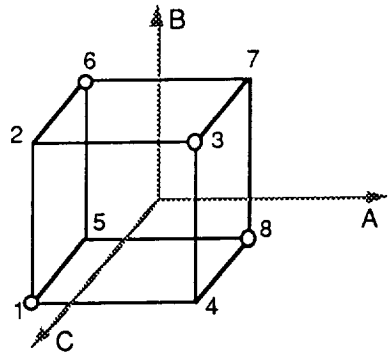

Figure 8c - L4 Orthogonal Array

The most important characteristic of orthogonal arrays is that they diagonalize the $[X^TX]^{-1}$ term in equation 30a which, in turn, makes the

calculation of the effect of each variable very easy. Consider the orthogonal design matrix from equation 31. Then the $[X^TX]^{-1}$ term would be

$$[X^TX]^{-1} = \frac{1}{4}\begin{bmatrix} 1 & 0 & 0 & 0 \\ 0 & 1 & 0 & 0 \\ 0 & 0 & 1 & 0 \\ 0 & 0 & 0 & 1 \end{bmatrix} \tag{33}$$

and the solution for the variable of coefficients, $\overline{\beta}$, is:

$$\overline{\beta} = [X^TX]^{-1}[X^T]\overline{y} = \begin{bmatrix} \beta_0 \\ \beta_1 \\ \beta_2 \\ \beta_3 \end{bmatrix} = \frac{1}{4}\begin{bmatrix} 1 & 1 & 1 & 1 \\ -1 & -1 & 1 & 1 \\ -1 & 1 & -1 & 1 \\ 1 & -1 & -1 & 1 \end{bmatrix}\begin{bmatrix} y_1 \\ y_2 \\ y_3 \\ y_4 \end{bmatrix} \tag{34}$$

The mean response β_0 is (as expected) the average of all four experimental responses and the other β's can be shown to be half of the difference between the average responses at one level of the variable and the average responses at the other level. That is,

$$\beta_0 = \frac{y_1 + y_2 + y_3 + y_4}{4} \tag{35a}$$

and using β_1 as an example

$$\beta_1 = \frac{1}{2}\left[\frac{y_3 + y_4}{2} - \frac{y_1 + y_2}{2}\right] \tag{35b}$$

The responses y_3 and y_4 were determined with A set to a value of +1, and the responses y_1 and y_2 were determined with A set to -1. With orthogonal arrays, the effect of a variable on the response can be determined by a simple difference of averages rather than by having to perform a complex matrix inversion. The same result is true for larger orthogonal arrays with more variables and more runs (and even interactions). This property of

orthogonal arrays makes them very easy for the average engineer to learn and apply and has contributed to the popularity of Taguchi methods.

To this point, only experimental arrays with two levels per variable have been discussed. Taguchi has published orthogonal arrays for three, four, and five level variables, and he has even created some arrays that have mixed levels (e.g. the L_{18} array). The mathematical interpretation of these other arrays is more difficult, but Taguchi maintains that the "averaging" method (called analysis of the mean , ANOM) is applicable for these arrays as well as two-level arrays [16, 17]. For example, a variable could have three levels (either discrete or discretized). When placed in a three-level orthogonal array, the effect of the variable can be determined from averaging the runs at each of the three levels and picking the level that produces the best average response. Three level arrays are able to capture some curvature effects using this technique. Because Taguchi relies on easy to analyze orthogonal arrays, his method is less concerned with "the mathematical model" and deals more with questions like "which variable setting (and which combination of settings) produces the best average result?". In fact, most historical applications of Taguchi methods deal with only main variable effects (no interaction terms) in an attempt to find the best overall combination. In advanced aerospace design, however, it is unwise to ignore the interactions. The following section illustrates that two variable interactions can be analyzed by the same ANOM techniques if the columns of the design array are carefully chosen to avoid aliasing problems.

As discussed in the DOE section, interactions can sometimes be aliased to (or confounded with) main variable terms. That is, certain columns in a design array could represent interactions and main effects. Taguchi methods have traditionally emphasized using orthogonal arrays to determine main effects only. If fact, critics of the method point out Taguchi's claim that two variable interactions do not need to be considered **at all** because a proper selection of design variables will minimize interactions [20]. However, there are provisions in the method to properly treat interactions. Taguchi developed

and published a graphical tool called *linear graphs* that can be used to help identify columns that contain two variable interactions. Linear graphs show all of the columns of the experimental array either as points (main effects) or lines between two points (a two variable interaction between two points) as shown in figure 9.

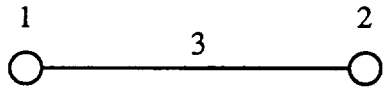

Figure 9 - Linear Graph for L_4 Array

By using the linear graph for the L_4 array, a designer can easily see that an interaction between the first and second columns of the array will be present in the third column. Therefore, any main effect variable placed in the third column will be confounded with the interaction. If the designer is interested in estimating the interaction, then the column should be left empty (i.e. no main effect in the third column). The resulting experimental array can be used to estimate the coefficient associated with the interaction term. In most cases, a given experimental array will have more than one linear graph indicating different ways that the columns can be used.

As an example, consider a problem that has four two-level design variables, and two variable interactions are likely to exist between three of the design variables. The linear graph for the L_8 array (figure 10) indicates that it is an acceptable orthogonal array that can determine the required terms in only 8 runs (a full factorial array would take $2^4 = 16$ runs).

Therefore, if variable A is assigned to column 1, variable B is assigned to column 2, variable C is assigned to column 4, and variable D is assigned to column 7, then the AB, AC, and BC interactions can all be estimated as shown in table 10. Note that only the four main variables are changed during the experimental process (i.e. the array is treated as four main columns and eight

rows). The interaction coefficients are estimated after the experiment is completed by calculating one-half of the difference between the average of the four runs with a setting of +1 and the average of the four runs with a setting of -1.

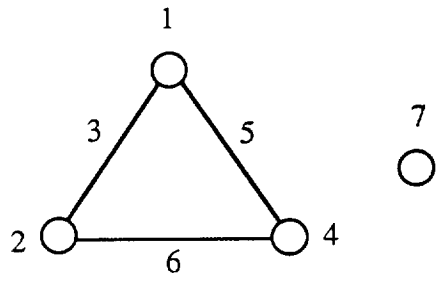

Figure 10 - Linear Graph for L_8 Array

Table 10 - L_8 Orthogonal Array

Run	A	B	AB	C	AC	BC	D
1	-1	-1	1	-1	1	1	-1
2	-1	-1	1	1	-1	-1	1
3	-1	1	-1	-1	1	-1	1
4	-1	1	-1	1	-1	1	-1
5	1	-1	-1	-1	-1	1	1
6	1	-1	-1	1	1	-1	-1
7	1	1	1	-1	-1	-1	-1
8	1	1	1	1	1	1	1

As mentioned previously, Taguchi methods place less emphasis on matrix operations to determine coefficients and model fits because by using

orthogonal arrays, the process can be reduced to simply averaging the responses at the different levels (analysis of the mean). Many applications of Taguchi methods simply present the results in a graphical format. For example, if variable A in the L_8 array was engine thrust and the response was gross weight, then the average responses could be plotted on a graph like that shown in figure 11. The value plotted for engine thrust of -1 is $(y_1+y_2+y_3+y_4)/4$ and the value plotted for engine thrust of +1 is $(y_5+y_6+y_7+y_8)/4$. If the objective is to minimize gross weight, then setting the engine thrust to its highest value would be the best choice (in the absence of large interactions). ANOM results are also frequently shown in tables called *mean response tables.*

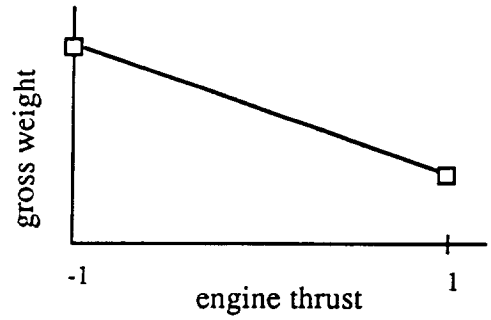

Figure 11 - ANOM Result for L_8 Array

Interactions can be analyzed graphically using ANOM or by using mean response tables. The mean response tables can either be shown as the difference of the averages of the interaction "levels" shown in the orthogonal array (the same method as used for main effects) or as separate average responses for each of the four combinations of the two variables (i. e. (-1,-1), (-1,+1), (+1,-1), and (+1,+1)). The first method is analogous to calculating the interaction term coefficient in the additive model, and it is useful for determining the magnitude of the interaction effect. The second method is useful for determining the best combination in the two variables involved in the interaction. Interactions can also be interpreted graphically as shown in

figure 12. Here, the interaction effect of a second variable (variable B – engine exit area) has been shown on the graph. For this example, there is a strong interaction between engine thrust and engine exit area. An engine thrust setting of 1 produces the lowest gross weight, but only if the exit area is also set to +1. As a rule of thumb, a strong interaction is said to exist if the lines on such a graph are crossed.

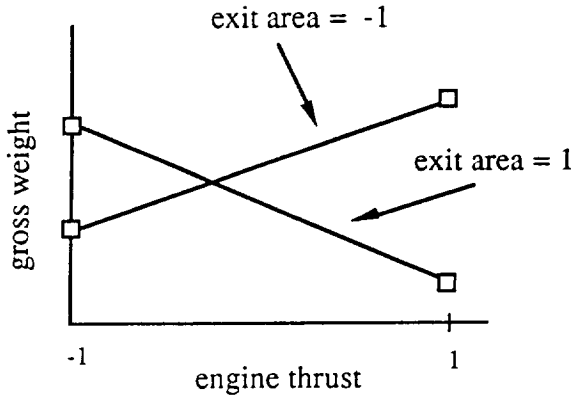

Figure 12 - Graphical Interpretation of an Interaction

An extension of the ANOM technique is the more powerful technique for determining the statistical information about the variables called Analysis of the Variance (ANOVA). ANOVA, while not used by many designers and not necessary for all situations, uses additional statistical techniques to further analyze the problem and provide additional data [27]. For example, ANOVA uses the standard deviation of the mean results from a particular parameter to insure that the changes in the overall response are statistically valid. That is, are the results inside or outside of the statistical noise of the experiments? Reference 29 contains ANOVA data from an experimental application of the Taguchi method to the design of a plastic container using finite element analysis. Using ANOVA, the designer was able to determine relative importance of the various design parameters on the overall product design [29]. References 16 and 27 provide additional information about the analysis of variance technique.

The second primary analysis tool within the Taguchi method is signal-to-noise ratio (S/N) analysis. As mentioned earlier, a good design is one that is fairly insensitive to uncontrollable outside influences. For example, a launch vehicle that is more tolerant to unexpected weight growth is more desirable than one that is not. Once the noise factors and appropriate levels are identified, a second orthogonal array is selected to create a noise array (also called the "outer array") [27]. The noise array is used in conjunction with the original controllable factors array (or "inner" array) such that for each row of the inner array, experiments are performed for all of the rows of the outer array. If the inner and outer arrays are both L_8 arrays, then the result would be 64 evaluations of the objective function. Using the objective function data for each case, an appropriate signal-to-noise ratio is calculated that, in effect, represents the ratio of the effect of the parameter on the mean of the objective function to the sensitivity of that parameter to the uncontrollable noises. A higher signal-to-noise ratio is the most desirable because it indicates a parameter that controls the objective function without being overly sensitive to uncontrollable noises. For the L_8 controllable factors array used in the previous example, assume a designer wants to test the sensitivity of the system to three noise factors at two levels each (e.g. 10% and 15% weight growth, two levels of cross winds during landing, and two launch delays periods). We can construct the noise array using an L_4 Taguchi orthogonal array. So, for each of the eight rows of the original array, we now perform experiments at four different noise combinations. The result is 32 evaluations of the objective function – vehicle gross weight (see figure 13).

Taguchi created several definitions for calculating signal-to-noise ratios. Since we are trying to minimize the vehicle weight, the appropriate signal-to-noise ratio to use is the "smaller-the-best" S/N. The S/N for each row of the controllable factors array is calculated using the following equation from reference 16.

$$S/N = -10*\log_{10} \left(\frac{1}{n}\sum_{i=1}^{n} y_i^2\right) \qquad (36)$$

where,

n = number of rows in the noise array (4)

y_i = objective function at each noise column

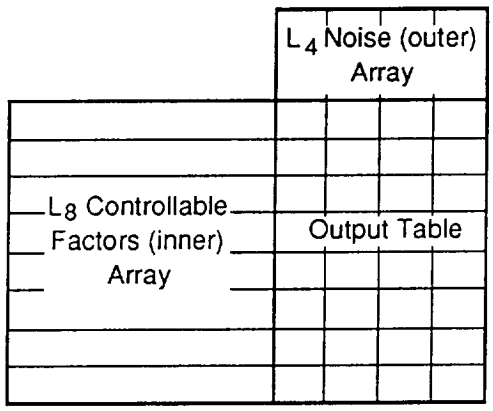

Figure 13 - Inner and Outer Arrays

After a single S/N is calculated for each row, an average S/N is then calculated for each of the controllable design parameters at each of its settings (similar to the ANOM calculation). Higher S/N's indicate a statistically lower vehicle weight even when noise is included and are, therefore, better settings for the parameters. Using S/N information, a designer can identify which parameter levels are most sensitive to uncontrollable noises. Therefore, a more robust, noise tolerant system can be designed. Figure 14 shows a case where knowledge of the noise sensitivities allows a designer to select a more robust design point rather than risk a more "optimum" setting that is overly sensitive to uncontrollable factors. The S/N formulas for cases where a specific output value is being targeted (i.e. nominal-the-best S/N) include additional terms such as the standard deviation and mean of the row [16]. In all S/N cases, however, a larger S/N is a more desirable case.

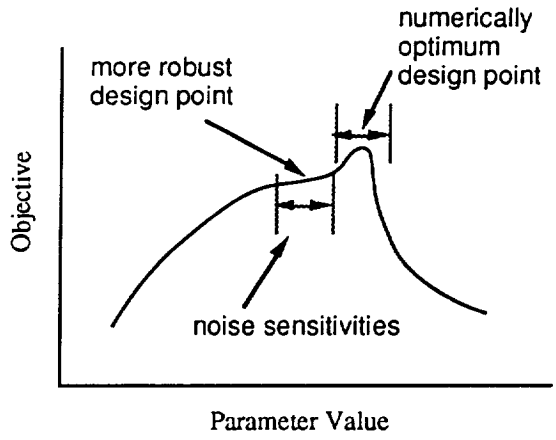

Figure 14 - Robust Design vs. Numerical Optimum

While many applications of the Taguchi method do not make use of signal-to-noise ratio techniques, it is perhaps the greatest strength of the method. In reference 30, Byrne and S. Taguchi give an example of signal-to-noise ratio analysis applied to the design of an elastomeric hose connector where the controllable factors are adhesive concentration, connector wall thickness, insertion depth, and interference fit. The noise factors are conditioning time, conditioning temperature, and conditioning humidity.

In general the Taguchi method is very easy to apply and does not require numerical gradients and derivatives to be generated for each step in an iteration process. The experimental runs, with or without noise factors, to be analyzed are established from the beginning of the design process. Existing detailed analysis codes can be retained. The method does not require the analysis experts to provide any "new" information as part of their individual analysis processes.

Because parametric ranges and levels are used, the process lends itself very well to the use of discrete variables. Structural material type, for example, could be one of the input parameters with the two levels representing

two completely different materials. Numerical optimization techniques would have a very difficult time dealing with such a parameter because derivatives do not exist for discrete variables.

In addition, the Taguchi method tends to characterize the entire design space rather than just finding the optimum answer. Interactions, parametric trends, and noise variances are all identified by the method. Armed with such information, a designer may have more confidence in the final design.

On the negative side, the results from the Taguchi method (like all DOE based methods) are not truly optimums in the sense of several decimal place accuracy. The results will only show trends over the range and levels given by the designer. The "near-optimum" solution will only be the best combination of the design variables as limited by their levels. In some cases, the ranges may be too large, and therefore, the "grid" may be too coarse to predict a suitable optimum. In that case, the ranges should be redefined, and the process should be repeated. Large ranges are useful for exploring the entire design space, but care should be taken to avoid infeasible regions in the design space. The method is not well suited to dealing with infeasible design points. Taguchi methods are also useful for screening variables to determine the most significant ones. Using the method, variable trends and interactions can be identified to enable one or two designs to be selected for more detailed study.

Because of the Taguchi method's ease of use, ability to deal with discrete variables, ability to find a near-optimum (if not an exact optimum), and ability to screen a set of variables over the entire design space, it may be most applicable to the early phases of a vehicle design – where many of the major configuration decisions remain open. This method is particularly attractive to the conceptual aerospace vehicle designer.

Central Composite Design

Methods based on two-level arrays (like 2^n full factorial arrays, 2^{n-p} fractional factorial arrays and Taguchi's L_4, L_8, and L_{32} arrays) are designed to capture linear main variable effects and interactions between variables. However, many aerospace designs contain curved design spaces. In order to capture curvature in a particular variable, it must be represented at least by three levels in the experimental array. In addition, curved models can be used to help locate a near-optimum within the design space – not just at the corners as with an additive model. Full factorial and fractional factorial three-level DOE arrays are candidates. However, full factorial 3^n arrays generally require many experimental runs and do not fractionate very cleanly (i.e. it is difficult to obtain simple aliasing structures). Taguchi's three-level orthogonal arrays are also candidates, but again they can be large and have complicated aliasing patterns [20].

Central composite designs (CCD's) are a class of designs that are able to capture curvature effects in the design space, specifically a quadratic model. CCD's were introduced in the 1950's by statistical researchers Box and Wilson as an alternative to three-level factorial designs [19]. CCD's are built from full or fractional factorial two-level arrays that already contain a sufficient number of runs to capture first order effects (and interactions) for a given number of design variables. Then, a point is added at the center of the design space and two points are added along each variable axis for which curvature is to be estimated. These "star" points are placed an even distance to the left and right of the center point. Figure 15 illustrates a CCD for a three variable problem for which all interactions are to be estimated and all three variables are expected to have curvature effects. The white circles represent the points from a 2^3 full factorial array, and the black circles represent the points added to form the central composite design (i.e. center point and the star points).

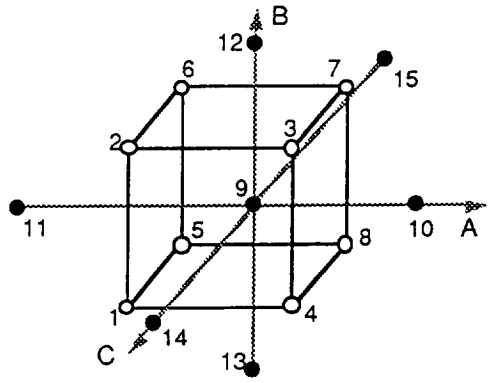

Figure 15 - Three Variable Central Composite Design

The star and center points add 2n+1 points to the experimental design. Table 11 lists the number of experiments required to estimate quadratic curvature and all 2 variable interactions for Taguchi and CCD. The number of runs required by the CCD is tabulated based on a suitable orthogonal fractional two level array (one that will capture all of the interactions) and based on a full factorial two level array. The full factorial three level array is also listed.

Table 11 - Comparison of CCD and Other Methods

# Variables	Full Factorial 3^n	3 Level Taguchi	Fractional 2^{n-p} based CCD	Full based 2^n CCD
2	9	9	9	9
3	27	9	15	15
4	81	81	25	25
5	243	81	27	43

As the number of variables increases, the efficiency of the fractional 2^{n-p} based CCD becomes evident. Note that the number of experiments required by the fractional arrays does not vary smoothly with number of variables because the amount of fractionating required to preserve an array that will capture all of the two variable interactions varies. CCD's are designed to be able to fit a model that captures all of the two variable interactions, all of the linear terms, and all of the second order terms. For example, consider a two variable CCD design. The model to be fitted is

$$y = \beta_0 + \beta_1 * A + \beta_2 * B + \beta_3 * AB + \beta_4 * A^2 + \beta_5 * B^2 \qquad (37)$$

This equation has six unknowns so there must be at least six experiments in the design array. The appropriate CCD design is

Table 12 - Two Variable CCD

Run	A	B
1	-1	-1
2	-1	1
3	1	-1
4	1	1
5	$-\alpha_1$	0
6	α_1	0
7	0	$-\alpha_2$
8	0	α_2
9	0	0

Note that the first four runs are a full factorial 2^2 array. The full factorial is required in this case to capture the two variable interaction. The

fifth through ninth experiments capture the quadratic term in variables A and B. The ninth experiment is the center point. Graphically, this array is the two dimensional graphic shown in figure 16.

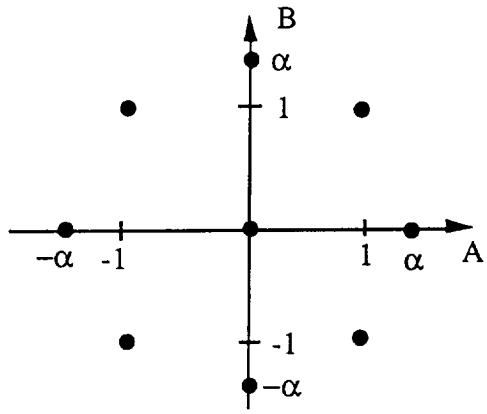

Figure 16 - Two Variable CCD

The selection of values for the coefficients α_1 and α_2 will have an effect on the characteristics of the second order model. If $\alpha_1=\alpha_1=1$, then the star points will lie in the same plane as the upper and lower settings for each variable. Counting the center point, each variable will be represented at three different levels. Such a design is said to be *face centered* [20]. Face centered designs have some advantages. They are simple to construct, and they are useful for cases when the high and low settings of a design variable are physically limited to the values within the assigned range of +1 and -1. For example, if a variable was engine throttle setting, and a normalized setting of +1 was given to a throttle setting of 100% in the fractional part of the design, then it would not make sense to assign a star point to a value higher than +1. It can be shown, however, that if α_1 and α_2 are carefully selected, then the variance of the fitted model will depend only on the distance from the center point and not on the direction. Variance is a statistical term that is analogous to the precision of the fit [20]. Such a design is called a *rotatable* design [19]. The term rotatable is derived from the fact that the design can be rotated about

its center point, and the variance at a given point would be unaffected (since its distance from the center point would not change).

The value for α in a rotatable design is given by:

$$\alpha = F^{\left(\frac{1}{4}\right)} \tag{38}$$

where,

F = the number of points in the factorial portion of the design

For the example CCD shown in figure 16 and table 12, F=4 and the design will be rotatable if α is set according to equation 39.

$$\alpha = 4^{\left(\frac{1}{4}\right)} = \sqrt{2} \tag{39}$$

Rotatability of the array is a desirable theoretical goal since the object of the design is to find the minimum point in the design space and rotatable designs provide equal precision in all directions [20]. Note that all orthogonal first order arrays are rotatable. 3^k arrays are not rotatable [20].

In practice, rotatability may be most useful only as a design guideline. In some cases, it may be impractical to select α such that it equals $F^{1/4}$. In those cases, a value close to the optimum will make a "near rotatable" design that should be sufficient. In fact, different values of α_1 and α_2 could be used if necessary. The second point to remember about using rotatable designs is that they calculate variance based on a second order model. It is highly likely that the actual physical design space may not be a true second order space. That is, there will likely be other sources of variance in the model.

One attractive characteristic of central composite designs is the fact that they can be created as "add-ons" to existing first order, two-level designs. A design space could be first explored with a simple fractional factorial array, and if the model is later found to be inadequate, then the design could be built into a CCD by the addition of a center point and star points. The new second

order model would take advantage of the previous work. It is a common practice to determine the accuracy of a first order model by performing a design at the center of the design space and comparing the result to the predicted center point. The predicted center point is the mean response of the first order model (the β_0 coefficient). If the actual center point differs significantly from the predicted center point, then it is highly likely that there is curvature in the design space. However, there is no indication of which of the variables is contributing the most to the curvature effect. It is not necessary to add star points for every variable in the design – only those for which a quadratic term is desired. In many cases, the majority of the curvature is the result of only one or two variables.

In summary, CCD's are a potentially very useful technique for use in advanced aerospace vehicle design. Unlike two-level methods, CCD's can capture second order effects in the design space (at the expense of additional runs compared to linear models). They are easy to construct, and they can be "built up" from a fractional factorial array. CCD's can be designed to be rotatable (equal precision in all directions), while three-level methods like a 3^k full factorial design cannot. They are more efficient and require fewer experimental runs than Taguchi's three-level orthogonal arrays. CCD's, however, are not orthogonal. They cannot be readily used with discrete variables using Taguchi's analysis of the mean technique, but they are very attractive for use with continuous variables.

Once a suitable design array has been selected using CCD techniques (either rotatable, near-rotatable, or face centered), then the individual experiments can be used to fit a mathematical model of the response. Generally, the actual process of determining the coefficients in the second-order model is part of a technique called response surface analysis or response surface methods. Response surface methods are discussed in the following section.

Response Surface Methods

Response surface methods (RSM) are very closely associated with arrays created with central composite design. RSM refers to the actual process of determining or "fitting" an approximate mathematical model for an experimental response (the objective function). RSM is not restricted to fitting experimental arrays formed with central composite design techniques, but it is one of the most common uses of RSM. RSM can be used to fit mathematical response models to full and fractional factorial two-, three-, and higher-level design of experiments arrays as well as other statistically derived three level arrays. However, RSM is **not** generally associated with Taguchi methods because orthogonal arrays can be analyzed with simple analysis of the mean techniques.

Central composite designs contain information to fit a mathematical response model of the form (containing all main effects, all two variable interactions, and all quadratic terms for a given number of design variables):

$$y = \beta_0 + \sum_{i=1}^{n} \beta_i x_i + \sum_{i=1}^{n} \sum_{j=i+1}^{n} \beta_k x_i x_j + \sum_{i=1}^{n} \beta_l x_i^2 \qquad (40)$$

where,

n= the number of design variables

k= (n+1) to n(n+1)/2 by 1's

$$l = \left[\frac{(n+1)(n+2)}{2} + (i-n) \right] - 1$$

Equation 40 can be written in the matrix form:

$$\bar{y} = [X]\bar{\beta} \qquad (41)$$

where $\bar{y}$ is the vector of experimental responses, $\bar{\beta}$ is the vector of unknown coefficients, and [X] is the design matrix. For the two variable CCD shown in table 12, second order model is

$$y = \beta_0 + \beta_1 * A + \beta_2 * B + \beta_3 * AB + \beta_4 * A^2 + \beta_5 * B^2 \qquad (42)$$

Taking $\alpha_1=\alpha_2=\sqrt{2}$ to make the design rotatable, the design matrix, [X], becomes

$$[X] = \begin{bmatrix} 1 & -1 & -1 & 1 & 1 & 1 \\ 1 & -1 & 1 & -1 & 1 & 1 \\ 1 & 1 & -1 & -1 & 1 & 1 \\ 1 & 1 & 1 & 1 & 1 & 1 \\ 1 & -\sqrt{2} & 0 & 0 & 2 & 0 \\ 1 & \sqrt{2} & 0 & 0 & 2 & 0 \\ 1 & 0 & -\sqrt{2} & 0 & 0 & 2 \\ 1 & 0 & \sqrt{2} & 0 & 0 & 2 \\ 1 & 0 & 0 & 0 & 0 & 0 \end{bmatrix} \qquad (43)$$

where the columns in the matrix are associated with the terms in the model as shown in table 13.

Table 13 - Column Assignments for 2 Variable CCD Design

term	mean	A	B	AB	A^2	B^2
column	1	2	3	4	5	6

Note that the design matrix formed from a central composite design is not orthogonal. Since the matrix is not square, the solution of equation 41 requires the use of the least squares method. The least squares method is appropriate for use with polynomial equations [20]. Solutions for coefficients in non-polynomial equations can be found by using various forms of regression analysis [see reference 20]. Regression analysis can also be used as

an alternative to matrix manipulation to solve for the coefficients in a polynomial equation. Regression analysis capabilities exist in many personal computer based data analysis packages.

Using the method of least squares, equation 41 becomes,

$$\overline{\beta} = [X^T X]^{-1}[X]^T \overline{y} \tag{44}$$

and the solution for $\overline{\beta}$ can be written

$$\begin{bmatrix} \beta_0 \\ \beta_1 \\ \beta_2 \\ \beta_3 \\ \beta_4 \\ \beta_5 \end{bmatrix} = \frac{1}{16} \begin{bmatrix} 0 & 0 & 0 & 0 & 0 & 0 & 0 & 0 & 16 \\ -2 & -2 & 2 & 2 & -\sqrt{8} & \sqrt{8} & 0 & 0 & 0 \\ -2 & 2 & -2 & 2 & 0 & 0 & -\sqrt{8} & \sqrt{8} & 0 \\ 4 & -4 & -4 & 4 & 0 & 0 & 0 & 0 & 0 \\ 1 & 1 & 1 & 1 & 3 & 3 & -1 & -1 & -8 \\ 1 & 1 & 1 & 1 & -1 & -1 & 3 & 3 & -8 \end{bmatrix} \begin{bmatrix} y_1 \\ y_2 \\ y_3 \\ y_4 \\ y_5 \\ y_6 \\ y_7 \\ y_8 \\ y_9 \end{bmatrix} \tag{45}$$

Once a model has been determined, the goal is to minimize (or maximize) the response. A non-linear, gradient-based optimization technique can be used to locate the minimum. Many of the techniques discussed previously in the classical optimization section are appropriate – steepest descend, Powell's Method, etc. If a central composite design is used (thereby allowing a quadratic response surface to be calculated) then it is possible that a minimum may exist within the design space. Recall that two-level methods will only locate a near-optimum along the edges of the design space. In addition, the RSM optimum is not limited to the best combination of the different levels of all of the variables (unlike Taguchi). Even though a variable may only be limited to a few levels in the experimental array (i.e. -1, 0, and 1), the optimum may be determined to be a value like 0.567. Therefore, RSM may allow a more optimum solution than Taguchi methods.

One of the most important advantages of response surface methods is the fact that constraints can be included in the process. At the same time that experiments are being performed to determine the objective function at various points in the design space, the value of an output to be constrained can also be recorded. A separate response surface can be created to model the value of the constraint, and a non-linear optimizer capable of treating constraints can be used to minimize the objective subject to the constraint. For example, a launch vehicle is being optimized for minimum weight using a CCD with RSM. The design variables are wing size, engine thrust, and engine mixture ratio. The vehicle is also constrained to a maximum landing speed. For each point in the CCD, a complete, converged vehicle point design is performed for the prescribed settings of the design variables. The vehicle weight and landing speed are recorded for each point, and RSM is used to fit second order models of both the objective function and the constraint function. An optimizer is then used to find the minimum vehicle weight subject to a maximum landing speed constraint. This same technique could be performed with several simultaneous constraints. Stanley, et. al. [7] provides an example of such an application to an advanced rocket design. In that example, the vehicle dry weight was minimized subject to minimum aerodynamic control constraints. The ability to handle constraints is one of the most powerful aspects of response surface methods. Such an ability is lacking in purely parametric methods like the Taguchi method.

Response surface methods are very well suited to advanced aerospace vehicle design. They are based on parametric design arrays which have already been shown to be useful (they retain existing analysis codes, explore the entire design space, are resistant to local minima, allow parallel execution of some analysis, they use a small number of point designs, etc.). In addition, RSM methods based on second order experimental arrays like central composite designs allow the determination of an optimum that is not just the best combination of the levels of the design variables (i.e. values between levels are possible). It is important to remember, however, that the model is

still just an approximation of the true design space. Using a second order RSM model does not mean that the design space will be quadratic. The numeric optimum of the model (determined by the optimizer) will not necessarily be the optimum of the true design space. Also, RSM based on CCD's require more point designs than two-level models (although they provide more information), and they are not well suited to the use of discrete variables. Taguchi methods are better suited for use of discrete variables. However, RSM appears to be a very attractive method for use in aerospace design.

SAMPLE DESIGN APPLICATION (ROCKET-BASED COMBINED-CYCLE LAUNCH VEHICLE)

In order to test some of the hypotheses concerning the applicability of the parametric class of multidisciplinary design methods to advanced aerospace vehicle conceptual design, a sample application was selected. The rocket-based combined-cycle (RBCC) vehicle is a single-stage-to-orbit (SSTO) launch vehicle of current interest. It is a highly multidisciplinary design – requiring separate analysis capabilities in propulsion, performance, aerodynamics, weights and sizing, structures, and aerodynamic heating. Ultimately, a converged point design is obtained from extensive iteration between existing, disciplinary analysis tools. The selected design variables are highly coupled (interrelated), and therefore interactions are expected to be present. Traditional one-variable-at-a-time optimization is not appropriate for this design. The objective of the RBCC SSTO design is to determine the settings of the design variables that will minimize vehicle dry weight. Dry weight is a better indicator of cost than gross weight since gross weight is primarily composed of propellant weight and propellant is relatively cheap. The objective of the application of the parametric methods to this problem is to verify their applicability, point out strengths and weaknesses, and contribute to the literature in the field by demonstrating an actual application of the methods.

The design was performed in three phases. An initial exploration of the design space was performed using a three-level Taguchi array (L_{27}) and eight design variables. The initial design phase contains two truly discrete variables. Based on the results of the initial array, a second L_8 experiment was performed using three of the design variables that required further study. The second experiment also used Taguchi's "noise" array (L_4) in order to determine a robust design. In this case, the vehicle sensitivity to three weight growth and engine performance degradation variables was to be minimized.

Finally, the experimental array was extended to a central composite design in the three main variables. Response surface methods were used to optimize the resulting quadratic response surface.

Vehicle Background

The next generation of piloted launch vehicles will have emphasis on low cost design, responsiveness, and reusability. In the past 10-15 years, advances in structural technologies (composites, advanced metallic alloys) and reductions in subsystems weights have made single-stage-to-orbit (SSTO) designs more feasible [31]. New SSTO vehicle designs are generally fully reusable and, if flight rates are high enough, they have potential to reduce recurring costs associated with expendable systems.

Among the SSTO designs currently being considered for initial operating capabilities (IOC's) in the 2005-2010 time frame are advanced rocket powered vehicles [7] and airbreathing concepts that are derivatives of the National Aerospace Plane (NASP). Rockets and airbreathing systems each have advantages and disadvantages. Rockets, which carry their own oxidizer, are characterized by high engine thrust-to-weight ratios (70-100) and relatively low trajectory averaged I_{sp}'s (350-450 sec for LH2/LOX systems). Rocket SSTO's have relatively high gross weights, high bulk propellant densities, and low dry weights (i.e. empty weight) (fig. 17). Airbreathing concepts do not carry a substantial amount of onboard oxidizer. Instead they derive it from the atmosphere. They have higher I_{sp}'s (1500 - 2500 sec. for LH2), but their complex airflow paths (inlets, cowls, nozzles) generally produce heavy engines with thrust-to-weight ratios around 5-15. Airbreathing SSTO concepts have low gross weights but higher dry weights when compared to rockets. Combined cycle propulsion concepts have potential to combine the best aspects of both rockets and airbreathing propulsion.

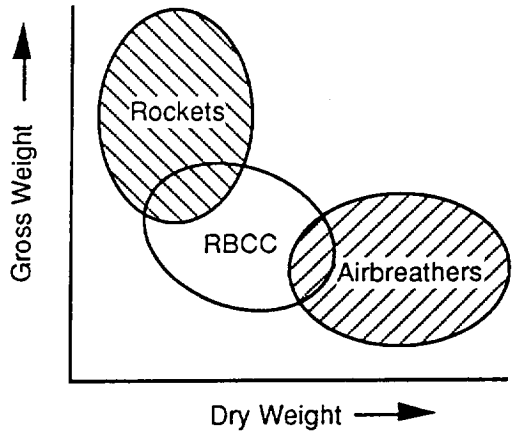

Figure 17 - Propulsion Concept Characteristics

Combined cycle engines merge the functions and operating modes of different engine cycles into a single unit. Rocket-based combined-cycle propulsion, sometimes referred to as an air-augmented rocket, utilizes a "ducted rocket" approach with a rocket primary embedded in the duct of an airbreathing engine (fig. 18).

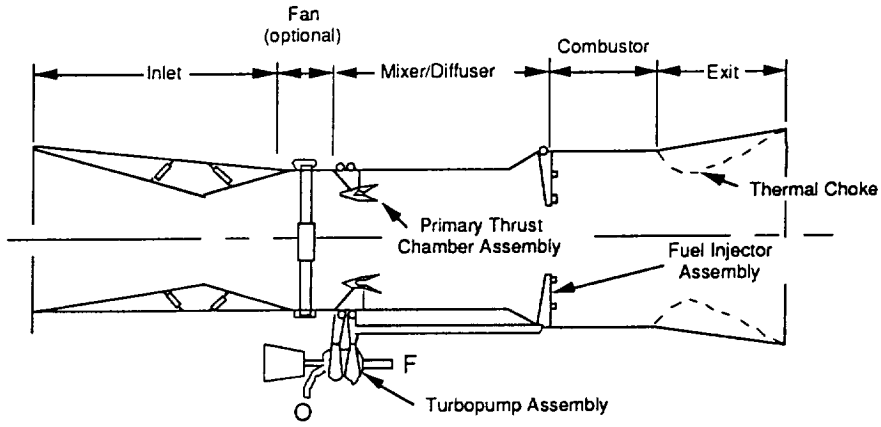

Figure 18 - Typical RBCC Engine Layout

RBCC engines have thrust-to-weight ratios of 25-40 and average Isp's that are higher than that for rockets (420-800 sec). RBCC engines function in four different operation modes. From 0 to Mach 3, the engine operates as an ejector. The rocket primary entrains additional air through the inlet to which LH2 fuel is added in an afterburning fashion. Beyond Mach 3 the engine operates in ramjet and scramjet modes. For terminal acceleration to orbit, the RBCC engine is capable of operating in rocket mode. The RBCC engine has been studied in some detail including work by the Marquardt Corp. in the 1960's [32] and Rocketdyne [33].

Airbreathers with an axisymmetric fuselage have been previously studied because of advantages in high engine capture area (thus high acceleration), relatively low drag, and simplified load paths associated with a circular tank cross section. [34, 35]. In fact, a conical vehicle configuration was considered a candidate early in the NASP program [35]. Preliminary work to combine the advantages of RBCC propulsion with the advantages of an axisymmetric fuselage was performed in the late 1980's by the Astronautics Corp. [36, 37]. The Astronautics Corp. work showed the potential weight and performance advantages in a vehicle like the one shown in figure 19, and it identified several key variables that have a significant impact on the vehicle design. However, that work was unable to identify the optimum settings for the variables because multidisciplinary design optimization techniques were not available to the researchers.

The research reported in this paper is an attempt to extend the previous work by employing multidisciplinary design optimization (MDO) techniques. It is hoped that parametric design methods can be used to locate a near-optimum setting for the design variables. In addition, it is hoped that this particular use of MDO methods will document an example aerospace vehicle conceptual design application and demonstrate the utility of multidisciplinary design optimization.

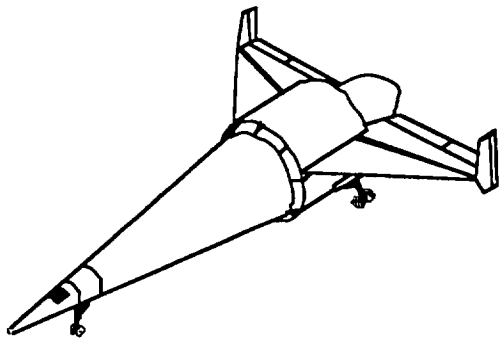

Figure 19 - RBCC SSTO Configuration

The baselined technologies chosen for this work are shown in table 14. These technologies are consistent with a vehicle of IOC 2005-2010 and are based on technology efforts that are currently in-work at NASA and in industry. Advanced technologies, particularly lightweight structures are critical to the feasibility of a RBCC SSTO vehicle.

Table 14 - Baselined RBCC SSTO Technologies

LH2 tank	graphite/PEEK, filament wound, integral loads
LOX tank	aluminum-lithium, integral loads
Structure	NASP-derived titanium-aluminide Beta 21S
OMS/RCS systems	LH2/LOX cryogenic pump-fed OMS, LH2/LOX pressure -fed RCS)
TPS (passive areas)	ACC and mechanically bonded metallic (Inconel and titanium standoff)
Active cooling	heat pipe and active hydrogen cooling for engine, nosecap, cowl and wing leading edges
Subsystems	lightweight avionics, ECLSS, crew systems, EMAs

Analysis Tools and Process

The analysis was performed using computer-based conceptual aerospace design tools that are available at the NASA - Langley Research Center's Vehicle Analysis Branch (analogous to the "design modules" discussed previously) and proceeded according to the flow chart shown in figure 20. The design was highly multidisciplinary – containing disciplinary analyses from aerodynamics, performance, aeroheating, weights and sizing, structures, and propulsion. The general RBCC SSTO vehicle layout is shown in figure 21. A general discussion of the analysis process follows.

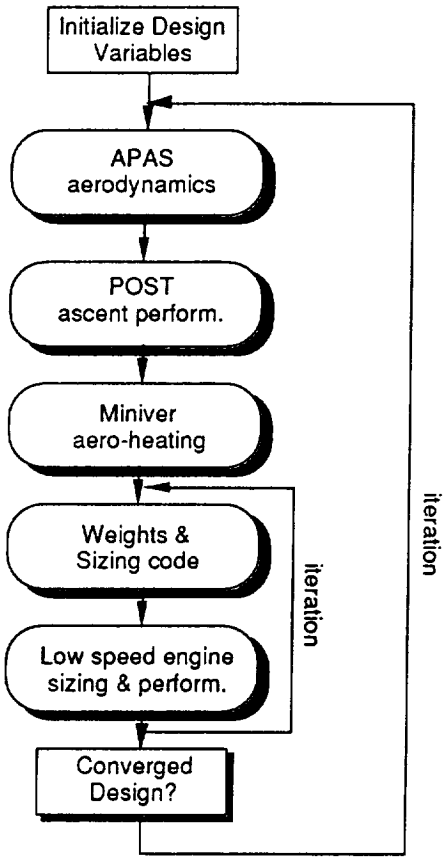

Figure 20 - Analysis Cycle

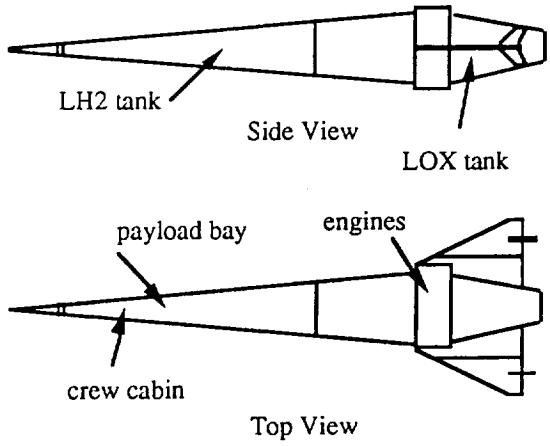

Figure 21 - General RBCC SSTO Vehicle Layout

APAS (the Aerodynamic Preliminary Analysis System) [38] was used to determine the lift and drag coefficients for each vehicle point design for Mach numbers from 0 to Mach 25. APAS is a conceptual level aerodynamic design tool that has been shown to produce relatively accurate answers when compared to wind tunnel tests on conical configurations [39, 40]. Additional confidence was placed in the data because APAS used a tangent cone solution at high Mach numbers – a solution originally derived from conical forebody aerodynamic data. Because the scramjet engine data was provided in cowl-to-tail form, the aerodynamic pressures on the conical forebody were treated as drag rather than as part of the engine cycle. For each design, the wing was kept at a constant leading edge sweep of 76°, aspect ratio of 1, and a thickness of 4% (the existing wind tunnel test values). The wing area was sized to provide a 200 kt. landing (or a 250 kt. take-off speed for the case of horizontal take-off vehicles). Wing location (fore to aft) was varied in order to maintain subsonic and hypersonic static stability.

The RBCC ejector mode engine characteristics for each engine from 0 to Mach 3 were determined using a quasi-1-D inlet, combustor, and nozzle

model with appropriate component efficiencies derived from reference 32. Engine uninstalled weights (less inlet) were also derived from references 32 and 36 as a function of maximum airbreathing Mach number, capture area, inlet height, and rocket primary mass flow rate. Ramjet and scramjet performance had been previously generated for a 5° cone half angle winged-cone concept by researchers at NASA - Langley and was taken from reference 39. This data exists as cowl-to-tail engine thrust coefficients and I_{sp} as a function of Mach number and fuel equivalence ratio (the normalized ratio of fuel flow rate to captured air flow rate with 1 being stoichiometric). Cowl-to-tail engine thrust was determined from C_t using the equation $T = C_t q A_c$ where A_c is the physical annular area between the outer engine cowl and the vehicle body. The engine data was originally generated for a reference A_c of 207 sqft. The reference engine area was scaled up or down for each point design. In order to account for the LH2 that is necessary to cool the engine at higher Mach numbers, a minimum cooling schedule for equivalence ratio was established. Equivalence ratio was required to be at least .5 at Mach 8, 1 at Mach 12, and 2.5 at Mach 18 with linear variation between design points.

The ascent trajectory was optimized using POST 3D [41]. POST is widely used in aerospace industry to perform numerical optimization of trajectories. Engine throttle settings and vehicle pitch angles were varied in order to minimize the mass ratio (MR) of the vehicle. The point designs were each flown to a 100 Nmi circular polar orbit (a NASP reference mission) from a fictitious launch site at Vandenberg Air Force Base in California. The reference payload was 10,000 lbs. The OMS propulsion system was designed to circularize the ascent orbit, perform a delta velocity maneuver of 50 fps on-orbit, and deorbit the vehicle. POST was slightly modified to allow the vehicle to fly a constant dynamic pressure boundary and later a constant stagnation point heating rate during ascent.

Vehicle take-off was either vertical or horizontal as determined by a design variable. Horizontal take-off versions (HTO) accelerated to 250 knots before lifting off. The vehicle operated in ejector (rocket primary on) until

Mach 3, then switched to ramjet and later scramjet mode. During this phase, the vehicle was constrained to fly a constant dynamic pressure boundary determined by the optimization process. Angles of attack, α, during this portion of the trajectory generally were between 2° and 5°. The stagnation heating rate to a reference one foot radius sphere (Chapman's equation heating) was monitored during the ramjet and scramjet portions of the trajectory. If the heating rate reached a prescribed value, again as set by a design variable, the vehicle left the constant dynamic pressure boundary and flew along the constant stagnation point heat rate boundary until the scramjet to rocket mode transition Mach number was reached. During ascent, the vehicle was limited to 3g sensed acceleration by throttling the engines.

After the ascent trajectory was determined, windward and leeward centerline heating was determined using Miniver [42]. Miniver uses simplified geometry representations and a choice of several accepted heating rate calculation methods to determine the aerodynamic heating to various sample points on the vehicle. TPS concepts for each vehicle were selected based on radiation equilibrium temperatures at different points along the cone, cowl, and wing. Active LH2 cooling was required on the nosecap, the wing leading edges, the cowl leading edges, the engine, and part of the engine nozzle. Advanced carbon-carbon TPS was used for areas reaching temperatures between 1800°F and 2800°F. Inconel superalloy constructed into standoff, mechanically attached panels was used for areas between 1200°F and 1800°F. Titanium standoff panels were used for areas below 1200°F. In areas where appropriate (such as the wings and upper cowl surface), the titanium-aluminide structure was allowed to get as hot as 1500° F without a protective TPS covering.

A complex, inter-related series of mass estimating relationships (MER's) was established for the current vehicle based on existing, historical data regression MER's obtained from the Vehicle Analysis Branch at NASA - Langley. The MER's used for this work are listed in Appendix A and Appendix B. Some equation constants were modified to reflect mass

reductions from expected technology and materials advancements. Structural sizing constants on a per area or per volume unit basis for tank weights, smeared primary and secondary structure, and each of the TPS concepts were updated to reflect the anticipated IOC for this vehicle of 2005 - 2010. In many cases, NASP-derived technology improvements were assumed to be available. For example, the primary vehicle structure was baselined to be an advanced NASP titanium- aluminide alloy - Beta 21S. The constants for the filament wound LH2 tank were established specifically for this vehicle through a finite element structural analysis including appropriate non-optimum factors. Subsystem MER's (avionics, ECLSS, etc.) were determined based on previous NASA - Langley VAB work on SSTO winged-cone concepts and expected NASP-derived improvements.

For each point design in the experimental array, a series of iterations was made through each of the analysis codes as shown in figure 20. Once the systems level design parameters were established, an initial gross weight and geometry was assumed in order to start the design cycle. The analysis then proceeded from one analysis code to the next with data being exchanged between each code. This process simulates the way a typical engineering design team functions. Each engineer in a team functions in the role of disciplinary expert. The disciplinary expert performs the required analysis in his or her field and then passes the results on to the next disciplinary expert.

Each cycle through the design codes took four to eight hours. A typical point design converged after about three iterations. A design was considered to be converged when the mass ratio (MR) from one POST run to the next changed by less than about 3%. As will be seen, however, some designs did not converge at all. For the designs that converged, the dry weight was recorded. Dry weight (i.e. no propellant, payload, or crew) was selected as the objective function because it is generally a better indicator of cost than gross weight.

Initial Screening Analysis (L_{27} Array)

Based on previous work on a conical RBCC SSTO by the Astronautics Corp. [36], eight key variables were selected for this study and are listed in table 15 along with the potential effects that each variable might be expected to have on the vehicle design. Figure 6 illustrates the location of both the cone half angle, Θ, and the cowl wrap around angle, Φ.

Table 15 - L_{27} Design Variables

Parameter	Potential trades
scramjet to rocket mode transition Mach number (M_{tr})	lower LOX propellant weight vs. smaller hydrogen tanks
max q of ascent (for a constant q boundary trajectory)	increased thrust-to-drag ratio vs. higher heating and aero. loads
engine cowl wrap around angle (Φ)	increased thrust-to-drag ratio vs. additional engine weight
Forebody cone half angle (Θ)	higher drag vs. improved propellant tank structural efficiency (volume/area)
Vehicle lift-off thrust-to- weight ratio (T/Wo)	lower gravity losses and LOX weight vs. increased engine weight
stagnation point heating limit boundary (heat rate) (referenced to 1' sphere)	improved high Mach number airbreathing performance vs. higher TPS weight
supercharged engine (Y/N)? (engine 12 or 10 from Marquardt work)	improved low speed RBCC performance vs. additional engine weight
take-off mode (vertical vs. horizontal)	higher engine weight vs. higher wing and gear weight

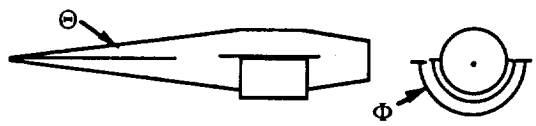

Figure 22 - Cone Half Angle and Cowl Wrap Angle

Of the eight design variables, two variables are discrete. Two take-off options, vertical or horizontal, were considered (the vehicle landed unpowered, horizontally in both cases), and the RBCC engine was treated with and without an optional supercharging fan. In previous work on a series of preliminary RBCC engine designs at the Marquardt Corp. [32], the non-supercharged engine was referred to as engine concept number 10. The supercharged engine concept was referred to as engine concept number 12. The same nomenclature was used to distinguish between the two options in this study as well. The other six variables are continuous, but have been discretized to three levels (or values) as required by the Taguchi method. A range for each of the design variables was established based on previous work and engineering experience. Refer to table 16 for the selected levels chosen for each variable.

Based on the number of variables being considered and the desired number of two variable interactions (three), a three-level orthogonal array of 27 point designs was selected using the Taguchi method. The L_{27} orthogonal array shown in table 17 outlines the runs performed and the levels for each of the eight design variables for each of the 27 required point designs. Note that the Taguchi array is a fractional array - that is, not every combination of all of the variables is required to be run. For comparison, a full factorial experimental array including every combination would take $3^6 x 2^2$ or 2916 runs.

Table 16 - Design Parameter Levels

Parameter	L	M	H
rocket trans. Mtr	12	15	18
max. q (psf)	1000	1500	2000
cowl angle (Φ)	180°	270°	360°
cone angle (Θ)	5°	6.5°	8°
T/Wo (VTO) (HTO)	1.2 0.6	1.3 0.7	1.4 0.8
heat rate limit (BTU/sqft-sec)	250	300	350
supercharger?	10 (N)		12 (Y)
take-off mode	HTO		VTO

The standard L_{27} Taguchi array was modified in two ways for this analysis. First, the two discrete variables are combined into a single three-level column of the array without loss of information about either variable. This technique is known as the *compound factor method* [16], and it is made possible by the fact that these two variables each have only two settings rather than three. Second, a technique known as *branching* [16] is used to establish two ranges for vehicle thrust-to-weight ratio depending on whether the design is horizontal or vertical take off. T/Wo ratios of 1.2, 1.3, and 1.4 are associated with VTO designs. T/Wo ratios of 0.6, 0.7, and 0.8 are associated with HTO designs.

The resulting dry weights for each of the 27 point designs are shown in the last column of table 17. Several designs (nine) represented points that were not feasible. That is, for reasons of low capture area, low dynamic pressure, or high cone angle, these designs exhibited an unacceptably low thrust-to-drag ratio. These infeasible points or "no-closure" cases were assigned a maximum dry weight value of 300,000 lbs. This somewhat arbitrary limit was set higher

than any converged case values in order to properly penalize the poor designs, but it was found that if it was set too high, it would completely "wash out" the real data. The value chosen seemed to represent a reasonable medium. However, as will be shown, the "no-closure" runs still have a negative impact on the analysis.

Table 17 - L_{27} Taguchi Array

Run	M_{tr}	Max. q bndry.	Φ	θ	Lift-off T/Wo	Max. stag. heat rate	Engine # & T.O. mode	**Dry Weight (lbs)**
1	12	1000 psf	180°	5.0°	0.8	250 BTU/ft2-s	10 & HTO	300,000
2	12	1000 psf	270°	6.5°	1.3	300 BTU/ft2-s	10 & VTO	114,220
3	12	1000 psf	360°	8.0°	1.4	350 BTU/ft2-s	12 & VTO	193,510
4	12	1500 psf	180°	6.5°	1.3	350 BTU/ft2-s	12 & VTO	109,320
5	12	1500 psf	270°	8.0°	0.6	250 BTU/ft2-s	10 & HTO	150,690
6	12	1500 psf	360°	5.0°	1.2	300 BTU/ft2-s	10 & VTO	118,330
7	12	2000 psf	180°	8.0°	1.4	300 BTU/ft2-s	10 & VTO	113,180
8	12	2000 psf	270°	5.0°	1.2	350 BTU/ft2-s	12 & VTO	124,110
9	12	2000 psf	360°	6.5°	0.7	250 BTU/ft2-s	10 & HTO	136,520
10	15	1000 psf	180°	6.5°	1.4	300 BTU/ft2-s	12 & VTO	300,000
11	15	1000 psf	270°	8.0°	0.8	350 BTU/ft2-s	10 & HTO	300,000
12	15	1000 psf	360°	5.0°	1.3	250 BTU/ft2-s	10 & VTO	124,720
13	15	1500 psf	180°	8.0°	1.2	250 BTU/ft2-s	10 & VTO	300,000
14	15	1500 psf	270°	5.0°	1.3	300 BTU/ft2-s	12 & VTO	122,520
15	15	1500 psf	360°	6.5°	0.6	350 BTU/ft2-s	10 & HTO	135,450

Table 17 (continued)

Run	M_{tr}	Max. q bndry.	Φ	θ	Lift-off T/Wo	Max. stag. heat rate	Engine # & T.O. mode	**Dry Weight (lbs)**
16	15	2000 psf	180°	5.0°	0.7	350 BTU/ft2-s	10 & HTO	124,040
17	15	2000 psf	270°	6.5°	1.4	250 BTU/ft2-s	10 & VTO	98,350
18	15	2000 psf	360°	8.0°	1.2	300 BTU/ft2-s	12 & VTO	155,590
19	18	1000 psf	180°	8.0°	1.3	350 BTU/ft2-s	10 & VTO	300,000
20	18	1000 psf	270°	5.0°	1.4	250 BTU/ft2-s	12 & VTO	208,860
21	18	1000 psf	360°	6.5°	0.8	300 BTU/ft2-s	10 & HTO	272,810
22	18	1500 psf	180°	5.0°	0.6	300 BTU/ft2-s	10 & HTO	300,000
23	18	1500 psf	270°	6.5°	1.2	350 BTU/ft2-s	10 & VTO	132,970
24	18	1500 psf	360°	8.0°	1.3	250 BTU/ft2-s	12 & VTO	300,000
25	18	2000 psf	180°	6.5°	1.2	250 BTU/ft2-s	12 & VTO	300,000
26	18	2000 psf	270°	8.0°	0.7	300 BTU/ft2-s	10 & HTO	300,000
27	18	2000 psf	360°	5.0°	1.4	350 BTU/ft2-s	10 & VTO	113,200

The "no-closure" cases have a very significant impact on the analysis of the mean process. The method relies on determining differences between average vehicle weights at different points in the design space. Since there is no difference between the dry weight for two designs that did not close, all of the variable effect information pertaining to the differences between the two runs is lost, even for the variables that did not contribute significantly to the problem. It could be argued that the analysis process might work better without these runs, but the orthogonality of a "true" Taguchi analysis would be lost. The method's inability to handle infeasible points is a serious weakness.

The no-closure cases are indicative of the complex interactions going on between the variables. In particular, every case of a cowl wrap angle (Φ) of 180° and a max dynamic pressure boundary of 1000 psf did not close. However, taken at other dynamic pressure limits, 180° cowl wraps do close. Additionally, every case of M_{tr} 18 scramjet to rocket mode transition and 180° cowl wrap angle did not close. The relationship between q, Φ, and M_{tr} suggests a three variable interaction. The Taguchi method is only capable of handling two variable interactions. In fact, three variable interactions tend to confound the method results. For the L_{27} array that was used in this experiment, a three variable interaction between M_{tr}, q, and Φ would tend to confound the results of the T/Wo and maximum stagnation point heat rate mean responses.

The sensitivities are calculated for each design variable by individually averaging the vehicle weights at each of its three levels - L, M, and H. Since the array is balanced, one-third of the runs corresponds to each of the three levels. The results of the analysis of the mean technique for dry weight are shown in the mean response tables 18, 19 , and 20 and graphically in figure 23. The selected levels to minimize dry weight have been circled in the tables. Judgment has been temporarily reserved on cowl angle and M_{tr} because of the possible interaction between them. However, the **H** setting for dynamic pressure (2000 psf), the **L** setting for cone half angle (5°), and the **H** setting for maximum stagnation heat rate (350 BTU/sqft-sec) seem fairly clear and are supported by engineering experience. High dynamic pressures produce higher accelerations and lower angles of attack (and therefore lower drag losses). The 5° half angle cone generates a relatively low drag and thus has a high thrust-to-drag ratio. Its low shock angle produces relatively few heating problems even at 2000 psf dynamic pressures. The maximum stagnation point heating value of 350 BTU/sqft-sec also makes engineering sense. The thrust penalty due to lost dynamic pressure incurred by leaving the q boundary and flying a heat rate boundary is significant in terms of lost acceleration capability.

Table 18 - Mean Responses for L_{27} Array

	Mtr	Max. q	Cowl Ang.	Cone Ang.	Max. Heat
L	151,098	234,902	238,504	170,642	213,238
M	184,519	185,476	172,413	177,738	199,628
H	247,538	162,777	172,237	234,774	170,289

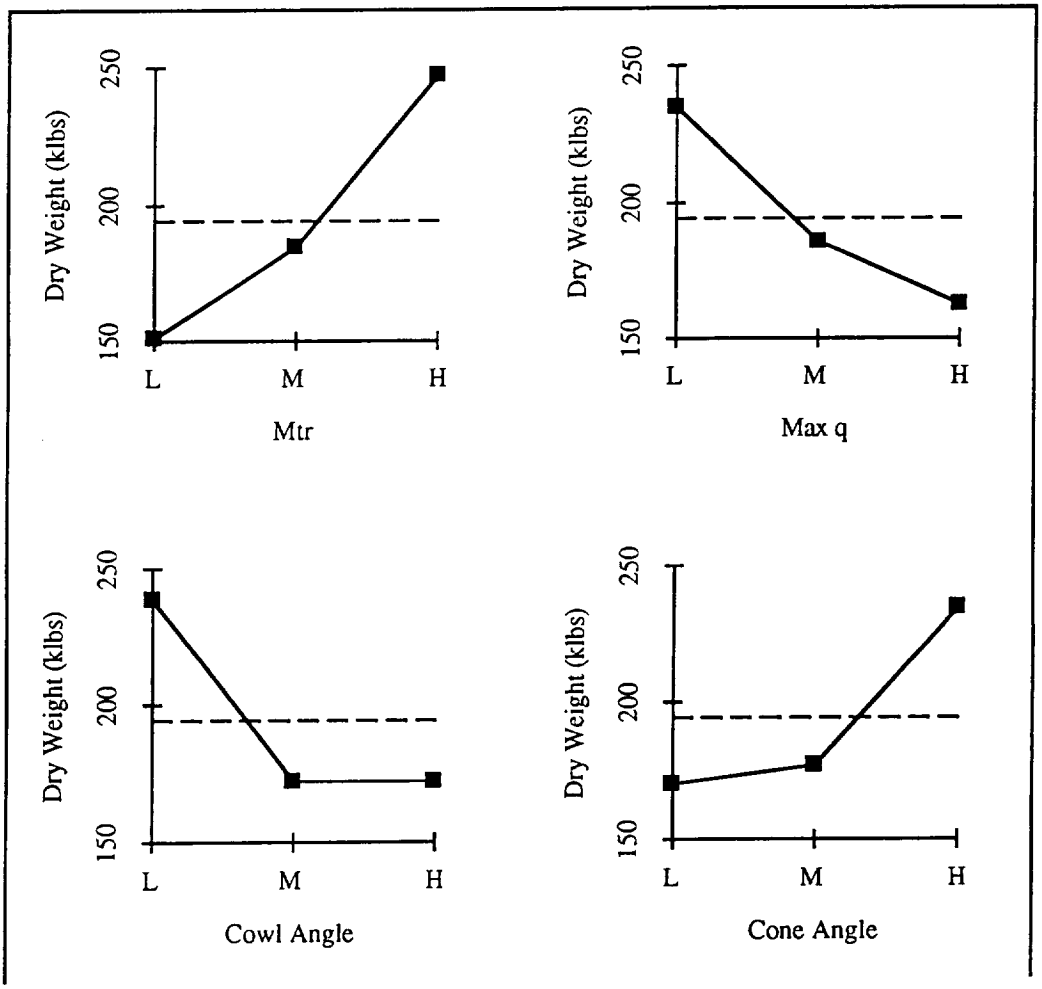

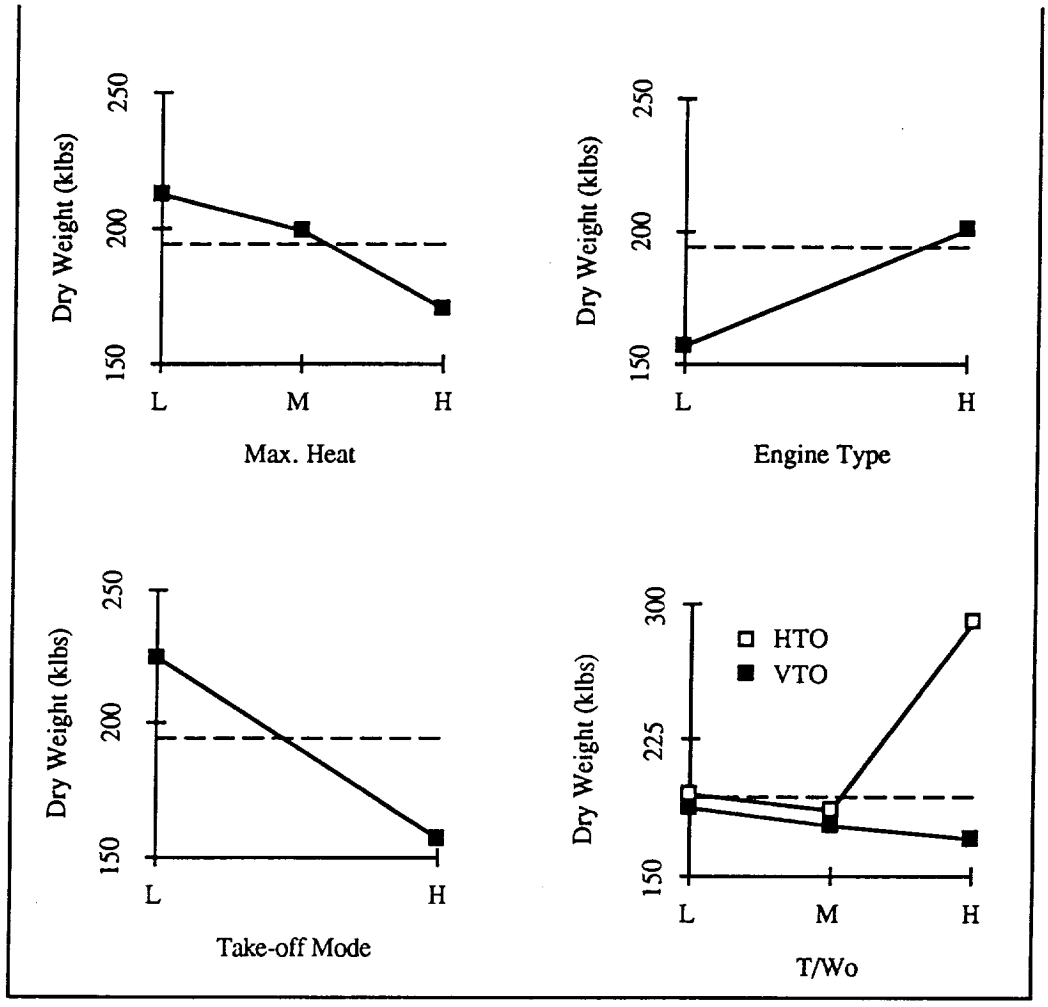

Figure 23 - Graphical Results of L_{27} Array

Table 19 - Engine Type and Take-off Mode Responses

	Engine #	T.O. Mode
L	157,219	224,390
H	201,546	157,219

Table 20 - T/Wo by Take-off Mode Responses

	T/Wo (VTO)	T/Wo (HTO)
L	188,500	195,380
M	178,463	186,853
H	171,183	290,937

The non-supercharged engine (**L**) produces a lower dry weight vehicle compared to the super-charged engine (table 19). However, before a final decision is made regarding supercharging, the operational advantages of a supercharged engine during landing, self ferry operations, subsonic loiter, etc. must be carefully weighed. This research only considered the impact of supercharging on ascent performance. For ascent, the small increase in engine I_{sp} is not worth the extra weight of the fan system. Table 19 also shows the advantage of vertical take-off (**H**) over horizontal take-off. Since the RBCC essentially behaves like a rocket at lift-off, it is easier and lighter to add additional engine thrust than it is to add wing size and landing gear weight.

Table 20 shows the results for the take-off thrust-to-weight ratio variable. Recall that the ranges for T/Wo depended on whether the vehicle was HTO or VTO. For vertical take-off, a T/Wo of **H** (1.4) produces the lowest dry weight. Engineering judgment suggests that this value may be somewhat high. As mentioned above, a three way interaction between M_{tr}, q, and Φ would tend to disrupt the results of this variable. Since the variable is considered to be one of the least critical (based on the relatively small difference in dry weight between its highest and lowest settings) it was left at the **H** setting. Additional work is recommended for this variable.

The L_{27} Taguchi array is capable of determining the interactions between three sets of two variable interactions. These interactions were

preplanned to be M_{tr} x q, M_{tr} x Φ, and q x Φ based on the placement of the variables within the L_{27} array and the L_{27} linear graph. The results are shown in tables 21-23. Interesting, but contradictory combinations have been circled.

Table 21 - M_{tr} x q Interaction

	1000 psf	**1500 psf**	**2000 psf**
12	202,577	126,113	124,603
15	241,573	185,990	125,993
18	260,557	244,323	237,733

Table 22 - M_{tr} x Cowl Angle Interaction

	180°	**270°**	**360°**
12	174,167	129,673	149,453
15	241,347	173,623	138,587
18	300,000	213,943	228,670

Table 23 - q x Cowl Angle Interaction

	1000 psf	**1500 psf**	**2000 psf**
180°	300,000	236,440	179,073
270°	207,693	135,393	174,153
360°	197,013	184,593	135,103

Unlike main effect response tables that average a particular variable effect over all of the simultaneous changes of the other variables, a two variable interaction can discern the effects of changing one variable while holding a second variable at each of its three levels. An interaction is usually

said to be strong if the graphical mean plots cross (i.e. figure 24, Mtr x Φ and q x Φ). Given such a strong interaction, the variable settings should be determined from the interaction plots rather than the mean responses for each variable. However, tables 21-23 show mixed results. In table 21 at 2000 psf q, M_{tr} of 12 and 15 appear to be very close together and show the lowest dry weights. In table 22, a Φ of 270° and a M_{tr} of 12 seem to produce the best combination. Also in table 22, M_{tr} of 15 doesn't seem to be as close to 12 as indicated in the previous table - the best M_{tr} 15 answer being found for a Φ of 360°. Finally, table 23 indicates that either Φ of 270° or 360° would be good choices, but for different dynamic pressure limits.

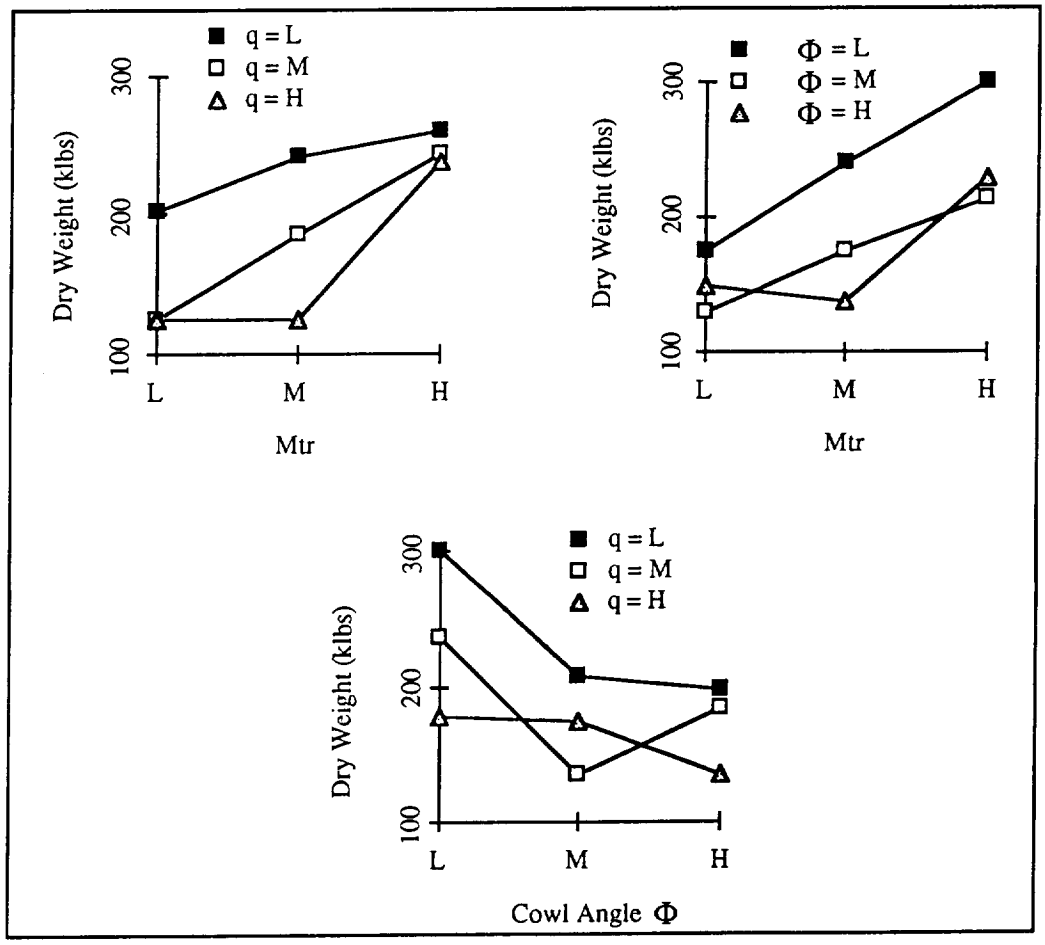

Figure 24 - Graphical Interaction Results for L_{27} Array

Confusing two-variable interaction information, coupled with the fact that a three way interaction between M_{tr}, q, and Φ is suspected, led to the performance of an additional set of runs outside of those required by the Taguchi method. The final set of runs to determine the best combination of Φ and M_{tr} (as shown in table 24) was performed by **fixing 6 of the 8 variables** of the study to values that the L_{27} analysis indicated to be their best settings. Max. q was set to 2000 psf, Θ was set to 5°, max. heat rate was set to 350 BTU/sqft-sec, the non-supercharged engine was used (#10), and the vehicle was VTO with an initial T/Wo of 1.4. With these variables held constant, a sweep of all nine combinations of Φ and M_{tr} was performed. The results show that a Φ of 180° and a M_{tr} of 15 results in the lowest dry weight. These results were somewhat unexpected, because Φ of 180° was not indicated by any of the main effect tables or the two variable interaction tables of the Taguchi method. The fact that Taguchi "missed" this result is probably a result of the high number of "no-closure" designs and the suspected three way interaction discussed above. It is interesting to note that the dry weight is relatively flat between M_{tr} of 12 and M_{tr} of 15. In light of operational and technical complexities due to higher Mach numbers, a designer might choose to select the M_{tr} 12 case for only a slight penalty in dry weight.

Table 24 - Dry Weight Extra Runs Results

	180°	270°	360°
12	85,210	99,470	116,930
15	84,090	93,460	105,960
18	100,110	102,880	113,200

In summary, a set of parameter levels was found that produces a very attractive dry weight for the conical RBCC SSTO. Table 25 lists the final

parameter levels that were chosen and table 26 lists some of the characteristics of the final vehicle. A more complete report of the final vehicle characteristics is included in Appendix C. Figure 25 lists some RBCC SSTO vehicle characteristics and those of the current U.S. Space Shuttle. The two vehicles are not directly comparable in terms of mission, payload, and technology. The information in figure 25 is included only for reference purposes.

Table 25 - Selected Parameter Levels

M_{tr}	15
max. q	2000 psf
cowl wrap angle (Φ)	180°
cone half angle (Θ)	5°
T/W_o	1.4
max. heat rate	350 BTU/sqft-sec
supercharged engine?	N (engine #10)
take-off mode	VTO

The Taguchi method was largely a success at determining the best levels for each of the parameters in order to determine the minimum vehicle dry weight. Six of the eight design variables were determined based on the results of the initial L_{27} Taguchi matrix. However, the method failed to capture the correct settings for cowl wrap angle, Φ, and M_{tr} (as determined by a full sweep of those variables) even though interaction information was also available for those variables. As noted in the analysis discussion, the fact that many of the point designs did not produce feasible "closed" designs most likely contributed to the Taguchi method's inability to correctly select the proper levels for Φ and M_{tr}. When designs did not close, the information used to compare variables between them was lost. This inability to deal with

infeasible points in the experimental array is a serious weakness of the method. An appropriate reaction to an infeasible point would be for the designer to redefine the variable ranges (i.e. limit the worst combinations of variables) and start over. However, since the designer is most likely unfamiliar with the design space, this could lead to time consuming restart situations. In addition, redefining and reducing variable ranges may eliminate some attractive regions of the design space.

It is also very likely that a three variable interaction was present between cowl wrap angle, q, and M_{tr}. Taguchi methods cannot handle three way interactions. However, it should be noted that if the suspected three way interaction is present, it could be confounding the results of the T/Wo. Follow-on research should attempt to verify the current selection for T/Wo and try to gain additional information about cowl wrap angle (Φ) and M_{tr}. Additionally, follow-on research should attempt to discover the most robust RBCC SSTO design. A robust vehicle design is one that is relatively insensitive to uncontrollable influences like weight growth and engine performance degradation. The ability to determine a robust design is a powerful, but often overlooked, capability of Taguchi methods.

The final results produced by this application of the Taguchi method can only be considered a "near optimum" because of the Taguchi method's inability to interpolate between variable levels. That is, Taguchi methods only determine the best combination of all of the possible combinations of the levels of the design variables (in this case, the best combination of 2916 alternatives). In some cases, this "near optimum" may be sufficient for a conceptual vehicle design. However, the results of this work could be used as a "front-end" for a more detailed optimization process if necessary. The more detailed process could either be another parametric study with refined variables and ranges or a gradient-based optimization (since all of the discrete variables have been satisfactorily determined by the current work).

Table 26 - Selected Vehicle Characteristics

Characteristic	Value
GLOW	416,000 lbs
dry weight	84,090
mass ratio	3.934 (ξ=.746)
LH2 prop wt./total prop	.354
payload to polar 100 Nm	10,000 lbs
payload to 28.5° 100 Nm	20,100 lbs
vehicle length	188.5 ft
max. body diameter	29.3 ft (w/ cowl)
wingspan	48.4 ft

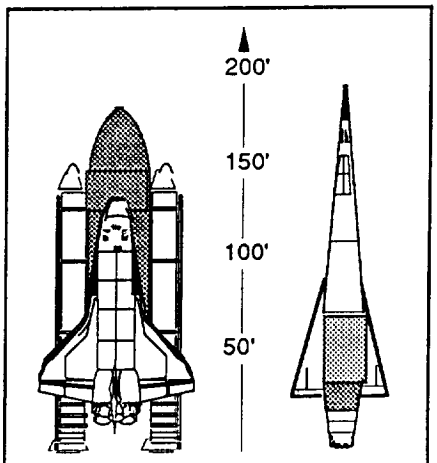

Crew	7 crew, 14 days	2 crew, 3 days
GLOW	4.5 Mlbs	420 Klbs
Landed Wt.	220 Klbs	100 Klbs
Payload (100 nm, 28.5°)	~45 Klbs	20 Klbs
	partially reusable	fully reusable

Figure 25 - Comparison of L_{27} Vehicle to STS

Second Design Analysis (L_8 by L_4 Arrays)

Based on the results of the initial L_{27} Taguchi study of eight design variables, three variables were selected for further study. They are the cowl wrap around angle (Φ), the airbreathing to rocket transition Mach number (M_{tr}), and the overall vehicle liftoff thrust-to-weight ratio (T/W_o). The other six variables investigated in the initial array were considered to be satisfactorily determined. For the current work, the dynamic pressure limit was set to 2000 psf, the cone half angle (Θ) was set to 5°, the maximum stagnation point heating rate was set to 350 BTU/ft^2-s, the engine was not supercharged (engine 10), and the vehicle took off vertically.

In order to study the three main variables and all three of their two-variable interactions, an L_8 two-level orthogonal array was selected. The L_8 orthogonal array was shown previously in table 10, and the linear graph showing the placement of the interaction columns was shown in figure 10. Note that the seventh column of the L_8 array was not used for this study because it is confounded with the three variable interaction between M_{tr}, Φ, and T/W_o. This was an attempt to avoid any three variable interaction problems like those encountered in the L_{27} array. The discretized levels for the three design variables are shown in table 27.

Table 27 - Variables and Levels for L_8 Array

Variable	L	H
T/W_o	1.2	1.4
M_{tr}	12	15
Cowl Angle (Φ)	180°	360°

In table 27, the variables T/Wo, Mtr, and Φ correspond to the A, B, and C variables in table 10, respectively. The column assignments and interaction columns are similar.

Because the variables are all two-level, an additive model of the following form can be estimated.

$$\text{Dry Weight} = \beta_0 + \beta_1 * \left(\frac{T}{W_0}\right) + \beta_2 * (M_{tr}) + \beta_3 * (\Phi) + \beta_4 * \left(\frac{T}{W_0}\right) * (M_{tr}) + \beta_5 * \left(\frac{T}{W_0}\right) * (\Phi) + \beta_6 * (M_{tr}) * (\Phi) \quad (46)$$

It is also a goal of this research to determine the settings of the three design variables that will produce the most robust vehicle design. Robustness is defined as insensitivity to different types of uncontrollable influence on the design. If a designer suspects that there may be an adverse change in the design conditions, then he or she could plan the original design to be able to accommodate the changes. In this case, there are three uncontrollable variables that may have an adverse effect on the vehicle – off nominal I_{sp} in the airbreathing cycles of the ascent, unexpected weight growth in the airbreathing components of the engine, and unexpected weight growth in the body structure and TPS weight.

The I_{sp} of the airbreathing components of the engine is very dependent on technological advances over the next 10-15 years. An I_{sp} schedule vs. Mach number and fuel equivalence ratio has been baselined in reference 39. However, given the likelihood of a reduction in Isp, the vehicle should be designed to be as insensitive as possible to changes in I_{sp}. Similarly, the baselined weights of the airbreathing components of the engine (as shown in Appendix B and derived from ref. 32) are likely to increase thereby reducing the uninstalled thrust-to-weight ratio of the engine. The airbreathing components of the engine are the inlet, the mixer/diffuser, the combustor, the fuel injectors, and the internal parts of the nozzle. The "smeared" fuselage

weight (including nosecap, crew cabin, tank structure, tank insulation, non-inlet sections of the cowl, tailcone, base area, and active and passive thermal protection systems) was also considered a potential growth variable. These three growth variables (often called *noise variables*) were each discretized to two levels as shown in table 28, and given the designations N_{isp}, N_{eng}, and N_{fuse} respectively. Note that the -20% setting of N_{isp} refers to a 20% degradation or **reduction** in airbreathing I_{sp}.

Table 28 - L_4 Outer Array Variable Levels

Variable	L	H
Airbreathing I_{sp} Change (N_{isp})*	-20%	0%
Airbreathing Engine Weight Growth (N_{eng})	0%	20%
Fuselage Smeared Weight Increase (N_{fuse})	0%	20%

* the 20% reduction in airbreathing I_{sp} actually follows the following linear schedule by Mach number: -15% for M=3, -6% for M=5, -20% for M>8. This is because ramjet I_{sp}'s were considered to be more predictable than scramjet I_{sp}'s.

Interactions between noise variables are typically ignored, so the three noise variables can be placed in the three columns of an L_4 orthogonal array. Here, the L_4 array is referred to as the "outer" array, and the array containing the main variables is called the "inner" array (i.e. the L_8 array). Each of the experiments in the L_8 array is then performed for each combination of noises in the L_4 array. The 32 resulting dry weights (measured in lbs.) are shown in table 29. The inner array is shown on the left, and the outer array is on the top. The actual design variable values are shown, not the normalized -1 and +1 levels.

The signal-to-noise ratio (S/N) is calculated in the last column of table 10 for each row. Taguchi documented several formulas for calculating signal-to-noise ratio. In this case, the dry weight is to be minimized, so the appropriate S/N is the "lowest is the best" [16].

$$S/N = -10*\log_{10} \left(\frac{1}{4}\sum_{i=1}^{4} y_i^2\right) \qquad (47)$$

where,

y_i = dry weight for each column in the row

Table 29 - Dry Weight and S/N Results for L_8 x L_4 Arrays

			0%	0%	-20%	-20%	N_{isp}
			0%	20%	0%	20%	N_{eng}
T/W_o	M_{tr}	Φ	0%	20%	20%	0%	N_{fuse} S/N
1.2	12	180°	92,498	118,623	119,865	109,261	-100.875
1.2	12	360°	125,091	161,283	154,076	151,943	-103.448
1.2	15	180°	92,121	123,229	131,979	117,139	-101.368
1.2	15	360°	118,731	162,323	166,299	165,534	-103.780
1.4	12	180°	92,871	120,909	122,145	110,463	-101.001
1.4	12	360°	124,903	161,361	153,085	151,701	-103.428
1.4	15	180°	91,685	124,938	135,532	118,943	-101.502
1.4	15	360°	118,690	161,095	164,714	163,823	-103.711

For the analyses that generated the dry weights in table 29, the mass estimating relationships (MER's) were slightly modified from those used in the L_{27} study. A separate 10% weight growth margin on the engines was eliminated (a 10% margin still exists on all dry weights at the vehicle level),

the engine side walls were modified to run the entire length of the inlet, and the payload bay volume was increased to 5300 ft^3 in order to accommodate larger sized payloads. Unfortunately, the exact dry weights are not directly comparable to those from the L_{27} set of experiments, but the differences are small (the current weight results are about 9% higher). The design variable trends and conclusions are expected to be similar, however. The MER's listed in Appendices A and B are the updated equations used in the current analysis.

L_8-Only Analysis

One of the goals of this phase of the research was to determine the β coefficients in equation 46. All but the first column of dry weights in table 29 can be temporarily ignored because the noise variables are set to their baseline values in column 1. Because the L_8 array is orthogonal, the simple analysis of the mean technique can be used to determine the coefficients. The averages of each variable and each interaction are listed in table 30. The "levels" of an interaction are determined from the -1 and +1 values for their assigned column in the L_8 array (see table 10). The mean responses are depicted graphically in figure 26. The overall mean of the 8 responses (β_0) is 107,074 lbs.

Table 30 - L_8 Mean Response Table

	T/W_0	M_{tr}	Φ	$T/W_0 \times M_{tr}$	$T/W_0 \times \Phi$	$M_{tr} \times \Phi$
L	107,110	108,841	92,294	107,157	107,095	108,450
H	107,037	105,307	121,854	106,991	107,053	105,698
β_i's	-37	-1,767	14,780	-83	-21	-1,376

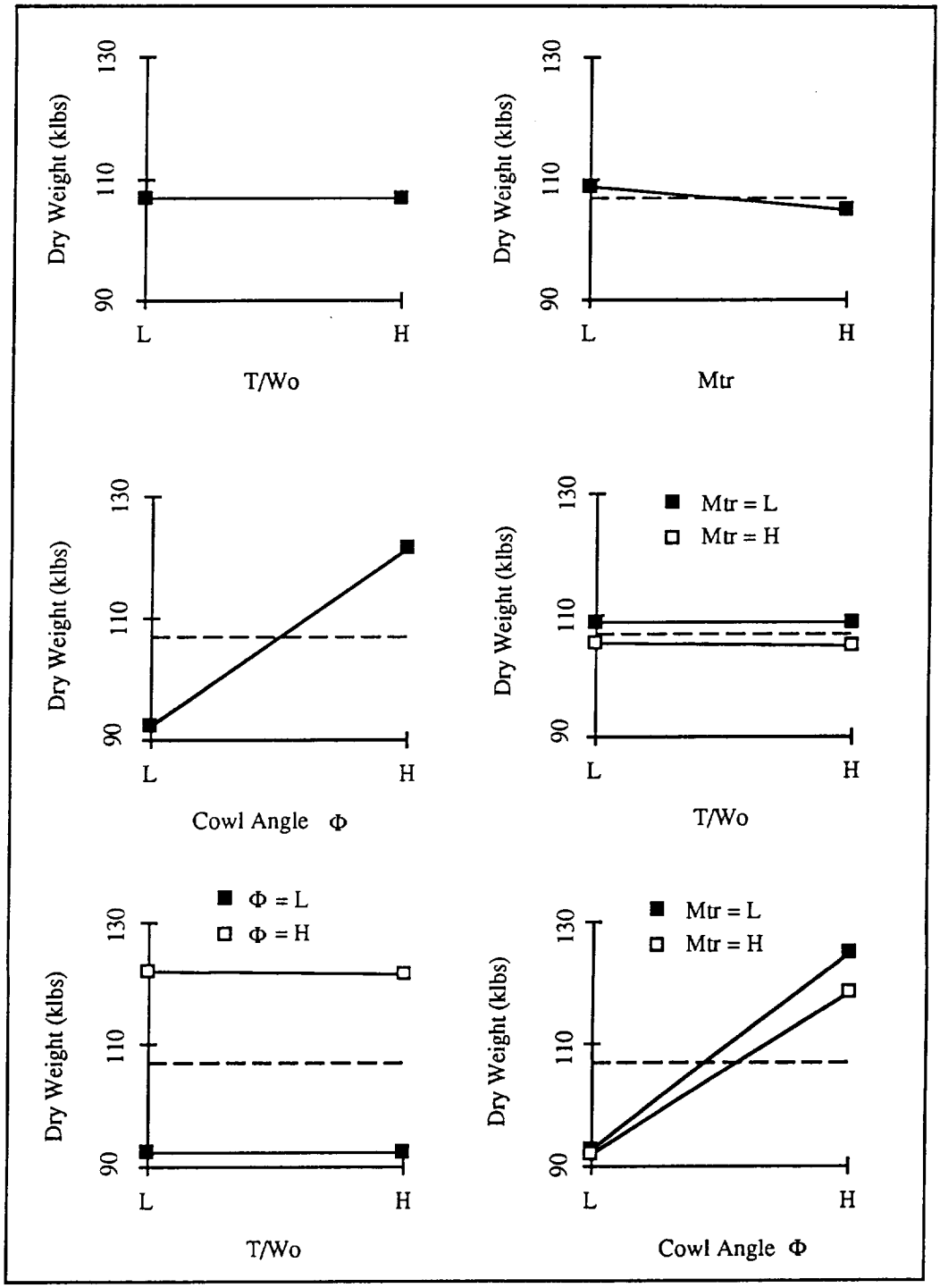

Figure 26 - L_8 Mean Responses and Interactions

The β coefficients in table 30 for the normalized variables are calculated by taking one-half of the difference between the average responses at the high and low values of each term in the equation. For example, β_1 is associated with T/W_0.

$$\beta_1 = \frac{1}{2}\left(\frac{(y_5 + y_6 + y_7 + y_8)}{2} - \frac{(y_1 + y_2 + y_3 + y_4)}{2}\right) = \frac{1}{2}(\overline{H} - \overline{L}) \\ = \frac{1}{2}(107{,}037 - 107{,}110) = -37 \tag{48}$$

The other β coefficients are determined from a similar process. The additive model (in terms of **normalized** design variables) is shown in equation 49. Note that a design matrix equation could have been formed to solve for $\overline{\beta}$, but the analysis of the mean process is much simpler.

$$\text{Dry Weight} = 107{,}074 - 37*\left(\frac{\hat{T}}{W_0}\right) - 1{,}767*(\hat{M}_{tr}) + 14{,}780*(\hat{\Phi}) \\ -83*\left(\frac{\hat{T}}{W_0}\right)*(\hat{M}_{tr}) - 21*\left(\frac{\hat{T}}{W_0}\right)*(\hat{\Phi}) - 1{,}376*(\hat{M}_{tr})*(\hat{\Phi}) \tag{49}$$

Based on the magnitude of the β coefficients and the graphically display of the mean effects, the cowl wrap angle, Φ, has the most significant effect on the dry weight as it is varied from 180° to 360°. M_{tr} and the M_{tr} x Φ interaction are also relatively strong effects. The other effects are insignificantly small. Most notably, the vehicle thrust-to-weight ratio has very little effect on the dry weight. This is probably due to the fact that the extra engine weight of a higher T/W_0 vehicle is counteracted by the fact that the vehicle accelerates to ramjet speed faster and therefore requires less on-board oxidizer. It is also interesting to note that if Φ is set to -1 (the strongest effect) then the interaction between M_{tr} and Φ indicates a preferred setting for M_{tr} of -1. However, the main effect for M_{tr} prefers a setting of +1. Since the magnitudes of β_2 and β_6 are roughly equal, the two terms nearly cancel each other out. The result is that the design space is very flat in terms of M_{tr}.

The best combination of settings for the L_8 array is shown in table 31.

Table 31 - L_8 Variable Settings

T/W_o	1.4
M_{tr}	15
Cowl Wrap Angle	180°

These settings are the same as those determined from the additional nine experiments performed after the initial L_{27} array (i.e. tables 24 and 25). However, the experiments performed in the L_8 array provide useful interaction information, and they are free from the influences of "no-closure" runs.

Using the variable settings in table 31, the predicted dry weight from equation 49 is 91,805 lbs. This combination of settings was actually performed during the experiment (row 7, column 1) and resulted in a dry weight of 91,685 lbs. The additive model over predicts the actual value by an extremely acceptable 0.13%.

L_8 by L_4 Robust Design

Taguchi's method for robust design uses the signal-to-noise ratios calculated for each row as shown in table 29. The column containing the S/N's is used in a similar manner as that used in locating a minimum dry weight for the L_8-only analysis described above. However, the objective is always to determine the variable settings that **maximize** the S/N. Since the S/N's are negative, the best one is the one that has the smallest magnitude.

The mean response table for the signal-to-noise ratios are displayed in table 32 and graphically in figure 27. The mean S/N (β_o) is -102.390.

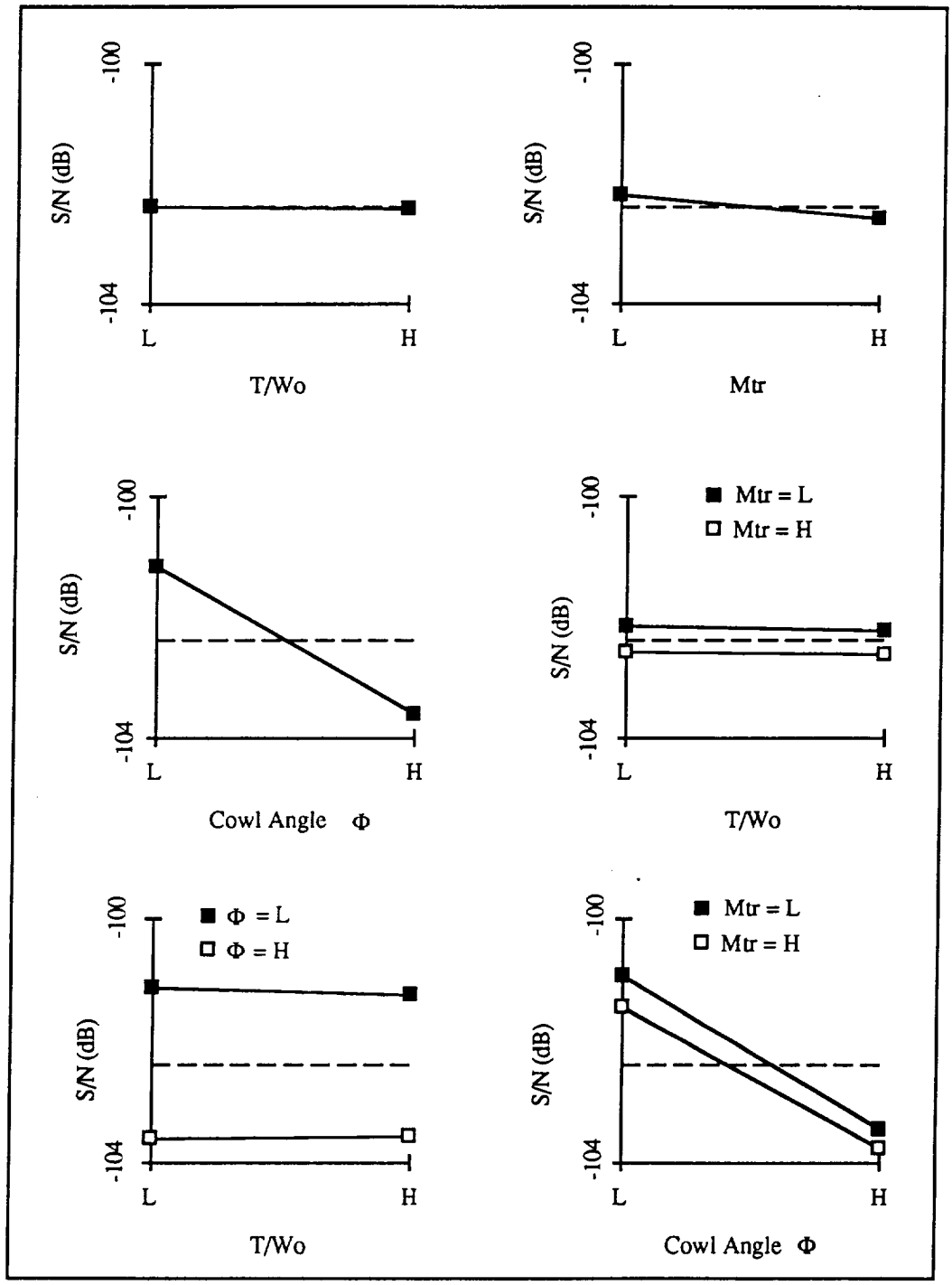

Figure 27 - S/N Mean Responses and Interactions

Table 32 - S/N Mean Responses for Robust Design

	T/W_0	M_{tr}	Φ	$T/W_0 \times M_{tr}$	$T/W_0 \times \Phi$	$M_{tr} \times \Phi$
L	-102.368	-102.188	-101.187	-102.394	-102.433	-102.437
H	-102.411	-102.590	-103.592	-102.384	-102.346	-102.342
β_i's	-0.021	-0.201	-1.203	0.005	0.044	0.047

Using the values of the β coefficients in table 32, the following model for S/N can be formed (for the **normalized** variables):

$$\frac{S}{N} = -102.39 - 0.021 * \left(\frac{\hat{T}}{W_0}\right) - 0.201 * (\hat{M}_{tr}) - 1.203 * (\hat{\Phi})$$
$$+0.005 * \left(\frac{\hat{T}}{W_0}\right) * (\hat{M}_{tr}) + 0.044 * \left(\frac{\hat{T}}{W_0}\right) * (\hat{\Phi}) + 0.047 * (\hat{M}_{tr}) * (\hat{\Phi}) \quad (50)$$

As with the L_8 dry weight minimization in the previous example, the cowl wrap around angle (Φ) has the largest effect on signal-to-noise ratio. A cowl wrap angle of -1 (180°) will help maximize S/N. This is not a surprising result since the S/N combines the effect of the lowest dry weight with insensitivity to the noise variables. Φ has already been shown to have a significant effect on the dry weight. The transition Mach number is the second most significant influence on S/N, but unlike the previous dry weight minimization example, M_{tr} should be set to -1 (M = 12) to maximize vehicle robustness. T/W_0 is still the least significant of the three main variables, but its value has also changed from the previous example. T/W_0 = -1 (1.2) will maximize robustness. The levels that maximize robustness are shown in table 33. The details of the resulting robust vehicle are listed in Appendix D.

Table 33 - Robust Design Variable Settings

T/W_o	1.2
M_{tr}	12
Cowl Wrap Angle	180°

The results of this robust design analysis present some extremely useful and interesting information to the vehicle designer. If the engine weight is expected to grow and the scramjet I_{sp} is expected to be reduced, then the designer should designer a vehicle with a smaller engine (i.e. a smaller T/W_o) and spend less time using airbreathing propulsion. These deductions may seem obvious, but given the highly multidisciplinary, coupled nature of this design, they would have been risky to make prior to such an analysis. Reducing cowl wrap angle to its lowest setting is beneficial both in reducing dry weight and making the vehicle insensitive to the noise variables. The airbreathing engine weight is significant, and while a higher wrap angle provides more thrust, the benefits are quickly outweighed by the extra engine weight. During the analysis process, a design was run at the settings recommended by the robust design results (row 1, column 1) and produced a dry weight of 92,498 lbs. The initial penalty for the selection of the robust design over the minimum dry weight design is small (only about 800 lbs), but the benefits are clearly evident as the noise variables are introduced (scanning across row 1 and row 7 of table 29). The weight growth of row 7 is higher than that associated with row 1 for every column (47% compared to only 30% for the worst column).

As mentioned in the previous section on Taguchi methods, the robust design capability of the method is often overlooked, but may actually be one of it's most useful attributes. The technique provides useful information on the sensitivity of a design to uncontrollable noise variables like weight growth and off-nominal engine performance. It should not be used to replace engineering

judgment, but it provides an excellent resource for making planning decisions. There are some drawbacks. For example, it requires more analysis runs than a simple minimization of the objective function, but the benefits are significant and make it a highly recommended tool for conceptual aerospace vehicle design.

RSM and Central Composite Design Analysis

The 32 experiments performed as part of the L_8 by L_4 robust design provide an excellent set of data for using response surface methods (RSM). Since the variables are all continuous, an approximate mathematical model of dry weight as a function of the main design variables, main variable interactions, noise variables, and the main variable-noise variable interactions can be determined with regression techniques. However, interactions among the noise variables cannot be estimated because the original L_4 noise array (the outer array) was not designed to capture these interactions. In fact, if two-variable interactions exist between the noise variables, they will be confounded with the noise variables themselves.

The 32 dry weights from the L_8 by L_4 robust design experiments can be written as a single experimental array as shown in table 34. The columns in the experimental array are all orthogonal, and, in fact they are columns associated with Taguchi's L_{32} orthogonal array. Specifically T/W_o is L_{32} column 1, M_{tr} is column 2, Φ is column 4, N_{isp} is column 8, N_{eng} is column 16, and N_{fuse} is column 24 (see reference 43 for the complete L_{32} array and associated linear graph). However, the interaction column created from N_{isp} x N_{eng} is the same as N_{fuse} and therefore they cannot both be included in the model. Similar confounding exists for the other two noise variable interactions.

Table 34 - L_8 by L_4 Experiments as a Single Array

Run	T/W_o	M_{tr}	Φ	N_{isp}	N_{eng}	N_{fuse}	Dry Weight
1	-1	-1	-1	1	-1	-1	92,498
2	-1	-1	-1	1	1	1	118,623
3	-1	-1	-1	-1	-1	1	119,865
4	-1	-1	-1	-1	1	-1	109,261
5	-1	-1	1	1	-1	-1	125,091
6	-1	-1	1	1	1	1	161,283
7	-1	-1	1	-1	-1	1	154,076
8	-1	1	1	-1	1	-1	151,943
9	-1	1	-1	1	-1	-1	92,121
10	-1	1	-1	1	1	1	123,229
11	-1	1	-1	-1	-1	1	131,979
12	-1	1	-1	-1	1	-1	117,139
13	-1	1	1	1	-1	-1	118,731
14	-1	1	1	1	1	1	162,323
15	-1	1	1	-1	-1	1	166,299
16	-1	1	1	-1	1	-1	165,534
17	1	-1	-1	1	-1	-1	92,871
18	1	-1	-1	1	1	1	120,909
19	1	-1	-1	-1	-1	1	122,145
20	1	-1	-1	-1	1	-1	110,463
21	1	-1	1	1	-1	-1	124,903
22	1	-1	1	1	1	1	161,361
23	1	-1	1	-1	-1	1	153,085
24	1	1	1	-1	1	-1	151,701
25	1	1	-1	1	-1	-1	91,685
26	1	1	-1	1	1	1	124,938
27	1	1	-1	-1	-1	1	135,532
28	1	1	-1	-1	1	-1	118,943
29	1	1	1	1	-1	-1	118,690
30	1	1	1	1	1	1	161,095
31	1	1	1	-1	-1	1	164,714
32	1	1	1	-1	1	-1	163,823

By examining the linear graph for the L_{32} array, it can be shown that if the N_{fuse} column was changed from column 24 to column 15 in the experimental array, then **all** of the interactions between the variables could be determined. This is a particularly interesting result because it points out a sacrifice that has to be made in order to perform robust design using Taguchi's inner and outer arrays. If a designer had started out with an L_{32} array, he or she could capture **all** of the variable effects and interactions. By having to place the noise variables in a separate L_4 array instead, the designer lost some of the interaction information.

Based on the 32 runs and available interaction columns, the following linear mathematical model for dry weight can be formed in terms of the **normalized** variables.

$$\begin{aligned}\text{Dry Weight} = {} & \beta_0 + \beta_1 * \left(\frac{\hat{T}}{W}\right) + \beta_2 * (\hat{M}_{tr}) + \beta_3 * (\hat{\Phi}) \\ & + \beta_4 * (\hat{N}_{isp}) + \beta_5 * (\hat{N}_{eng}) + \beta_6 * (\hat{N}_{fuse}) \\ & + \beta_7 * \left(\frac{\hat{T}}{W} * \hat{M}_{tr}\right) + \beta_8 * \left(\frac{\hat{T}}{W} * \hat{\Phi}\right) + \beta_9 * \left(\frac{\hat{T}}{W} * \hat{N}_{isp}\right) \\ & + \beta_{10} * \left(\frac{\hat{T}}{W} * \hat{N}_{eng}\right) + \beta_{11} * \left(\frac{\hat{T}}{W} * \hat{N}_{fuse}\right) + \beta_{12} * (\hat{M}_{tr} * \hat{\Phi}) \\ & + \beta_{13} * (\hat{M}_{tr} * \hat{N}_{isp}) + \beta_{14} * (\hat{M}_{tr} * \hat{N}_{eng}) + \beta_{15} * (\hat{M}_{tr} * \hat{N}_{fuse}) \\ & + \beta_{16} * (\hat{\Phi} * \hat{N}_{isp}) + \beta_{17} * (\hat{\Phi} * \hat{N}_{eng}) + \beta_{18} * (\hat{\Phi} * \hat{N}_{fuse})\end{aligned} \tag{51}$$

Equation 51 can be written in matrix form.

$$\bar{y} = [X]\bar{\beta} \tag{52}$$

where,

$\bar{y}$ is the vector of 32 dry weight responses

$\bar{\beta}$ is the vector of 19 unknown coefficients

and [X] is the design matrix containing 32 rows and 19 columns

Using a personal computer based data analysis program , the following results were determined for the coefficients in equation 51. When the coefficients from equation 53 are inserted in equation 51, the resulting model characterizes the design space in terms of the main variables and the three noise variables.

$$\begin{bmatrix} \beta_0 \\ \beta_1 \\ \beta_2 \\ \beta_3 \\ \beta_4 \\ \beta_5 \\ \beta_6 \\ \beta_7 \\ \beta_8 \\ \beta_9 \\ \beta_{10} \\ \beta_{11} \\ \beta_{12} \\ \beta_{13} \\ \beta_{14} \\ \beta_{15} \\ \beta_{16} \\ \beta_{17} \\ \beta_{18} \end{bmatrix} = \begin{bmatrix} 132{,}089 \\ 214 \\ 2{,}709 \\ 18{,}202 \\ -7{,}692 \\ 6{,}821 \\ 10{,}502 \\ -85 \\ -584 \\ -55 \\ 29 \\ 167 \\ -349 \\ -3{,}005 \\ 508 \\ 963 \\ -914 \\ 2{,}771 \\ -263 \end{bmatrix} \tag{53}$$

This RSM model is more useful than the signal-to-noise ratio analysis in many ways. Rather than relying on a single S/N ratio that includes a "smeared" effect of all of the noises, the RSM model specifies the individual sensitivities of each noise variable. By inspecting the β coefficients, it can be seen that the dry weight sensitivity to increases in the fuselage weight (N_{fuse}) is the largest of all of the noise variables (adding 21,004 lbs to the dry weight as it varies from -1 to 1). In fact, the sensitivity to N_{fuse} is second in

magnitude only to the sensitivity to cowl wrap angle (Φ). The other noise variables are also very significant. The designer can use the linear RSM equation to determine information about the vehicle for unlimited "what-if" scenarios. For example, what would be the best settings for T/W_o, M_{tr}, and Φ if the airbreathing engine components grew in weight by 10%, but the other noise variables remained at their baselined settings?

The linear RSM model for the L_{32} analysis can be optimized to produce the design variable settings in table 35.

Table 35 - Variables Optimums for L_{32} RSM Model

T/W_o	1.2
M_{tr}	15
Cowl Angle, Φ	180°
N_{isp}	0%
N_{eng}	0%
N_{fuse}	0%

Note that the noise variables are all optimized to their baseline values as expected. Compared to the results of the additive model (equation 49 and table 31), only the thrust-to-weight variable has changed settings. However, it has been shown that the T/W_o variable has a very small effect on the dry weight. For the current combination of variables, the predicted dry weight is 90,413 lbs. The actual experiment was run in row 9 of the L_{32} array and produced an actual dry weight of 92,121 lbs. The model under predicts the actual dry weight by 1.9% at this point in the design space.

In summary, the application of response surface methods to this problem produces a useful linear equation for approximating the dry weight

for various points in the design space (but actually yielded no improvement in the vehicle dry weight over the L_8-only study). Unlike Taguchi's robust design analysis, sensitivity information is available for each of the noise variable individually. However, the determination of a robust design would still require the designer to create a combined effect of all the noise variables for which he or she would determine the least sensitive setting for the design variables. That is, the "smearing" effect of Taguchi's signal-to-noise ratios is actually desirable if the design is to be made insensitive to all three noise variables simultaneously.

As discussed previously, the 32 runs in this RSM analysis were derived from the L_8 by L_4 experimental runs. Because of this limitation, all of the noise variable interaction terms could not be included in equation 51. However, if the original goal of the research was to produce a response surface equation involving all of the possible terms, then the result could have been accomplished by selecting a slightly different configuration of the experimental array and still performing only 32 runs. The runs required by Taguchi's robust design method are slightly less efficient than the runs required to fit the "full" RSM model in this case.

Central Composite Design (with RSM)

As discussed in the previous section on central composite designs, CCD's are an excellent tool for extending a first-order experimental array to include the effects of curvature. In order to check for curvature in the RBCC SSTO design, an experiment was performed at the center of the design space. T/Wo was set to 1.3, M_{tr} was set to 13.5, and Φ was set to 270°. The three noise variables were all set at their midpoint (0) levels (i.e. N_{isp} = -10%, N_{eng} = 10%, N_{fuse} = 10%). The actual dry weight result is compared to the mean of the L_{32} array in table 36.

Table 36 - Actual vs. Predicted Design Center Point

Predicted - Mean of L_{32} Array	132,089 lbs
Actual - Verification Run	127,552 lbs

The difference between the predicted mean and the actual center point is relatively small (only 3.5%). In most cases, it would be assumed that the linear model is adequate, and if a more detailed optimum is desired, the designer could use a gradient-based MDO method on the true design space (response surfaces are only approximations of the true design space). However, in this case a quadratic RSM can be used to demonstrate the CCD with RSM method, and it may be able to locate an optimum design point inside the design space rather than along the edges. Linear models like the one in equation 51 are only capable of determining an optimum along the edges of the design space. By adding a center point and star points for each of the three main variables, the following model can be determined.

$$\begin{aligned}\text{Dry Weight} = {} & \beta_0 + \beta_1 * \left(\frac{\hat{T}}{W}\right) + \beta_2 * (\hat{M}_{tr}) + \beta_3 * (\hat{\Phi}) \\ & + \beta_4 * (\hat{N}_{isp}) + \beta_5 * (\hat{N}_{eng}) + \beta_6 * (\hat{N}_{fuse}) \\ & + \beta_7 * \left(\frac{\hat{T}}{W} * \hat{M}_{tr}\right) + \beta_8 * \left(\frac{\hat{T}}{W} * \hat{\Phi}\right) + \beta_9 * \left(\frac{\hat{T}}{W} * \hat{N}_{isp}\right) \\ & + \beta_{10} * \left(\frac{\hat{T}}{W} * \hat{N}_{eng}\right) + \beta_{11} * \left(\frac{\hat{T}}{W} * \hat{N}_{fuse}\right) + \beta_{12} * (\hat{M}_{tr} * \hat{\Phi}) \\ & + \beta_{13} * (\hat{M}_{tr} * \hat{N}_{isp}) + \beta_{14} * (\hat{M}_{tr} * \hat{N}_{eng}) + \beta_{15} * (\hat{M}_{tr} * \hat{N}_{fuse}) \\ & + \beta_{16} * (\hat{\Phi} * \hat{N}_{isp}) + \beta_{17} * (\hat{\Phi} * \hat{N}_{eng}) + \beta_{18} * (\hat{\Phi} * \hat{N}_{fuse}) \\ & + \beta_{19} * \left(\frac{\hat{T}}{W}\right)^2 + \beta_{20} * (\hat{M}_{tr})^2 + \beta_{21} * (\hat{\Phi})^2\end{aligned} \tag{54}$$

In order to have a rotatable design, central composite design requires the placement of star points at a distance of $\alpha = F^{1/4}$ from the center point. For the L_{32} experimental array, F=32 and $\alpha = 2.38$. However, there are some difficulties in creating a rotatable design with the current design. An α of 2.38 would place variables settings for actual T/W_o at 1.063 and 1.537. Physically, it is unwise to design a vertical lift off launch vehicle with a thrust-to-weight of less than around 1.1. Vehicles with very low lift-off T/W_o's are susceptible to cross winds and might drift into the launch tower. Therefore, α_1 was set to 2. α_2 for M_{tr} was set near the optimum value at 2.33 corresponding to M_{tr} star points of 13.5 and 17. However, since 360° is the maximum physical cowl wrap around angle, α_3 can be no higher than 1 (face centered). The resulting array is not rotatable, but it is reasonably close. The seven additional runs (2n+1) required to form a CCD in the three main variables and the selected levels are shown in table 37.

Table 37 - Additional Runs Required for CCD

Run	T/W_o	M_{tr}	Φ	N_{isp}	N_{eng}	N_{fuse}	Dry Weight
33	0	0	0	0	0	0	127,552
34	-2	0	0	0	0	0	129,163
35	2	0	0	0	0	0	128,921
36	0	-2.33	0	0	0	0	128,467
37	0	2.33	0	0	0	0	136,295
38	0	0	1	0	0	0	109,221
39	0	0	-1	0	0	0	149,310

Because the CCD is "built up" from the L_{32} two-level array, the additional runs are numbered 33 through 39. The entire CCD consists of all 39 runs. Note that the noise variables were set to their midpoint levels for every point

in the additional set. The curvature effects due to the noise variables were assumed to be small and were not included in the model.

Using a computer based regression analysis program, the 22 β coefficients in equation 54 can be determined. The resulting coefficients are

$$\begin{bmatrix} \beta_0 \\ \beta_1 \\ \beta_2 \\ \beta_3 \\ \beta_4 \\ \beta_5 \\ \beta_6 \\ \beta_7 \\ \beta_8 \\ \beta_9 \\ \beta_{10} \\ \beta_{11} \\ \beta_{12} \\ \beta_{13} \\ \beta_{14} \\ \beta_{15} \\ \beta_{16} \\ \beta_{17} \\ \beta_{18} \\ \beta_{19} \\ \beta_{20} \\ \beta_{21} \end{bmatrix} = \begin{bmatrix} 126,668 \\ 159 \\ 2,447 \\ 18,310 \\ -7,692 \\ 6,821 \\ 10,502 \\ -85 \\ -584 \\ -55 \\ 29 \\ 167 \\ -349 \\ -3,005 \\ 508 \\ 963 \\ -914 \\ 2,771 \\ -263 \\ 657 \\ 1,084 \\ 3,616 \end{bmatrix} \tag{55}$$

The last three terms in equation 55 correspond to $(T/W_O)^2$, $(M_{tr})^2$, and $(\Phi)^2$ respectively. The largest quadratic effect is due to the cowl wrap angle. The other variables generally follow the trends established in the L_{32} study. The largest linear influence on the dry weight is also the cowl wrap angle. The

three noise variables represent the next largest influence on the design. It is interesting to note the fairly large M_{tr} x N_{isp} term represented by β_{13}. Since the coefficient is negative, the signs of the normalized M_{tr} and N_{isp} variables should be the same to reduce dry weight. As N_{isp} goes to -1 (indicating a 20% degradation in airbreathing mode I_{sp}), then the transition Mach number should also go to -1 (M_{tr} = 12). The result makes good engineering sense because a lower M_{tr} will spend less time in airbreathing mode.

When the β coefficients in equation 55 are combined with equation 54, the resulting response surface is a quadratic approximation of the RBCC design space. The dry weight can be minimized with a non-linear optimizer to produce the variable settings shown in table 38. Unlike all of the previous examples, the optimum variable settings do not necessarily lie at the edge of the design space. Φ, however, has been consistently limited by its artificially determined lower limit of 180°. The "true" optimum for Φ probably lies below 180°. Additional work is recommended for this variable.

Table 38 - CCD Optimum Variable Settings

T/W_O	1.27
M_{tr}	14.6
Cowl Angle, Φ	180°
N_{isp}	0%
N_{eng}	0%
N_{fuse}	0%

The predicted optimum dry weight is 89,660 lbs. An actual verification run at the settings shown in table 38 produced an actual dry weight of 91,578 lbs. The quadratic RSM model under predicted the actual dry weight by 2.1%. The detailed datasheets for the actual verification run are listed in Appendix E.

Since the design space is relatively linear, no large improvement in the optimum dry weight was expected by adding the quadratic terms. However, there is a slight (almost negligible) improvement. The best design produced by the linear model was 92,121 lbs. The current design is 91,578 lbs. It should be pointed out that the optimum design predicted above is the optimum of the **approximate** model given by equation 54. The true optimum of the design space may be slightly lower than the dry weight predicted above. If the designer is interested in a more accurate optimum, gradient-based MDO methods could be employed. In fact, since the linear RSM had already been proved to be an adequate approximate model, a gradient-based technique like system sensitivity analysis could have been used in place of the current CCD application for the next step in the analysis.

While the quadratic model formed from a central composite design showed only a small improvement over the linear RSM model for this particular design, the potential of the method for aerospace applications is significant. Advanced aerospace design problems are typically non-linear, and an approximate model of the entire design space is a valuable design aid for an engineer. Once the model is formed, endless "what-if" questions can be answered about the design. Although the method cannot handle discrete variables (the Taguchi method can), CCD with RSM equation fitting is a highly recommended technique for use in conceptual aerospace design.

Final Vehicle Configuration

The final, "best" vehicle configuration is the minimum weight result of the 39 point design CCD with RSM analysis (see figure 28). The vehicle characteristics did not change significantly from the configuration selected following the initial L_{27} screening array (figure 25). In fact, most of the changes in dry weight and gross weight are due to the change in the mass estimating relationships from the L_{27} array to the subsequent analyses.

The final selected RBCC SSTO has a dry weight of 91,578 lbs and a gross weight of 463,943 lbs (see Appendix E for a full weight statement on the final vehicle). The vehicle lifts-off vertically and glides to a horizontal landing (the engine has no supercharger). The initial T/W_0 is 1.27 at lift-off, but it has been shown that a T/W_0 of 1.2 will make the vehicle less sensitive to engine weight growth. After flying along a constant dynamic pressure boundary of 2000 psf from Mach 3 to Mach 14.6, the vehicle transitions to rocket mode for the final acceleration to orbit. The cone half angle is 5°, and the cowl wrap around angle is 180°. As discussed above, the "true" optimum for cowl wrap angle (Φ) probably lies below 180.

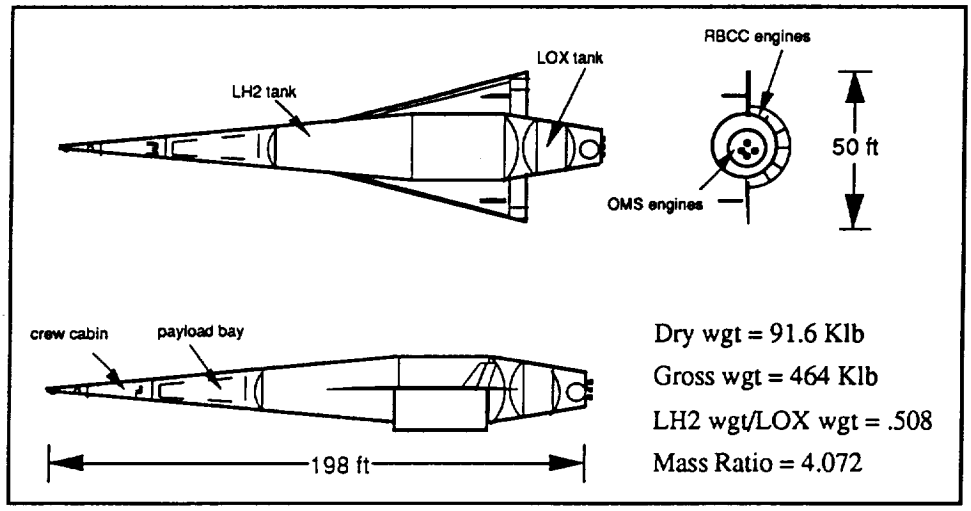

Figure 28 - Final Vehicle Configuration

The conical RBCC SSTO is designed to deliver a 10,000 lb payload to a 100 Nmi. x 100 Nmi. polar orbit from a fictitious launch site at Vandenberg Air Force Base in California. The same vehicle is capable of delivering slightly over 20,000 lbs to a 100 Nmi. x 100 Nmi. x 28.5° orbit from Kennedy Space Center in Florida. The vehicle is fully reusable, carries a crew of two for two days, and could begin operations in the 2005 - 2010 time frame.

Summary

In this research, several techniques from the parametric class of multidisciplinary design optimization methods were applied to the optimization of an advanced rocket-based combined-cycle SSTO launch vehicle. It was a primary goal of this work to provide some insight into the use of these methods for aerospace vehicle conceptual design, and to contribute to the experience base in the field of MDO. The parametric methods studied included Taguchi methods (both three-level and two-level), Taguchi's method of robust design, central composite design (CCD), and first and second order response surface methods (RSM).

Taguchi methods proved to be very useful for characterizing the design space, for determining the effects of the individual variables, and for locating a near-optimum region of the design space. Taguchi's use of orthogonal arrays (with proper attention to interaction terms) makes the method very easy to apply and the results easy to analyze. Of the methods tested, only Taguchi methods are capable of handling truly discrete variables. However, as evident in the application of an L_{27} array to the RBCC SSTO design, the method's inability to deal with infeasible or unconverged designs is a serious weakness of the method. Since all of the required point designs are determined prior to the start of a parametric method, the designer is required to know enough about the design space ahead of time so that the variable ranges can be chosen accordingly. Unfortunately, such knowledge is not always available.

One of the primary strengths of the Taguchi method is its ability to perform robust design. Using signal-to-noise ratio analysis, the design variables can be selected so that the vehicle is least sensitive to uncontrollable, and potentially negative, influences on the design. For the RBCC SSTO vehicle, two of the three design variable settings were found to be different

when designing the vehicle to be most robust versus designing the vehicle for the lowest dry weight. However, the penalty associated with the robust design is very small. Taguchi's method of robust design does not allow the designer to determine the **individual** effects of each noise factor, but instead provides a smeared effect of all of the noises on the design.

The use of central composite design techniques (and associated second order response surfaces) on the RBCC SSTO design was not expected to provide much improvement in the optimum dry weight because the linear model was shown to be fairly accurate for the selected design variables. In the end, the 39 experiment CCD analysis provided less than a 2% reduction in dry weight over the near-optimum solution produced by the eight run L_8 Taguchi array. In practice, a designer would probably not have chosen to perform the additional 31 experiments (based on the center point check), and this particular application was more of an attempt to understand the method than to improve the dry weight. In general, a linear model cannot be expected to be adequate in all cases.

First and second order RSM provides the designer with very useful information about the design space and the variables. The mathematical model of the response (the response surface) can be used to ask "what-if" type questions about the design and quickly determine the results. The coefficients of the model provide information about the effects of the main variables and their interactions. The model can be optimized to help locate a point inside the design space that might be optimum. However, response surfaces are only approximations to the actual design space. Just because the model is quadratic does not mean that the true design space is quadratic or that the optimums are at the same place. At some point, it becomes more prudent to change to a gradient-based optimization of the true design space rather than to add additional point designs to the RSM model. This "point of diminishing returns" is very problem dependent, but for the RBCC SSTO design, the improvements in dry weight from the addition of extra CCD runs was negligible.

The parametric MDO methods researched in this work all have their strengths and weaknesses. They each can be very helpful to the conceptual vehicle designer if used in the correct situation. The methods used here are not the only MDO methods useful for this type of design, but they form an initial set to which new methods can be added. It is hoped that the demonstrated applicability of these MDO methods will contribute to the growing literature in the field and provide a basis from which additional research can begin.

RBCC SSTO Vehicle Specific Conclusions

The optimization of the rocket-based combined-cycle vehicle was a highly multidisciplinary process that would have been difficult, if not impossible, without the aid of multidisciplinary design optimization. It served as an excellent test case for evaluating the potential of the methods.

For the reference mission, the minimum dry weight for the RBCC SSTO vehicle is around 91,600 lbs. Vertical take-off produces a lower dry weight than horizontal take-off primarily due to the extra gear and wing weight associated with the HTO option. Based solely on performance, the extra weight of the supercharging fan is not worth the additional weight of the engine. The 5° cone half angle reduces drag and heating, and therefore saves weight. The highest tested dynamic pressure boundary on ascent (2000 psf) produces the most beneficial amount of thrust during the airbreathing portions of the trajectory. The (one foot sphere) stagnation point heating limit was set to the maximum feasible 350 BTU/ft^2-s in order to allow the airbreathing portion of the trajectory to stay on a maximum dynamic pressure boundary as long as possible.

The RBCC SSTO dry weight is very insensitive to changes in the lift-off thrust-to-weight ratio. There are competing effects as the T/W_o is varied from low to high. A high T/W_o ratio will require a larger engine, but the vehicle will accelerate to ramjet speeds (Mach 3) faster and therefore have reduced requirements for on-board oxygen and lower lift-off thrust

requirements. These effects essentially cancel each other. A final value for T/W_0 of 1.27 was selected to minimize dry weight by using a quadratic response surface model.

The airbreathing to rocket mode transition Mach number (M_{tr}) should be set at near 15 (14.6 by quadratic RSM) in order to minimize the vehicle dry weight. M_{tr} of 15 allows a larger percentage of the fuel to be lightweight LH2 (due to the longer use of airbreathing propulsion). At higher transition Mach numbers, the scramjet engine thrust and fuel efficiency are reduced.

The most significant design variable is the cowl wrap around angle, Φ. In all cases except the initial L_{27} array (which was influenced by several "no-closure" designs), Φ of 180° proved to provide the lowest vehicle dry weight, and Φ was always the most influential design variable. Varying Φ from 180° to 360° can add as much as 36,000 lbs to the dry weight of the vehicle. Since Φ was always limited by the lower part of the allowable range, it is likely that the "true" optimum for cowl wrap around angle lies below 180°. Additional work is recommended to extend the range of Φ from 180° down to 90°. Since the original two-variable interaction between the dynamic pressure boundary, q, and Φ was performed under the influence of several no-closure runs (the L_{27} array), an additional investigation of that interaction is also recommended.

Some of the most useful information about the design was provided by the Taguchi robust design analysis. If the engine weight is likely to increase, the body structure and thermal protection system weights are likely to increase, and the airbreathing engine I_{sp} is likely to decrease, then the vehicle should be designed to be least sensitive to those "noises". A lift-off T/W_0 of 1.2 will reduce the engine weight sensitivity, and a M_{tr} of 12 will reduce the sensitivity to tank weight growth and scramjet I_{sp} degradation. Φ remains at 180°. The baseline design dry weight penalty for this robust design option is very small compared to the minimum dry weight design. Given the uncertainty in high speed airbreathing engine development, it would be wise to choose the design variable settings that maximize vehicle robustness.

RECOMMENDATIONS FOR FURTHER WORK

The current research characterized key aspects of the RBCC SSTO design space, but there are several areas in the design that would benefit from additional research.

1) As pointed out after the initial L_{27} set of experiments, there is a likely three variable interaction between the dynamic pressure (q), the transition Mach number (M_{tr}), and the cowl wrap angle (Φ). The two variable interaction between M_{tr} and Φ was investigated in subsequent research, but the q-M_{tr} and the q-Φ interactions have yet to be adequately studied. It is highly likely that these interactions exist and have a significant impact on the design.

2) The cowl wrap angle consistently optimized to the lower end of its preestablished range (i.e. 180°). Given the fact that Φ is the most dominant variable in the design in terms of dry weight, additional research should be conducted to locate the optimum setting for Φ. It is almost certain that a Φ of less than 180° will produce a lower dry weight than the best reported here. Use of a method that will capture the curvature effect of Φ is recommended.

3) The use of noise variables in the robust design and L_{32} RSM experiments provided an excellent insight into the overall design space and the sensitivity of the RBCC to expected negative influences. Future research should include additional noise variables. Dry weight margin growth, payload growth, and boundary layer transition criteria (for heating) are candidate noises.

While the current research focused only on the application of methods from the parametric class, gradient-based MDO methods are also applicable to conceptual vehicle design – particularly after the near-optimum region of interest has been so well identified by the current research.

4) System sensitivity analysis techniques should be applied to the optimization of RBCC SSTO design variables like cowl wrap angle and transition Mach number. Unlike the response surface method used in this research, SSA can be used to locate an optimum of the true design space rather than just a quadratic approximation of the true design space.

5) As shown in the L_{27} study, Taguchi methods have difficulty dealing with infeasible points in the design space. Additional research is recommended in order to determine the best options for addressing this deficiency.

6) MDO methods from both classes should continue to be applied to conceptual aerospace vehicle design problems of various types. Additional applications will provide insight into the methods and contribute to the growing experience base in this emerging field.

References

1. U. S. Congress, Office of Technology Assessment, "Launch Options for the Future: Buyer's Guide." OTA-ISC-383, July 1988.

2. Sobieski-Sobieszczanski, J., and J. Tulinius. "MDO Can Help Resolve the Designer's Dilemma." Aerospace America, September 1991.

3. Sobieski-Sobieszczanski, J. "Multidisciplinary Design Optimization: An Emerging New Engineering Discipline." Presented at the World Congress on Optimal Design of Structural Systems, Rio de Janeiro, Brazil, August 1993.

4. Olds, J. R. "The Suitability of Selected Multidisciplinary Design Techniques to Conceptual Aerospace Vehicle Design." AIAA Paper 92-4791, September 1992.

5. Stanley, D., R. Unal, and R. Joyner. "Application of Taguchi Methods to Dual Mixture Ratio Propulsion System Optimization for SSTO Vehicles." AIAA Paper 92-0213, January 1992.

6. Bush, L., and R. Unal. "Preliminary Structural Design of a Lunar Transfer Vehicle Aerobrake." AIAA Paper 92-1108, February 1992.

7. Stanley, D., et. al. "SSTO Configuration Selection and Vehicle Design." AIAA Paper 93-1053, February 1993.

8. Olds, J. R., and G. Walberg. "Multidisciplinary Design of a Rocket-Based Combined-Cycle SSTO Launch Vehicle using Taguchi Methods." AIAA Paper 93-1096, February 1993.

9. Fox, R. L. Optimization Methods for Engineering Design. Reading, MA: Addison-Wesley Publishing Company, 1971.

10. Gill, P., W. Murray, and M. Wright. Practical Optimization. London: Academic Press, 1981.

11. Rogers, J. L. "DeMaid - A Design Manager's Aid for Intelligent Decomposition, User's Guide." NASA TM-101575, March 1989.

12. Barthelemy, J-F. "Engineering Applications of Heuristic Multilevel Optimization Methods." NASA CP - 3031, Recent Advances in Multidisciplinary Analysis and Optimization Conference, part 3, pg. 1029, September 1988.

13. Sobieski-Sobieszczanski, J. "Sensitivity of Complex, Internally Coupled Systems." AIAA Journal, January 1990.

14. Malone, B. and W. H. Mason. "Multidisciplinary Optimization in Aircraft Design Using Analytic Technology Models." AIAA Paper 91-3187, September 1991.

15. Sobieski-Sobieszczanski, J. "Sensitivity Analysis and Multi-disciplinary Optimization for Aircraft Design : Recent Advances and Results." Journal of Aircraft, December 1990.

16. Phadke, Madhav. Quality Engineering Using Robust Design. NJ : Prentice-Hall, 1989.

17. Taguchi, G., E. Elsayed, T. Hsiang. Quality Engineering in Production Systems. NY:McGraw-Hill, 1989.

18. Taguchi, G. Introduction to Quality Engineering. Dearborn, MI: American Supplier Institute, 1989.

19. Khuri, A., and J. Cornell. Response Surfaces. NY: Marcel Dekker, Inc., 1987.

20. Montgomery, D. Design and Analysis of Experiments. NY: John Wiley and Sons, 1991.

21. Unal, R. "Engineering Design for Quality Using the Taguchi Approach." Engineering Management, vol. 4, number 1; March 1992.

22. Box,G., W. Hunter, and J. Hunter. Statistics for Experimenters - An Introduction to Design, Data Analysis and Model Building. NY: John Wiley and Sons, 1978.

23. Box, G., and N. Draper. Evolutionary Operations: A Statistical Method for Process Improvement. NY: Wiley and Sons, 1969.

24. Hicks, C. Fundamental Concepts in the Design of Experiments. NY: Holt, Rinehart, and Winston, 1973.

25. Box, G., and N. Draper. "On-minimum Second-Order Designs." Technometrics, vol. 16, number 4; November 1974.

26. McElroy, John. "Dr. Taguchi - Japan's Secret Weapon." Automotive Industries, August 1984, pg. 18.

27. Roy, Ranjit. A Primer on the Taguchi Method. NY : Van Nostrand Reinhold, 1990.

28. McElroy, John. "Experimental Design Hits Detroit." Automotive Industries, February 1985, pg. 48.

29. Pilon, G. "Product Design Optimization Using Taguchi Methods with Finite Element Analysis." 1989 ASME Design Technical Conferences - 8th Biennial Conference on Failure Prevention and Reliability, Montreal, Canada, September 1989, pg. 145.

30. Byrne, D. and S. Taguchi. "The Taguchi Approach to Parameter Design." 40th Annual Quality Congress Transactions, The Taguchi Approach to Parameter Design, 1987.

31. Freeman, D. C., et. al. "Design Options for Advanced Manned Launch Systems (AMLS)." AIAA paper 90-3816, September 1990.

32. Anon. "A Study of Composite Propulsion Systems for Advanced Launch Vehicle Applications." NASA contract NAS7-377, September 1966.

33. Escher, W. J. D. "Combined-Cycle and Hypersonic Propulsion - A Renewed Rocketdyne Initiative." Threshold - Rocketdyne's internal engineering journal of power technology, Issue No. 3, Summer 1988.

34. Hunt, J. L., and J. Martin. "Aero-space Plane Figures of Merit." presented at the 4th International Aerospace Planes Conference, December 1992.

35. Wilhite, A. W.. et. al. "Concepts Leading to the National Aero-Space Plane Program." AIAA paper 90-0294, January 1990.

36. Foster, R. W., W. Escher, and J. Robinson. "Air Augmented Rocket Propulsion Concepts." USAF Astronautics Laboratory Report AFAL-TR-88-004, April 1988.

37. Foster, R. W., W. Escher, and J. Robinson. "Studies of an Extensively Axisymmetric Rocket Based Combined Cycle (RBCC) Engine Powered SSTO Vehicle." AIAA Paper 89-2294, July 1989.

38. Sova, G. and P. Divan. "Aerodynamic Preliminary Analysis System II Part II - User's Manual. NASA CR 182077, April 1991.

39. Shaughnessy, J. D., et. al. "Hypersonic Vehicle Simulation Model." NASA TM-102610, November 1990.

40. Phillips, W. P., et. al. "Experimental Investigation of the Aerodynamic Characteristics for a Winged-Cone Concept." AIAA Paper 87-2484, August 1987.

41. Brauer, G. L., et. al. "Program to Optimize Simulated Trajectories (POST)." NASA contract NAS1-18147, September 1989.

42. Engel, C. D., and C. Schmitz. "Miniver Upgrade for the AVID System." NASA CR-172213, August 1983.

43. Taguchi, G, and S. Konishi. Orthogonal Arrays and Linear Graphs. American Supplier Institute, 1987.

Appendices

Appendix A

Vehicle Mass Estimating Relationships

RBCC SSTO Mass Estimating Relationships

These mass estimating relationships have been compiled from various sources (some not yet published), and are intended for use on specific advanced vehicle configurations. They are listed by categories used on the standard RBCC weight statement (Appendices C, D, E). These MER's are not to be used for general weight estimation for broad classes and technology levels of advanced spacecraft. Much of the supporting data (developed partially from NASA LaRC in-house work) has been omitted here.

1.0 Wing Group

$$\textbf{Exposed Wing} = .82954 * \left[\frac{(1 + taper\_ratio)}{\left(\frac{t}{c}\right)}\right]^{0.4} * \left[\frac{safety\_factor * max\_wing\_normal\_force}{1000}\right]^{.48} * S_{exp}^{.67} * AR_{exp}^{.64} * (1 - technology\_factor)$$

where:

safety factor = 1.5

"*exp*" refers to exposed wing (rather than theoretical wing)

max_wing_normal_force varies depending on ascent trajectory and loads

t/c = .04 (airfoil thickness to chord ratio)

taper_ratio = 0 (delta wing)

S = wing planform area

AR = wing aspect ratio (b^2/S)

technology_factor= .40 (from Aluminum skin/stringer to Ti_3Al Beta 21S w/SiC)

notes:

equation derived from military aircraft wings (Lepsch)

$$\textbf{Wing Carry Through} = .00636 * \left[(1 + taper\_ratio)AR_{exp}\right]^{.5} * \left[\frac{safety\_factor * max\_wing\_normal\_force}{1000}\right] * \frac{b_{str\_exp} * body\_width}{root\_chord\_thickness_{exp}} * (1 - technology\_factor)$$

where:

safety_factor = 1.5

b_{str_exp} refers to the total exposed span along the chord centerlines

max_wing_normal_force varies depending on ascent trajectory and loads

technology_factor= .40 (from Aluminum carry-through to Ti_3Al Beta 21S w/SiC)

notes:

equation derived from military aircraft wings (Lepsch)

2.0 Tail Group

$$\textbf{Vertical tail} = 5.0 * S_{vert}^{1.09} * (1 - technology\_factor)$$

where:

S_{vert} = 2*.025*S_{ref_wing} (planform area of both vertical surfaces)

technology_factor = .2 (estimate from Aluminum to Ti3Al Beta 21S)

notes:

original equation based on standard Aluminum construction (Lepsch)

3.0 Body Group

$$\textbf{Nosecone} = structural\_unit\_weight * surface\_area$$

where:

structural_unit_weight = 2.21 lb/ft^2 (est. Ti_3Al Beta 21S materials from AIAA 91-0540)

$$\textbf{Crew Cabin (structure)} = 1455 * (number\_crew)^{0.5}$$

notes:

pressurized volume (and therefore cabin weight) is related to the number of crew

Payload Bay (structure) = structure (excluding doors) + P/L bay doors + P/L accommodations

1) structure (excluding doors) =*structural_unit_weight* surface_area(excluding doors)*

where:
structural_unit_weight = 2.21 lb/ft^2 (Ti3Al Beta 21S materials)

2) P/L bay doors = *structural_unit_weight*surface_area_doors*

where:
structural_unit_weight = 3.5 lb/ft^2 (20% less than STS honeycomb doors, includes fittings, mechanisms, etc.)

3) P/L accommodations = .15 * payload

where:
P/L accommodations include extra longerons, fittings, mounts, etc. to hold payload

LH2 tank = LH2 tank structure + LH2 tank cryo. insulation

1) LH2 tank structure = *volume_unit_weight*total_LH2_tank_volume*

where:
volume_unit_weight = .255 lb/ft^3 (Gr/PEEK, wound, integral, axisymmetric tank, Olds)

notes:
LH2 tank ullage of 4.25% used on volume

2) LH2 tank cryo. insulation = *insulation_unit_weight* total_LH2_tank_surface_area*

where:
insulation_unit_weight = .26 lb/ft^2 (based on Rohacell insulation)

LOX tank = LOX tank structure + LOX tank cryo. insulation

1) LOX tank structure = *volume_unit_weight*total_LOX_tank_volume*

where:
volume_unit_weight = .33 lb/ft^3 (advanced Al-Li, non-integral, Stanley)

notes:
LOX tank ullage of 4.25% used on volume

2) LOX tank cryo. insulation = *insulation_unit_weight* total_LOX_tank_surface_area*

where:
insulation_unit_weight = .20 lb/ft^2 (based on Rohacell insulation)

Aft Body = Tail cone(frustrum) + Base

1) Tail cone = *structural_unit_weight*surface_area*

where:
structural_unit_weight = 2.21 lb/ft^2 (Ti_3Al Beta 21S materials)

1) Base = *structural_unit_weight*surface_area*

where:
structural_unit_weight = 1.99 lb/ft^2 (secondary struct., 10% lower than baseline)

Cowl = Cowl ring + Cowl struts

1) Cowl ring = *non_inlet_struct_unit_weight*non_inlet_surface_area+ 2*inlet_struct_unit_weight*_inlet_surface_area*

where:
*non_inlet_struct_unit_weight**= 2.21 lb/ft^2 (Ti_3Al Beta 21S materials)
*inlet_struct_unit_weight**= 2.75 lb/ft^2 (advanced materials, 150 psi, top&bottom req'd)

1) Cowl struts = *structural_unit_weight*inlet_height* inlet_length*number_struts*

where:
structural_unit_weight = 2.21 lb/ft^2 (baseline structural unit weight)

4.0 Thermal Protection

Active Cooling = Nosecap + Cowl leading edge + Wing leading edges + Engine nozzle exit

1) Nosecap = 150 lb

notes:
fixed weight including cooling panels, heat pipes, supports, pumps, etc

2) Cowl leading edge = *cowl_leading_edge_length** *active_cooling_per_length*

where:
active_cooling_per_length = 2.70 lb/ft (based on 5° cone, Wilhite)

3) Wing leading edges = *wing_exposed_leading_edges** *active_cooling_per_length*

where:
active_cooling_per_length = 2.70 lb/ft (based on 5° cone, Wilhite)

4) Engine nozzle exit = *engine_nozzle_exit_cooled_area** *active_cooling_per_area*

where:
active_cooling_per_area = 3.50 lb/ft^2 (based on 5° cone, Wilhite)

Advanced Carbon/Carbon TPS = Body/cowl + wing/tails

1) Body/cowl = *(body_passive_area+cowl_area)*body/cowl_%_ACC* ACC_unit_weight*

where:
body/cowl_%_ACC = percent of body/cowl area covered by ACC (T_{eq}>1800° F)
ACC_unit_weight = 2.0 lb/ft^2 (based on advanced NASP TPS, Shideler)

2) Wing/tails = *(wing_wetted_area+tail_wetted_area)* wing/tail_%_ACC*ACC_unit_weight*

where:
wing/tail_%_ACC = percent of wing/tail wetted area covered by ACC (T>1800° F)

ACC_unit_weight = 2.0 lb/ft^2 (based on advanced NASP TPS, Shideler)

Superalloy standoff TPS = Body/cowl + wing/tails

1) Body/cowl = *(body_passive_area+cowl_area)*body/cowl_%_superaly* superaly_unit_weight*

where:

body/cowl_%_superaly= percent of body/cowl area covered by superalloy (T_{eq}>1200° F)

superaly_unit_weight = 1.06 lb/ft^2 (based on advanced metallic NASP TPS, Shideler)

2) Wing/tails = *(wing_wetted_area+tail_wetted_area)* wing/tail_%_superaly*superaly_unit_weight*

where:

wing/tail_%_superaly= percent of wing/tail wetted area covered by superaly (T>1200° F)

superaly_unit_weight = 1.06 lb/ft^2 (based on advanced metallic NASP TPS, Shideler)

Titanium standoff TPS = Forebody

1) Forebody = *(body_passive_area)*forebody_%_ti*ti_unit_weight*

where:

forebody_%_ti= percent of forebody area covered by titanium TPS (T_{eq}<1200° F)

ti_unit_weight = .508 lb/ft^2 (based on advanced metallic NASP TPS, Shideler)

notes:

cowl, tailcone, base, vertical tail, and wing areas made from Ti_3Al Beta 21S and with temperatures below 1500 °F do not require external TPS because the material is capable of sustaining that temperature already. However, all forebody (crew cabin and LH2 tank) areas will require TPS reqardless of temperature. For example, titanium standoff TPS is required on the tank because they are constructed of lower temperature capability materials and sometimes contain cryogenic fluids.

5.0 Landing Gear

Landing Gear = Nose gear + Main Gear

1) Nose gear = .15 * .026 * *landing_weight*

2) Main gear = .85 * .026 * *landing_weight*

notes:
total advanced landing gear is 2.6% of landing weight (or takeoff weight if horizontal take-off)
nose gear/main gear ratio is 15%/85% (MacConochie')

6.0 Main Propulsion (less cowl)

$$\textbf{RBCC Engines} = gross\_weight * \frac{\left(\frac{T}{W}\right)_{vehicle\_liftoff}}{\left(\frac{T}{W}\right)_{engine\_uninstall}}$$

where:
engine uninstalled T/W is a function of the engine selected (#10, #12, etc.) and is calculated based on formulas in Appendix B. Uninstalled weight includes pumps, cooling, diffuser, combustor, fan (if applicable), short nozzle, rocket ejectors, and gas generator. Only the inlet weight (cowl) is excluded. Cowl weight is included in the body weight.

notes:
engine weight is subdivided to component level according to data available in Astronautics Corp. report for rocket primaries, airbreathing components, and supercharging fan.

$$\textbf{Pressurization and feed systems} = 1.616 * gross\_weight * \frac{\left(\frac{T}{W}\right)_{vehicle\_liftoff}}{Isp_{sea\_level}}$$

notes:

pressurization and propellant feed systems based on propellant mass flow rate

Purge System = $(.05*V_{LH2} + .075*V_{LOX})*(1\text{-}technology\_factor)$

where:
technology_factor = 0.6 (advanced AMLS data, Lepsch)

notes:
for purging lines and tanks with He

7.0 RCS Propulsion

Forward RCS = Thrusters + Propellant tanks + Press. tank + Pressurants + Lines, Manifolds, etc

1) Thrusters = $number\_vernier\_thrusters * \frac{T_{req}}{\left(\frac{T}{W}\right)_{vernier}}$

where:
number_thrusters = 15 (3 verniers in each direction plus forward)
T_{req} = [*entry_weight*body_length*//(147141 lbs*143 ft)]* 50 lbs per thruster
$(T/W)_{vernier}$ = 9.4 (includes mounts, supports, ignitors, etc)

notes:
thrusters are pressure fed LH2/LOX based on Rockwell IHOT study required thrust calculation based on reference AMLS weight and length

2) Propellant tanks = $.01295*P_{design}*V_{tank}$

where:
P_{design} = 195 psia for both LH2 and LOX tanks

notes:
propellant tanks weight based on AL 2219 tanks sized for yield stress at 140% of design pressure with a 1.75 factor for extra items (fittings, dewer constr.).
RCS propellant tanks include 5% ullage factor on volume

3) Pressurant tank(He) = $.0143*P_{design}*V_{He}*(1\text{-}technology\_factor)$

where:
P_{design} = 3000 psia for He pressurant tank
technology_factor = .25 (composite wound tanks reduction)
$V_{He} = .24*(V_{LOX} + V_{LH2})$ (based on 3000 psia and 195 psia tanks)

notes:
pressurant tank based on Ti-6Al-4V sized for yield stress at 400% of design pressure with a 1.25 factor for extra items

4) Pressurant weight (He) = $.671*(V_{LOX} + V_{LH2})$

notes:
based on 400° R storage temperature

5) Lines, Manifolds, Valves, etc = .74**thruster_weight*

notes:
based on Rockwell IHOT study for LOX/LH2 RCS

Aft RCS = Thrusters + Propellant tanks + Pressurant tank + Pressurants + Lines, Manifolds, etc

1) Thrusters =

$$num\_vernier\_thrusters * \frac{T_{req\_vernier}}{\left(\frac{T}{W}\right)_{vernier}} + num\_prim\_thrusters * \frac{T_{req\_primary}}{\left(\frac{T}{W}\right)_{primary}}$$

where:
num_vernier_thrusters = 12 (2 verniers in each direction plus 4 aft)
$T_{req\_vernier}$ = [*entry_weight*body_length*//(147141 lbs*143 ft)]* 50 lbs per thruster
$(T/W)_{vernier}$ = 9.4 (includes mounts, supports, ignitors, etc)
num_prim_thrusters = 10 (2 primaries in each direction plus 2 aft)
$T_{req\_primary}$= [*entry_weight*body_length*//(147141 lbs*143 ft)]* 870 lbs per thruster
$(T/W)_{primary}$ = 39.5 (includes mounts, supports, ignitors, etc)

notes:
thrusters are pressure fed LH2/LOX based on Rockwell IHOT study
required thrust calculation based on reference AMLS weight and length

2) Propellant tanks = $.01295*P_{design}*V_{tank}$

where:
P_{design} = 195 psia for both LH2 and LOX tanks

notes:
propellant tanks sizing based on AL 2219 tanks designed for yield stress at 140% of design pressure with a 1.75 factor for extra items(fittings, dewer constr.)
RCS propellant tanks include 5% ullage factor on volume

3) Pressurant tank(He) = $.0143*P_{design}*V_{He}*(1\text{-}technology\_factor)$

where:
P_{design} = 3000 psia for He pressurant tank
$technology\_factor$ = .25 (composite wound tanks reduction)
$V_{He} = .24*(V_{LOX} + V_{LH2})$ (based on 3000 psia and 195 psia tanks)

notes:
pressurant tank based on Ti-6Al-4V sized for yield stress at 400% of design pressure with a 1.25 factor for extra items

4) Pressurant weight (He) = $.671*(V_{LOX} + V_{LH2})$

notes:
based on 400° R storage temperature

5) Lines, Manifolds, Valves, etc = $.74*thruster\_weight$

notes:
based on Rockwell IHOT study for LOX/LH2 RCS

8.0 OMS Propulsion

$$\textbf{Engines} = \frac{T_{req\_OMS}}{\left(\frac{T}{W}\right)_{OMS\_engines}}$$

where:
$T_{req\_OMS} = entry\_weight/16$ (1/16 g acceleration/deceleration)
$(T/W)_{OMS\_engines}$ = 22 (includes mounts, supports, ignitors, etc)

$$\textbf{Propellant tanks} = .01295*P_{design}*V_{tank}$$

where:

P_{design} = 25 psia for both LH2 and LOX tanks (low pressure for pump fed sys.)

notes:
propellant tanks based on AL 2219 tanks designed for yield stress at 140% of design pressure with a 1.75 factor for extra items(fittings, dewer constr.) OMS propellant tanks include 5% ullage factor on volume

Pressurant tank(He) = $.0143*P_{design}*V_{He}*(1\text{-}technology\_factor)$

where:
P_{design} = 3000 psia for He pressurant tank
technology_factor = .25 (composite wound tanks reduction)
$V_{He} = .06*(V_{LOX} + V_{LH2})$ (based on 3000 psia and 25 psia tanks)

notes:
pressurant tank based on Ti-6Al-4V sized for yield stress at 400% of design pressure with a 1.25 factor for extra items

Pressurant weight (He) = $.167*(V_{LOX} + V_{LH2})$

notes:
based on 400° R storage temperature

Lines, Manifolds, Valves, etc = $.76*thruster\_weight$

notes:
based on Rockwell IHOT study for LOX/LH2 RCS

9.0 Primary Power

Fuel Cells = 396 lbs

notes:
based on NASP technology AMLS (Stanley)

Reactant Dewers(wet) = $176.9*(mission\_duration+1)$

where:
mission_duration = 2 days

Batteries = .05166*(*surface_control_actuators_weight*)

notes:
surface_control_actuator weight is proportional to power requirements

10.0 Electrical Conversion & Distribution

Power conversion and distribution = 1875 lb

notes:
based on NASP technology AMLS (Stanley)

EMA controllers = .324*(*surface_control_actuators_weight*)

notes:
controller weight proportional to actuator weight

Circuitry and wiring =
*shape_factor*8.56*(*vehicle_length+vehicle_width+vehicle_height*)

where:
shape_factor = 0.6 for RBCC SSTO due to proximity of P/L bay and crew cabin

EMA Cabling =
.00043*(*vehicle_length+wingspan*)*(*surface_control_actuators_weight*)

notes:
cabling weight proportional to power requirements and run length

11.0 Hydraulic Systems

Hydraulic systems = 0

notes:
hydraulics replaced with EMAs for advanced vehicles

12.0 Surface Control Actuators

Elevon EMAs =
.01613**elevon_control_surface_percent*entry_weight*

where:
elevon_control_surface_percent = .25 (fraction of exposed wing that is control surface)

Verticals EMAs =
.00428**verticals_control_surface_percent*entry_weight*

where:
verticals_control_surface_percent = .20 (fraction of exposed tails that is control surface)

13.0 Avionics

Avionics = 3300 lbs

notes:
fixed weight from NASP technology AMLS SSTO (Stanley)

14.0 Environmental Control

Personnel Systems = 141 lbs

notes:
based on AMLS SSTO (Stanley)

Equipment Cooling = 729 lbs

notes:
based on AMLS SSTO (Stanley)

Heat transport loop =
*shape_factor**6.79*(*vehicle_length*+*vehicle_width*+*vehicle_height*)

where:
shape_factor = .6 (radiators located in P/L bay doors for RBCC SSTO)

Heat rejection system = Radiators + Flash Evaporators

1) Radiators = 512 lbs

notes:
based on AMLS SSTO (Stanley)

2) Flash Evaporators = 163 lbs

notes:
based on AMLS SSTO (Stanley)

15.0 Personnel Equipment

Food(galley), water, waste management systems= 502 lbs

notes:
based on NASP technology AMLS (Stanley)

Seats, etc = 150**number_crew*

where:
number_crew = 2

notes:
seat weight based on historical seat weight data (Talay)

16.0 Dry Weight Margin

Dry weight margin = .10*dry_weight

notes:

use a 10% dry weight margin to account for growth and uncertainties (Stanley)

Dry Weight

$$\text{Dry Weight} = \sum_{i=1}^{16} w_i$$

17.0 Crew and Gear

Crew and Gear = 1176 + (311+23**mission_duration*)**number_crew*

where:
mission_duration = 2 days
number_crew = 2

notes:
includes crew consumables (food), personal items, crew, and suits (Talay)

18.0 Payload Provisions

Payload provisions = 0

notes:
payload specific items (special power supplies, umbilicals, etc) are charged to the payload

19.0 Cargo (up and down)

Payload = 10,000 lb

notes:
baseline mission is 10,000 lb delivery to polar orbit from VAFB

20.0 Residual Propellants

OMS/RCS residuals = .05**OMS/RCS_usable_propellant*

notes:
residuals trapped in tanks and lines is 5% of usable (not including reserves) for OMS/RCS

Main Propellant residuals = .005**usable_main_propellant*

notes:
residuals trapped in tanks and lines is 0.5% of usable (not including reserves) for main

21.0 OMS/RCS Reserve Propellants

OMS/RCS reserves = .10**OMS/RCS_usable_propellant*

notes:
OMS/RCS reserves are 10% of usable (not including reserves or residuals) propellants
OMS/RCS reserves are returned to the landing site

Landed Weight

$$\text{Landed Weight} = \sum_{i=1}^{21} w_i$$

22.0 RCS Entry Propellants

$$\text{RCS Entry Propellants} = landed\_weight * \left(e^{\frac{\Delta V_{RCS\_entry}}{Isp_{RCS} * g_c}} - 1 \right)$$

where:

ΔV_{RCS_entry} = 25 fps

Isp_{RCS} = 420 secs

g_c = 32.2 fps^2

notes:

RCS thruster Isp based on pressure-fed cryogenic thrusters from Rockwell IHOT work

LOX/LH2 proportions calculated using RCS thruster mixture ratio of O/F=4

distribution between fore and aft RCS calculated based on same ratio as on-orbit ΔV's

Entry Weight

$$\text{Entry Weight} = \sum_{i=1}^{22} w_i$$

23.0 RCS/OMS Propellants (on-orbit)

$$\textbf{Forward RCS Propellants} = entry\_weight * \left(e^{\frac{\Delta V_{RCS\_forward}}{Isp_{RCS} * g_c}} - 1 \right)$$

where:
$\Delta V_{RCS\_forward}$= 15 fps
Isp_{RCS} = 420 secs
g_c = 32.2 fps^2

notes:
RCS thruster Isp based on pressure-fed cryogenic thrusters from Rockwell IHOT work
LOX/LH2 proportions calculated using RCS thruster mixture ratio of O/F=4

$$\textbf{Aft RCS Propellants} = entry\_weight * \left(e^{\frac{\Delta V_{RCS\_aft}}{Isp_{RCS} * g_c}} - 1 \right)$$

where:
ΔV_{RCS_aft}= 35 fps
Isp_{RCS} = 420 secs
g_c = 32.2 fps^2

notes:
RCS thruster Isp based on pressure-fed cryogenic thrusters from Rockwell IHOT work
LOX/LH2 proportions calculated using RCS thruster mixture ratio of O/F=4

$$\textbf{OMS Propellants} = entry\_weight * \left(e^{\frac{\Delta V_{OMS}}{Isp_{RCS} * g_c}} - 1 \right)$$

where:
ΔV_{OMS} = varies depending on ascent trajectory (range 500 - 800 fps). Includes 50 fps on-orbit and 200 fps deorbit ΔV.
Isp_{RCS} = 462 secs
g_c = 32.2 fps^2

notes:
OMS engine Isp based on pump-fed cryogenic engine from Rockwell IHOT work
LOX/LH2 proportions calculated using OMS mixture ratio of O/F=6
OMS ΔV includes both circularization and deorbit burns

24.0 Cargo Discharged

Cargo discharged = 0

notes:
ascent cargo is also returned

25.0 Ascent Propellant Reserves

Main propellant reserves = .005**usable_main_propellants*

notes:
main propellant reserves are 0.5% of ascent (not residuals or reserves) propellants
main propellant reserves are vented on orbit or transferred to SSF (not returned to landing)

26.0 Inflight Losses and Vents

Inflight losses and vents = .10**entry_weight*

notes:
vents and losses include waste, purge gases, excess fuel cell reactants, etc

Insertion Weight

$$\text{Insertion Weight} = \sum_{i=1}^{26} w_i$$

27.0 Ascent Propellants

LH2 ascent propellant =

$$LH2\_prop\_fraction * gross\_weight * \left(1 - \frac{1}{mass\_ratio}\right)$$

where:

LH2_prop_fraction = LH2 ascent prop/total prop. (varies depending on engine and ascent)

mass_ratio = $(gross\ weight/insertion\ weight)_{required}$ (determined by ascent trajectory)

notes:

during the sizing process, the volume of the LH2 tank (and therefore the ascent prop. mass) is varied in order to match the actual vehicle mass ratio to the required mass ratio determined from the trajectory optimization program.

LH2 density = 4.43 lb/ft^3

LOX ascent propellant =

$$LH2\_ascent\_propellent * \left(\frac{1}{LH2\_prop\_fraction} - 1\right)$$

notes:

LOX ascent prop. mass (and therefore volume) is sized from LH2 ascent propellant

Gross (liftoff) Weight

Gross Weight = $\sum_{i=1}^{27} w_i$

28.0 Startup Losses

$$\text{Startup propellants} = 2 * gross\_weight * \frac{\left(\frac{T}{W}\right)_{vehicle\_liftoff}}{Isp_{sea\_level}}$$

notes:
4 second ramp-up from 0% to 100% throttle during hold down.
main propellant tanks also sized to hold start-up propellants (ratio of O/F determined by engine sea level mixture ratio)

Maximum Pre-launch Weight

$$\text{Maximum Pre-launch Weight} = \sum_{i=1}^{28} w_i$$

Appendix B

Engine Mass Estimating Relationships

Engine 10 Weight Equations (less inlet)
(No Supercharging Fan)

Assume: Rocket components scale with rocket prop. mass flow rate
Assume: Airbreathing components scale with mixer cross sectional area
Reference engine 10 (from reference NAS7-377, page 57):

Thrust = 250 klb, m_p = 563 lbm/s, A_{mixer} = 32 ft^2

Weight Adjustments (weights in lbs)

Component	NAS7-377 wgt.	Technology fact.*	New weight
Fan Assembly	N/A		N/A
Gas Generator	N/A		N/A
Struct. & Actuat.	N/A		N/A
Fan Cover Struct.	N/A		N/A
Primary Rockets	677	.81	548
Turbopumps	706	.81	572
Rocket structure	1254	.90	1129
Mixer**	852	.875	746
Diffuser**	432	.875	378
Combuster**	712	.875	623
Exit/Nozzle**	2172	.875***	1901
Total	6805		5897

Note: percentage weight margin added at vehicle level
* - from ref. AFAL-TR-88-004 page 88 (1985 reductions*1995 reductions)
** - increase by 15% to scale from 100 psi to 150 psi duct pressure
(based on engine 9 & engine 10 comparison)
*** - includes reduction to eliminate ref. engine centerbody

Rocket components = (primary rockets+turbopumps+rock. structure)
= 2249 lbs
= 2249/563 = 3.99 lb/lbm/s rocket prop. flow

A/B components = (other weights)
= 3648 lbs
= 3648/32 = 114 lbm/ft^2 mixer area

Engine 10 Wgt. = 3.99 lb/lbm/s rocket prop flow + 114 lb/ft2 mixer area

Engine 12 Weight Equations (less inlet) (with Supercharging Fan)

Assume: Rocket components scale with rocket prop. mass flow rate
Assume: Airbreathing components scale with mixer cross sectional area
Reference engine 12 (from reference NAS7-377, page 96):

Thrust = 250 klb, m_p = 501 lbm/s, A_{mixer} = 32 ft^2

Weight Adjustments (weights in lbs)

Component	NAS7-377 wgt.	Technology fact.*	New weight
Fan Assembly	1009	.88	888
Gas Generator	895	.88	788
Struct. & Actuat.	665	.88	585
Fan Cover Struct.	350	.88	308
Primary Rockets	602	.81	488
Turbopumps	661	.81	535
Rocket structure	1114	.90	1003
Mixer**	1081	.875	946
Diffuser**	432	.875	378
Combuster**	712	.875	623
Exit/Nozzle**	2172	.875***	1901
Total	9693		8443

Note: percentage weight margin added at vehicle level
* - from ref. AFAL-TR-88-004 page 88 (1985 reductions*1995 reductions)
** - increase by 15% to scale from 100 psi to 150 psi duct pressure (based on engine 9 & engine 10 comparison)
*** - includes reduction to eliminate ref. engine centerbody

Rocket components =(primary rockets+turbopumps+rock. structure)
= 2046 lbs
= 2046/501 = 4.04 lb/lbm/s rocket prop. flow

A/B components = (other weights)
= 6417 lbs
= 6417/32 = 200.5 lbm/ft^2 mixer area

Engine 12 Wgt. = 4.04 lb/lbm/s rocket prop flow + 200.5 lb/ft2 mixer area

Appendix C

Initial L_{27} Vehicle Datasheets

RBCC Single-stage-to-orbit Weights and Sizing
L27 Array Results

5 degree cone, VTO RBCC SSTO with engine #10
q = 2000 psf, Mtr =15, stag. heat rate = 350 BTU/sqft-sec

Vehicle Overall Parameters

Forebody cone half angle	5.00 deg	
Afterbody cone half angle	9.00 deg	
Mass Ratio (required)	3.834	
LH2 ascent/total ascent prop	0.354	
Forebody cone half angle	0.087 rads	
Afterbody cone half angle	0.157 rads	
Total vehicle length	186.54 ft	
Mass Ratio (actual)	3.834	Eng. Thrust
Gross Weight (actual)	416,015 lb	84713
Dry Weight (actual)	84,066 lb	
Landing c.g. (PA in)	107.75 ft	
Landing c.g. (PA out)	114.32 ft	
Gross Weight c.g. (PA in)	145.71 ft	

Nosecone Data

Nosecap Radius	0.50 ft
Structural unit weight	2.21 lb/ft2
Aft diameter	3.50 ft
Nosecone length	14.77 ft
Nosecone surface area	182.88 ft2
Nosecone volume	62.8 ft3

Crew Cabin Data

Crew cabin volume	768.8 ft3
Number of crew	2
Mission duration	2.00 days
Aft diameter	8.16 ft
Cabin length	26.66 ft

Payload Bay Data

PL bay volume	2888.6 ft3
PL bay struct. unit weight	2.21 lb/ft2
PL bay doors str. unit weight	3.50 lb/ft2
PL bay length	27.84 ft
PL bay doors surface area	465.32 ft2
PL bay area (excluding doors)	673.83 ft2

LH2 Main Tank Data

Eng. Exit 32.15

Aft diameter (incl. insulation)	32.15 ft
Tank structural unit weight	0.26 lb/ft2
Tank insulation unit weight	0.26 lb/ft2
Cryo insulation thickness	0.17 ft
Tank ullage volume/total vol	0.0425
LH2 density	4.43 lb/ft3
Tank dome height/radius	0.707
Fore diameter	13.96 ft
Fore dome height	4.81 ft
Aft dome height	7.84 ft
Tank surface area (total)	5567.6 ft2
Tank volume (total)	26245.2 ft3
Tank length	82.13 ft

LOX Main Tank Data

Tank structural unit weight	0.33 lb/ft2
Tank insulation unit weight	0.26 lb/ft2
Cryo insulation thickness	0.13 ft
Tank ullage volume/total vol	0.0425
LOX density	71.2 lb/ft3
Tank dome height/radius	0.707
Aft LH2 tank dome to LOX dome	3.00 ft
Fore diameter	16.84 ft
Fore dome height	5.86 ft
Aft diameter	13.86 ft
Aft dome height	4.81 ft
Tank surface area (total)	805.68 ft2
Tank volume (total)	2998.5 ft3
Tank length	20.22 ft

Tailcone/Base Data

Base diam/LH2 tank max diam	0.5
Tailcone struct. unit weight	2.21 lb/ft2
Base structural unit weight	1.00 lb/ft2
Base diameter	11.08 ft
Base area	96.44 ft2
Tailcone surface area	1040.42 ft2
Tailcone length	34.96 ft
Aft compartment volume	588.7 ft3

Engine Data

Vehicle sfleft T/W	1.40	
Total Engine length	32.14 ft	
Inlet section length	23.38 ft	
AB/Rocket Trans. Mach #	15.00	
Engine T/W (less cowl/inlet)	61.77	
Engine Isp (sea level)	424.4 sec	
Lift/f mixture (LOX/LH2)	6.00	
Ejectors weight %	0.41	
Fan/GG/stowage weight %	0.00	
Cowl wrap angle	180.00 deg	
Cowl strut/s separation angle	20.00 deg	
Cowl unit weight(non-inlet)	2.21 lb/ft2	
Inlet section unit wgt (lbp)	2.75 lb/ft2	
Inlet height	3.58 ft	Eng. Inlet 16.08
Engine inlet rel. area	144.71 ft2	
Cowl surface area	1298.55 ft2	
Cowl leading edge length	45.06 ft	
Max. inlet hgt. (shock on lip)	3.58 ft	

TPS Data

Nose cap active cooling weight	158.88 lb
Active cooling weight/length	2.78 lb/ft
Active cooling weight/area	3.58 lb/ft2
Tailcone active cooled length	2.00 ft
ACC area/body area	0.34
ACC area/wing&tail area	0.10
ACC unit weight	2.00 lb/ft2
Superalloy area/body area	0.40
Supraly. area/wing&tail area	0.00
Superalloy unit weight	1.00 lb/ft2
Titanium area/body area	0.00
Titanium standoff unit weight	0.51 lb/ft2
Body & cowl passive TPS area	8644.0 ft2
Wing (top&btm) wetted area	1438.92 ft2
Tail wetted area (both)	233.97 ft2
Nozzle exit active TPS area	137.26 ft2

Wing/Tail Data

Wing leading edge sweep	76.00 deg
Wing Aspect ratio	1.80
Landing weight/Sref	42.000
Landing speed	200 kias
Thes. wing c.p. loc. (%l_ref)	68.0%
Tail area(ea.)/wing ref. area	0.025
Wing thickness ratio	0.04
Cruise norm. lift/gross wgt	0.430
Wing Reference area	2336.7 ft2
Wing exposed planform	719.5 ft2
Tail planform area(each)	58.5 ft2
Wingspan	48.37 ft
Wing T.E. to body base length	28.08 ft
Wing exp. leading edge (ea.)	61.54 ft
Span through half-chords	108.16 ft
Theoretical center chord	96.74 ft
Thickness at expos. root chord	2.08 ft
Body diam@exp wing apex	16.58 ft
Landing wing loading	42.8 lb/ft2
Design(max.) wing limit load	437,315 lb

RCS Data

Forward RCS on-orbit ΔV	15 ft/sec
Aft RCS on-orbit ΔV	35 ft/sec
RCS Isp	420.0 sec
RCS mixture ratio (O/F)	4

Forward RCS

Total forward RCS LH2 prop.	37.67 lb
Forward RCS LH2 tank vol.	8.8 ft3
Forward RCS LH2 tank diam.	2.57 ft
Total forward RCS LOX prop.	150.67 lb
Forward RCS LOX tank vol.	2.2 ft3
Forward RCS LOX tank diam.	1.62 ft
Forward He tank diameter	1.72 ft

Aft RCS

Total aft RCS LH2 prop.	87.84 lb
Aft RCS LH2 tank vol.	20.6 ft3
Aft RCS LH2 tank diam.	3.41 ft
Total aft RCS LOX prop.	351.77 lb
Aft RCS LOX tank vol.	5.2 ft3
AFT RCS LOX tank diam.	2.15 ft
Aft He tank diameter	2.29 ft

OMS Data

OMS on-orbit ΔV (incl circ.)	650 ft/sec
OMS Isp	462.9 sec
OMS mixture ratio (O/F)	6
Total OMS LH2 prop.	722.36 lb
OMS LH2 tank vol.	171.2 ft3
OMS LH2 tank diam.	6.88 ft
Total OMS LOX prop.	4334.17 lb
OMS LOX tank vol.	63.8 ft3
OMS LOX tank diam.	4.86 ft
Aft He tank diameter	3.00 ft

Vehicle Weight Statement
5 degree cone, VTO RBCC SSTO with engine #10
q = 2000 psf, Mtr =15, stag. heat rate = 350 BTU/sqft-sec

	Level 3	Level 2	Level 1	local x c.g.	c.g. moment (i
1.0 Wing Group			3,912		
2.0 Tail Group			759	130.59	99152
3.0 Body Group			26,604	0.00	
4.0 Thermal Protection			11,740	0.00	
5.0 Landing Gear			2,555	0.00	0
6.0 Main Propulsion (less cowl)			16,776 lb	0.00	0
7.0 RCS Propulsion			965	0.00	
8.0 OMS Propulsion			1,062	0.00	
9.0 Primary Power			952	0.00	0
10.0 Electrical Conversion & Dist.			3,276	0.00	0
11.0 Hydraulic systems			0	0.00	0
12.0 Surface Control Actuation			481	0.00	0
13.0 Avionics			3,300	21.43	70717
14.0 Environmental control			2,494	0.00	
15.0 Personnel Equipment			802	0.00	
16.0 Dry Weight Margin (10%)			8,409		
				Dry weight c.g. (excl. margin)	
Dry Weight			**84,086**	115.02 ft	61.01%
17.0 Crew and Gear			1,890	28.09	53096
18.0 Payload Provisions			0	0.00	0
19.0 Cargo (up and down)			10,000	55.34	553412
20.0 Residual Propellents			1,798	0.00	
21.0 OMS/RCS Reserve Propellents			494	0.00	
				Landing weight c.g. (P/L in)	
Landed Weight			**98,269**	107.75 ft	57.15%
				Landing weight c.g. (P/L out)	
22.0 RCS Entry Propellents (ΔV = 25 fps)			182	114.32 ft	60.63%
				Entry weight c.g. (P/L in)	
Entry Weight			**98,450**	107.80 ft	57.18%
				Entry weight c.g. (P/L out)	
23.0 RCS/OMS Propellents (on-orbit)			4,761	114.35 ft	60.65%
24.0 Cargo Discharged			0	55.34	0
25.0 Ascent Reserve Propellents			1,551	0.00	
26.0 Inflight Losses and Vents			985	94.27	92810
				Insertion weight c.g. (P/L in)	
Insertion Weight			**105,748**	111.77 ft	59.28%
27.0 Ascent Propellents			310,267	0.00	
				Gross weight c.g. (P/L in)	
Gross Liftoff Weight			**416,015**	145.71 ft	77.28%
28.0 Startup Losses			2,745		
Maximum Pre-launch Weight			**418,760**		

Vehicle Weight Statement
5 degree cone, VTO RBCC SSTO with engine #10
q = 2000 psf, Mv =15, stag. heat rate = 350 BTU/sqft-sec

		Level 3	Level 2	Level 1	local x c.g.	c.g. moment /
1.0 Wing Group				3,912		
	Exposed wing		3,233		140.55	454368
	Carry through		679		140.55	95447
2.0 Tail Group				759	130.59	99152
3.0 Body Group				26,604	0.00	
	Nosecone		227		4.92	1119
	Crew Cabin		2,058		29.87	61462
	Payload Bay Structure		4,618		0.00	
	Structure	1,489			56.55	84220
	P/L Bay Doors	1,629			56.55	92093
	P/L Accommodations	1,500			55.34	83012
	LH2 Tank		8,140		0.00	
	Tank Structure	6,693			118.86	795470
	Tank Insulation	1,448			118.86	172065
	LOX Tank		1,160		0.00	
	Tank Structure	984			174.51	171629
	Tank Insulation	177			174.51	30819
	Aft Body		4,279		0.00	
	Tail cone	4,087			169.11	691178
	Base	192			188.54	36183
	Cowl		6,122		0.00	
	Cowl ring	5,980			137.49	822122
	Cowl struts	142			137.49	19575
4.0 Thermal Protection				11,740	0.00	
	Active Cooling		1,087		0.00	
	Nosecap	150			0.50	75
	Cowl leading edge	124			121.42	15099
	Wing leading edges	332			130.59	43409
	Engine nozzle exit	480			154.56	74264
	Advanced Carbon/Carbon		6,469		0.00	0
	Body/cowl	5,880			94.27	554341
	Wing/tails	589			122.55	72203
	Superalloy standoff		4,183		0.00	0
	Body/cowl	4,183			113.12	473212
	Wing/tails	0			128.21	0
	Titanium Standoff		0		0.00	0
	Body/cowl	0			141.41	0
	Wing/tails	0			133.86	0
5.0 Landing Gear				2,555	0.00	0
	Nosegear		383		55.34	21209
	Main gear		2,172		147.13	319531
6.0 Main Propulsion (less cowl)				16,776 lb	0.00	0
	RBCC Engines		13,944		0.00	0
	Ejector rockets (incl. pumps)	5,717			132.13	755383
	Diff./Comb./Noz. (w/ cooling	8,227			137.49	1131082
	Fan/gas generator/storage	0			132.13	0
	Pressurization and feed systems		2,218		161.40	357934
	Purge Systems		615		162.90	100158
7.0 RCS Propulsion				965	0.00	
	Forward RCS		244		0.00	
	Thrusters (15 pressure fed)	70			4.92	346
	Prop. tanks/empty(195 psia)	28			9.84	277
	He presant. tank(3000 psia)	86			7.38	636
	He pressurant	7			7.38	55
	Lines,manifolds,valves,etc.	52			4.92	256
	Aft RCS		720		0.00	
	Thrusters (22 pressure fed)	251			185.54	46498
	Prop. tanks/empty(195 psia)	66			181.54	11938
	He presant. tank(3000 psia)	201			181.54	36494
	He pressurant	17			181.54	3171
	Lines,manifolds,valves,etc.	185			181.54	33668
8.0 OMS Propulsion				1,062	0.00	
	Engines (4 pump fed)		280		188.54	52733
	Prop. tanks/empty(25 psia)		76		179.80	13697
	He presant. tank(3000 psia)		454		179.80	81613
	He pressurant (for low pressure tanks)		39		179.80	7060
	Lines,manifolds,valves,etc.		213		179.80	38218
9.0 Primary Power				952	0.00	0
	Fuel cells		396		69.26	27428
	Reactant dewers		531		69.26	36757
	Batteries		25		162.90	4050
10.0 Electrical Conversion & Dist.				3,276	0.00	0
	Power conversion and distribution		1,875		162.90	305428
	EMA controllers		156		157.45	24552
	Circuitry & wiring		1,196		62.85	75165
	EMA cabling		49		160.17	7853
11.0 Hydraulic systems				0	0.00	0
12.0 Surface Control Actuation				481	0.00	0
	Elevon EMAs		397		157.45	62510

	Verticals EMAs		84		157.45	13269
13.0 Avionics				3,300	21.43	70717
14.0 Environmental control				2,494	0.00	
	Personnel systems		141		28.09	3961
	Equipment cooling		729		28.09	20480
	Heat transport loop		949		41.42	39296
	Heat rejection system		675		0.00	0
	Radiators	512			55.34	28335
	Flash evaporators	163			55.34	9021
15.0 Personnel Equipment				802	0.00	
	Food, water, waste manag.		502		28.09	14103
	Seats, etc.		300		23.65	7095
16.0 Dry Weight Margin (10%)				8,409		
					Dry weight c.g.	(excl. margin)
Dry Weight				**84,086**	115.02 ft	61.01%
17.0 Crew and Gear				1,890	28.09	53096
18.0 Payload Provisions				0	0.00	0
19.0 Cargo (up and down)				10,000	55.34	553412
20.0 Residual Propellents				1,798	0.00	
	OMS/RCS residuals		247		0.00	
	Fore LH2 RCS residuals	2			9.84	16
	Fore LOX RCS residuals	7			9.84	64
	Aft LH2 RCS residuals	4			181.54	694
	Aft LOX RCS residuals	15			181.54	2777
	LH2 OMS residuals	31			179.80	5647
	LOX OMS residuals	188			179.80	33881
	Main Propellent residuals		1,551		0.00	
	LH2 residuals	549			123.25	67686
	LOX residuals	1,002			174.51	174884
21.0 OMS/RCS Reserve Propellents				494	0.00	
	RCS reserves		55		0.00	
	Fore LH2 reserves	3			9.84	32
	Fore LOX reserves	13			9.84	129
	Aft LH2 reserves	8			181.54	1388
	Aft LOX reserves	31			181.54	5553
	OMS reserves		440		0.00	0
	LH2 reserves	63			179.80	11294
	LOX reserves	377			179.80	67762
					Landing weight c.g.	(P/L in)
Landed Weight				**86,269**	107.75 ft	57.15%
					Landing weight c.g.	(P/L out)
22.0 RCS Entry Propellents (ΔV = 25 fps)				182	114.32 ft	60.63%
	Forward RCS Propellents		55		0.00	
	LH2	11			9.84	107
	LOX	44			9.84	429
	Aft RCS Propellents		127		0.00	0
	LH2	25			181.54	4620
	LOX	102			181.54	18480
					Entry weight c.g.	(P/L in)
Entry Weight				**86,450**	107.80 ft	57.18%
					Entry weight c.g.	(P/L out)
23.0 RCS/OMS Propellents (on-orbit)				4,761	114.35 ft	60.65%
	Forward RCS Propellents		109		0.00	
	LH2	22			9.84	215
	LOX	87			9.84	860
	Aft RCS Propellents		255		0.00	0
	LH2	51			181.54	9263
	LOX	204			181.54	37052
	OMS Propellents		4,397		0.00	0
	LH2	628			179.80	112937
	LOX	3,769			179.80	677622
24.0 Cargo Discharged				0	55.34	0
25.0 Ascent Reserve Propellents				1,551	0.00	
	LH2 reserves		549		123.25	67686
	LOX reserves		1,002		174.51	174884
26.0 Inflight Losses and Vents				985	94.27	92810
Insertion Weight				**105,748**	Insertion weight c.g.	(P/L in)
					111.77 ft	59.28%
27.0 Ascent Propellents				310,267	0.00	
	LH2 ascent		109,835		123.25	13537101
	LOX ascent		200,433		174.51	34976832
Gross Liftoff Weight				**416,015**	Gross weight c.g.	(P/L in)
					145.71 ft	77.28%
28.0 Startup Losses				2,745		
	LH2 startup		392			
	LOX startup		2,353			
Maximum Pre-launch Weight				**418,760**		

			Engine 10 (No Fan)				
mp (lbm/s)	146.15	129.91	Engine Performance				
A max inlet	16.08						
A max exit	32.15		Primary area ratio	18		eta Ustar	0.980
Astar ejt/A max inlet	0.35		Primary Ae (ft2)	2.04		eta primary	0.975
Max inlet height (ft)	3.58		Primary Pc (psi)	2000		eta mixer	0.900
Max. Mach number	15		Primary ho (BTU/lbm)	5550		eta combustor	0.950
Astar ejector	4.90		Primary Ustar (fps)	13340		eta nozzle	0.980
A4 (ft2)	13.98						
A4/A3	2.00		Inlet length (ft)	23.36			
A3 (ft2)	6.99		Total engine length (ft)	32.14			
Fuel Ho (BTU/lbm)	50000						
Cone Half angle	5		**Weight (no inlet)(lb)**	**1549.83**			
			Engine T/W (SLS)	**41.77**			
Altitude (ft)	0		Ejector% Weight	0.41			
Pa (psi)	14.7		Fan % Weight	0.00			
Tinf (°R)	519						
Minf	Uinf (fps)	Thrust (lb)	Isp (sec)	Toinf (°R)	hoinf (BTU/lbm	Poinf (psi)	Approx Beta (deg
0.00	0.00	64,730	424.43	519.00	124.56	14.70	0.00
0.25	279.16	63,792	417.65	525.49	126.12	15.35	0.00
0.50	558.31	63,601	415.49	544.95	130.79	17.44	0.00
0.75	837.47	65,038	423.01	577.39	138.57	21.35	0.00
1.00	1116.62	68,680	443.26	622.80	149.47	27.83	0.00
1.25	1395.78	75,542	481.31	681.19	163.49	38.08	0.00
1.50	1674.93	87,954	548.63	752.55	180.61	53.96	42.34
1.75	1954.09	108,049	651.18	836.89	200.85	78.26	35.40

Appendix D

Robust Vehicle Design Datasheets

RBCC Single-stage-to-orbit Weights and Sizing
Taguchi Robust Design

5 degree cone, VTO RBCC SSTO with engine #10
q = 2000 psf, Mtr =12, stag. heat rate = 350 BTU/sqft-sec

Vehicle Overall Parameters

Forebody cone half angle	5.00 deg	
Afbody cone half angle	7.50 deg	
Mass Ratio (required)	4.393	
LH2 ascent/total ascent prop	0.761	
Forebody cone half angle	0.087 rads	
Afbody cone half angle	0.131 rads	
Total vehicle length	188.06 ft	
Mass Ratio (actual)	4.383	Eng. Thrust
Gross Weight (actual)	506,576 lb	67543
Dry Weight (actual)	92,486 lb	
Landing c.g. (FA in)	113.71 ft	
Landing c.g. (FA out)	119.38 ft	
Gross Weight c.g. (FA in)	156.18 ft	

Nosecone Data

Nosecap Radius	0.50 ft
Structural unit weight	2.21 lb/ft2
Aft diameter	2.58 ft
Nosecone length	14.77 ft
Nosecone surface area	102.88 ft2
Nosecone volume	62.8 ft3

Crew Cabin Data

Crew cabin volume	760.8 ft3
Number of crew	2.
Mission duration	2.00 days
Aft diameter	8.16 ft
Cabin length	26.66 ft

Payload Bay Data

PL bay volume	6300.0 ft3
PL bay struct. unit weight	2.21 lb/ft2
PL bay doors str. unit weight	1.50 lb/ft2
PL bay length	44.71 ft
PL bay doors surface area	851.36 ft2
PL bay area (excluding doors)	1185.16 ft2

LH2 Main Tank Data

		Eng. Exit
Aft diameter (incl. insulation)	22.30 ft	37.32
Tank structural unit weight	0.28 lb/ft2	
Tank insulation unit weight	0.20 lb/ft2	
Cryo insulation thickness	0.17 ft	
Tank ullage volume/total vol.	0.0425	
LH2 density	4.43 lb/ft3	
Tank dome height/radius	0.707	
Fore diameter	17.04 ft	
Fore dome height	6.03 ft	
Aft dome height	7.86 ft	
Tank surface area (total)	4954.6 ft2	
Tank volume (total)	24413.8 ft3	
Tank length	77.49 ft	

LOX Main Tank Data

Tank structural unit weight	0.33 lb/ft2
Tank insulation unit weight	0.20 lb/ft2
Cryo insulation thickness	0.13 ft
Tank ullage volume/total vol.	0.0425
LOX density	71.9 lb/ft3
Tank dome height/radius	0.707
Aft LH2 tank dome to LOX da	3.00 ft
Fore diameter	17.78 ft
Fore dome height	6.29 ft
Aft diameter	13.86 ft
Aft dome height	4.90 ft
Tank surface area (total)	1224.30 ft2
Tank volume (total)	4312.1 ft3
Tank length	26.87 ft

Tailcone/Base Data

Base diam/LH2 tank max diam	0.5
Tailcone struct. unit weight	2.21 lb/ft2
Base structural unit weight	1.88 lb/ft2
Base diameter	11.15 ft
Base area	97.64 ft2
Tailcone surface area	2244.21 ft2
Tailcone length	42.35 ft
Aft compartment volume	776.5 ft3

Engine Data

Vehicle liftoff T/W	1.20	
Total Engine length	33.53 ft	
Inlet section length	23.40 ft	
AB/Rocket Trans. Mach #	12.00	
Engine T/W (sea cav/Area)	46.90	
Engine Isp (sea level)	472.8 sec	
Lift/Jet mixture (LOX/LH2)	6.00	
Ejectors weight %	0.17	
Fan/GG/stowage weight %	0.00	
Cowl wrap angle	180.00 deg	
Cowl strut/i separation angle	90.00 deg	
Cowl unit weight(non-inlet)	2.21 lb/ft2	
Inlet section unit wgt (top)	2.73 lb/ft2	
Inlet height	4.50 ft	
		Eng. Inlet
Engine inlet ref. area	188.44 ft2	21.85
Cowl surface area	1411.52 ft2	
Cowl leading edge length	49.17 ft	
Max. inlet hgt. (shock on lip)	4.87 ft	

TPS Data

Nose cap active cooling weigh	150.00 lb
Active cooling weight/length	2.70 lb/ft
Active cooling weight/area	2.50 lb/ft2
Tailcone active cooled length	2.00 ft
ACC area/body area	0.33
ACC area/wing&tail area	0.18
ACC unit weight	2.00 lb/ft2
Superalloy area/body area	0.34
Supraly. area/wing&tail area	0.00
Superalloy unit weight	1.00 lb/ft2
Titanium area/body area	0.00
Titanium standoff unit weight	0.51 lb/ft2
Body & cowl passive TPS area	8261.8 ft2
Wing (top&bott) wetted area	1863.00 ft2
Tail wetted area (both)	255.05 ft2
Nozzle exit active TPS area	138.47 ft2

Wing/Tail Data

Wing leading edge sweep	78.00 deg
Wing Aspect ratio	1.80
Landing weight/Sref	42.000
Landing speed	200 knots
Theo. wing c.p. loc. (%l_ref)	66.8%
Tail area(ea.)/wing ref. area	0.025
Wing thickness ratio	0.04
Cruise norm. force/gross wgt	0.427
Wing Reference area	2558.5 ft2
Wing exposed planform	831.5 ft2
Tail planform area(each)	63.8 ft2
Wingspan	50.50 ft
Wing T.E. to body base length	29.72 ft
Wing exp. leading edge (ea.)	63.93 ft
Span through half-chords	112.93 ft
Theoretical center chord	101.00 ft
Thickness of expos. root cho	2.25 ft
Body diam@exp wing apex	18.57 ft
Landing wing loading	42.0 lb/ft2
Design(max.) wing limit load	525,218 lb

RCS Data

Forward RCS on-orbit ΔV	15 ft/sec
Aft RCS on-orbit ΔV	35 ft/sec
RCS Isp	420.0 sec
RCS mixture ratio (O/F)	4
Forward RCS	
Total forward RCS LH2 prop.	41.06 lb
Forward RCS LH2 tank vol.	8.7 ft3
Forward RCS LH2 tank diam.	2.65 ft
Total forward RCS LOX prop.	164.24 lb
Forward RCS LOX tank vol.	2.4 ft3
Forward RCS LOX tank diam.	1.67 ft
Forward He tank diameter	1.77 ft
Aft RCS	
Total aft RCS LH2 prop.	85.86 lb
Aft RCS LH2 tank vol.	22.7 ft3
Aft RCS LH2 tank diam.	3.51 ft
Total aft RCS LOX prop.	343.45 lb
Aft RCS LOX tank vol.	5.7 ft3
AFT RCS LOX tank diam.	2.21 ft
Aft He tank diameter	2.35 ft

OMS Data

OMS on-orbit ΔV (incl circ.)	820 ft/sec
OMS Isp	462.0 sec
OMS mixture ratio (O/F)	6
Total OMS LH2 prop.	758.32 lb
OMS LH2 tank vol.	177.8 ft3
OMS LH2 tank diam.	6.96 ft
Total OMS LOX prop.	4561.90 lb
OMS LOX tank vol.	66.4 ft3
OMS LOX tank diam.	5.02 ft
Aft He tank diameter	3.04 ft

Vehicle Weight Statement
5 degree cone, VTO RBCC SSTO with engine #10
q = 2000 psf, Mfr =12, stag. heat rate = 350 BTU/sqft-sec

	Level 3	Level 2	Level 1	local x c.g.	c.g. moment /i
1.0 Wing Group			4,715		
2.0 Tail Group			834	137.35	114562
3.0 Body Group			32,136	0.00	
4.0 Thermal Protection			11,297	0.00	
5.0 Landing Gear			2,785	0.00	0
6.0 Main Propulsion (less cowl)			17,809 lb	0.00	0
7.0 RCS Propulsion			1,082	0.00	
8.0 OMS Propulsion			1,128	0.00	
9.0 Primary Power			954	0.00	0
10.0 Electrical Conversion & Dist.			3,347	0.00	0
11.0 Hydraulic systems			0	0.00	0
12.0 Surface Control Actuation			525	0.00	0
13.0 Avionics			3,300	21.43	70717
14.0 Environmental control			2,534	0.00	
15.0 Personnel Equipment			802	0.00	
16.0 Dry Weight Margin (10%)			9,250		
				Dry weight c.g. (excl. margin)	
Dry Weight			**92,498**	**119.78 ft**	**60.47%**
17.0 Crew and Gear			1,890	28.09	53096
18.0 Payload Provisions			0	0.00	0
19.0 Cargo (up and down)			10,000	63.78	637768
20.0 Residual Propellents			2,214	0.00	
21.0 OMS/RCS Reserve Propellents			516	0.00	
				Landing weight c.g. (P/L in)	
Landed Weight			**107,119**	**113.71 ft**	**57.40%**
				Landing weight c.g. (P/L out)	
22.0 RCS Entry Propellents (ΔV = 25 fps)			198	**119.39 ft**	**60.27%**
				Entry weight c.g. (P/L in)	
Entry Weight			**107,317**	**113.75 ft**	**57.43%**
				Entry weight c.g. (P/L out)	
23.0 RCS/OMS Propellents (on-orbit)			4,964	**119.43 ft**	**60.29%**
24.0 Cargo Discharged			0	63.78	0
25.0 Ascent Reserve Propellents			1,956	0.00	
26.0 Inflight Losses and Vents			1,073	99.04	106289
				Insertion weight c.g. (P/L in)	
Insertion Weight			**115,311**	**117.84 ft**	**59.49%**
27.0 Ascent Propellents			391,265	0.00	
				Gross weight c.g. (P/L in)	
Gross Liftoff Weight			**506,576**	**156.10 ft**	**78.80%**
28.0 Startup Losses			2,881		
Maximum Pre-launch Weight			**509,457**		

Vehicle Weight Statement
5 degree cone, VTO RBCC SSTO with engine #18
q = 2000 psf, Mtr =12, stag. heat rate = 350 BTU/sqft-sec

			Level 3	Level 2	Level 1	local x c.g.	c.g. moment /i
1.0 Wing Group					4,715		
	Exposed wing			3,894		147.69	575113
	Carry through			821		147.69	121304
2.0 Tail Group					834	137.35	114562
3.0 Body Group					32,136	0.00	
	Nosecone			227		4.92	1119
	Crew Cabin			2,058		29.67	61462
	Payload Bay Structure			7,055		0.00	
		Structure	2,575			66.40	170984
		P/L Bay Doors	2,980			66.40	197861
		P/L Accommodations	1,500			63.78	95665
	LH2 Tank			7,513		0.00	
		Tank Structure	6,225			126.65	788439
		Tank Insulation	1,288			126.65	163150
	LOX Tank			1,653		0.00	
		Tank Structure	1,414			179.66	254101
		Tank Insulation	239			179.66	42891
	Aft Body			5,154		0.00	
		Tail cone	4,960			174.56	865760
		Base	194			198.08	38490
	Cowl			8,475		0.00	
		Cowl ring	6,373			138.97	885654
		Cowl struts	2,102			138.97	292187
4.0 Thermal Protection					11,297	0.00	
	Active Cooling			1,113		0.00	
		Nosecap	150			0.50	75
		Cowl leading edge	133			122.21	16223
		Wing leading edges	345			137.35	47416
		Engine nozzle exit	485			156.74	75965
	Advanced Carbon/Carbon			6,835		0.00	0
		Body/cowl	6,205			99.04	614588
		Wing/tails	630			128.75	81103
	Superalloy standoff			3,350		0.00	0
		Body/cowl	3,350			118.85	398098
		Wing/tails	0			134.79	0
	Titanium Standoff			0		0.00	0
		Body/cowl	0			148.56	0
		Wing/tails	0			140.64	0
5.0 Landing Gear					2,785	0.00	0
	Nosegear			418		63.78	26644
	Main gear			2,367		149.03	352808
6.0 Main Propulsion (less cowl)					17,809 lb	0.00	0
	RBCC Engines			14,863		0.00	0
		Ejector rockets (incl. pumps)	5,499			133.38	733518
		Diff./Comb./Noz. (w/ cooling	9,364			138.97	1301291
		Fan/gas generator/storage	0			133.38	0
	Pressurization and feed systems			2,328		163.62	380934
	Purge Systems			618		165.12	101983
7.0 RCS Propulsion					1,082	0.00	
	Foreward RCS			273		0.00	
		Thrusters (15 pressure fed)	81			4.92	397
		Prop. tanks/empty(195 psia)	31			9.84	302
		He pressnt. tank(3000 psia)	94			7.38	693
		He pressurant	8			7.38	60
		Lines,manifolds,valves,etc.	60			4.92	294
	Aft RCS			809		0.00	
		Thrusters (22 pressure fed)	287			195.08	55991
		Prop. tanks/empty(195 psia)	72			189.62	13591
		He pressnt. tank(3000 psia)	219			189.62	41549
		He pressurant	19			189.62	3610
		Lines,manifolds,valves,etc.	212			189.62	40272
8.0 OMS Propulsion					1,128	0.00	
	Engines (4 pump fed)			305		198.08	60392
	Prop. tanks/empty(25 psia)			79		187.50	14837
	He pressnt. tank(3000 psia)			471		187.50	88403
	He pressurant (for low pressure tanks)			41		187.50	7647
	Lines,manifolds,valves,etc.			232		187.50	43445
9.0 Primary Power					954	0.00	0
	Fuel cells			396		86.13	34109
	Reactant dewers			531		86.13	45711
	Batteries			27		165.12	4475
10.0 Electrical Conversion & Dist.					3,347	0.00	0
	Power conversion and distribution			1,875		165.12	309605
	EMA controllers			170		165.37	28109
	Circuitry & wiring			1,246		66.03	82299
	EMA cabling			56		165.24	9267
11.0 Hydraulic systems					0	0.00	0
12.0 Surface Control Actuation					525	0.00	0
	Elevon EMAs			433		165.37	71563

	Verticals EMAs		92		165.37	15191
13.0 Avionics				3,300	21.43	70717
14.0 Environmental control				2,534	0.00	
	Personnel systems		141		28.09	3961
	Equipment cooling		729		28.09	20480
	Heat transport loop		989		41.42	40953
	Heat rejection system		675		0.00	0
	Radiators	512			63.78	32654
	Flash evaporators	163			63.78	10396
15.0 Personnel Equipment				802	0.00	
	Food, water, waste manag.		502		28.09	14103
	Seats, etc.		300		23.65	7095
16.0 Dry Weight Margin (10%)				9,250		
					Dry weight c.g.	(excl. margin)
Dry Weight				**92,498**	**119.78 ft**	**60.47%**
17.0 Crew and Gear				1,890	28.09	53096
18.0 Payload Provisions				0	0.00	0
19.0 Cargo (up and down)				10,000	63.78	637768
20.0 Residual Propellents				2,214	0.00	
	OMS/RCS residuals		258		0.00	
	Fore LH2 RCS residuals	2			9.84	18
	Fore LOX RCS residuals	7			9.84	70
	Aft LH2 RCS residuals	4			189.62	790
	Aft LOX RCS residuals	17			189.62	3161
	LH2 OMS residuals	33			187.50	6117
	LOX OMS residuals	196			187.50	36700
	Main Propellent residuals		1,956		0.00	
	LH2 residuals	511			129.14	65941
	LOX residuals	1,446			179.66	259733
21.0 OMS/RCS Reserve Propellents				516	0.00	
	RCS reserves		60		0.00	
	Fore LH2 reserves	4			9.84	35
	Fore LOX reserves	14			9.84	141
	Aft LH2 reserves	8			189.62	1581
	Aft LOX reserves	33			189.62	6322
	OMS reserves		457		0.00	0
	LH2 reserves	65			187.50	12233
	LOX reserves	391			187.50	73400
					Landing weight c.g.	(P/L in)
Landed Weight				**107,119**	**113.71 ft**	**57.40%**
					Landing weight c.g.	(P/L out)
22.0 RCS Entry Propellents (ΔV = 25 fps)				198	**119.38 ft**	**60.27%**
	Forward RCS Propellents		59		0.00	
	LH2	12			9.84	117
	LOX	48			9.84	468
	Aft RCS Propellents		139		0.00	0
	LH2	28			189.62	5260
	LOX	111			189.62	21040
					Entry weight c.g.	(P/L in)
Entry Weight				**107,317**	**113.75 ft**	**57.43%**
					Entry weight c.g.	(P/L out)
23.0 RCS/OMS Propellents (on-orbit)				4,964	**119.43 ft**	**60.29%**
	Forward RCS Propellents		119		0.00	
	LH2	24			9.84	234
	LOX	95			9.84	938
	Aft RCS Propellents		278		0.00	0
	LH2	56			189.62	10546
	LOX	222			189.62	42185
	OMS Propellents		4,567		0.00	0
	LH2	652			187.50	122333
	LOX	3,915			187.50	733996
24.0 Cargo Discharged				0	63.78	0
25.0 Ascent Reserve Propellents				1,956	0.00	
	LH2 reserves		511		129.14	65941
	LOX reserves		1,446		179.66	259733
26.0 Inflight Losses and Vents				1,073	99.04	106289
Insertion Weight				**115,311**	Insertion weight c.g.	(P/L in)
					117.84 ft	**59.49%**
27.0 Ascent Propellents				391,265	0.00	
	LH2 ascent		102,120		129.14	13188147
	LOX ascent		289,145		179.66	51946679
Gross Liftoff Weight				**506,576**	Gross weight c.g.	(P/L in)
					156.10 ft	**78.80%**
28.0 Startup Losses				2,881		
	LH2 startup		412			
	LOX startup		2,470			
Maximum Pre-launch Weight				**509,457**		

			Engine 10 (No Fan)				
mp (lbm/s)	152.4	135.47	Engine Performance				
A max inlet	21.05						
A max exit	37.32		Primary area ratio	18		eta Ustar	0.980
Astar ejt/A max inlet	0.35		Primary Ae (ft2)	2.13		eta primary	0.975
Max inlet height (ft)	4.5		Primary Pc (psi)	2000		eta mixer	0.900
Max. Mach number	12		Primary ho (BTU/lbm)	5550		eta combustor	0.950
Astar ejector	6.95		Primary Ustar (fps)	13340		eta nozzle	0.980
A4 (ft2)	18.30						
A4/A3	2.00		Inlet length (ft)	23.49			
A3 (ft2)	9.15		Total engine length (ft)	33.53			
Fuel Ho (BTU/lbm)	50000						
Cone Half angle	5		**Weight (no inlet)(lb)**	**1651.42**			
			Engine T/W (SLS)	**40.90**			
Altitude (ft)	0		Ejector% Weight	0.37			
Pa (psi)	14.7		Fan % Weight	0.00			
Tinf (°R)	519						
Minf	Uinf (fps)	Thrust (lb)	Isp (sec)	Toinf (°R)	hoinf (BTU/lbm	Poinf (psi)	Approx Beta (deg
0.00	0.00	67,541	422.01	519.00	124.56	14.70	0.00
0.25	279.16	66,024	412.11	525.49	126.12	15.35	0.00
0.50	558.31	66,442	413.34	544.95	130.79	17.44	0.00
0.75	837.47	69,148	427.40	577.39	138.57	21.35	0.00
1.00	1116.62	74,989	458.35	622.80	149.47	27.83	0.00
1.25	1395.78	85,546	513.21	681.19	163.49	38.08	0.00
1.50	1674.93	104,416	607.51	752.55	180.61	53.96	42.34
1.75	1954.09	135,274	749.10	836.89	200.85	78.26	35.40

Appendix E

CCD (w/ RSM) Vehicle Datasheets

RBCC Single-stage-to-orbit Weights and Sizing
CCD/RSM - Best Dry Weight

5 degree cone, VTO RBCC SSTO with engine #10
q = 2000 psf, Mir =14.6, stag. heat rate = 350 BTU/sqft-sec

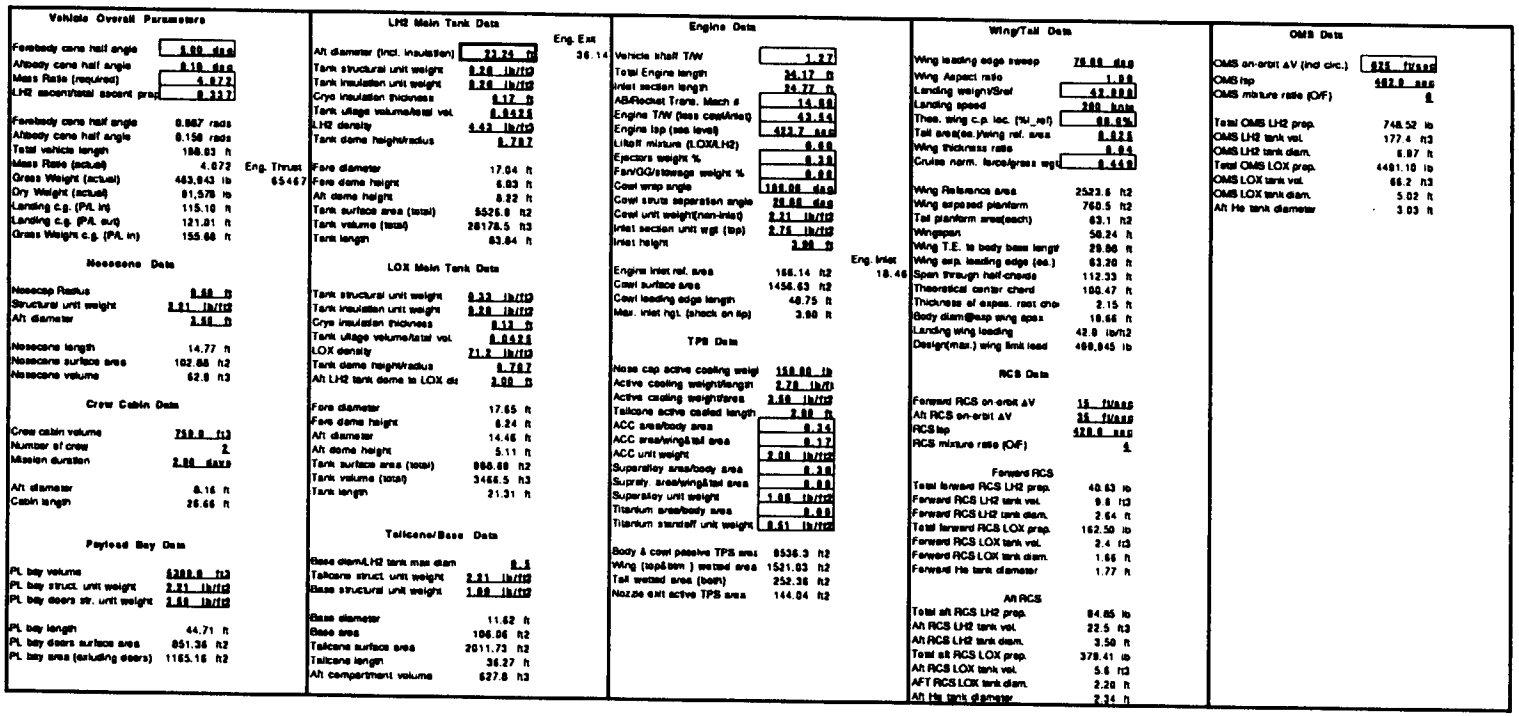

Vehicle Overall Parameters

Forebody cone half angle	5.00 deg	
Afterbody cone half angle	8.10 deg	
Mass Ratio (required)	4.072	
LH2 ascent/total ascent prop	0.337	
Forebody cone half angle	0.087 rads	
Afterbody cone half angle	0.150 rads	
Total vehicle length	188.83 ft	
Mass Ratio (actual)	4.072	Eng. Thrust 6546.7
Gross Weight (actual)	463,843 lb	
Dry Weight (actual)	81,578 lb	
Landing c.g. (P/L in)	115.10 ft	
Landing c.g. (P/L out)	121.01 ft	
Gross Weight c.g. (P/L in)	155.66 ft	

Nosecone Data

Nosecap Radius	0.50 ft
Structural unit weight	2.21 lb/ft2
Aft diameter	3.50 ft
Nosecone length	14.77 ft
Nosecone surface area	102.86 ft2
Nosecone volume	62.8 ft3

Crew Cabin Data

Crew cabin volume	750.0 ft3
Number of crew	2
Mission duration	2.00 days
Aft diameter	8.16 ft
Cabin length	26.66 ft

Payload Bay Data

PL bay volume	4388.0 ft3
PL bay struct. unit weight	2.21 lb/ft2
PL bay doors str. unit weight	1.66 lb/ft2
PL bay length	44.71 ft
PL bay doors surface area	851.36 ft2
PL bay area (excluding doors)	1165.16 ft2

LH2 Main Tank Data

		Eng. Exit 36.14
Aft diameter (incl. insulation)	21.24 ft	
Tank structural unit weight	0.26 lb/ft2	
Tank insulation unit weight	0.26 lb/ft2	
Cryo insulation thickness	0.17 ft	
Tank ullage volume/total vol.	0.0425	
LH2 density	4.43 lb/ft3	
Tank dome height/radius	0.707	
Fore diameter	17.04 ft	
Fore dome height	6.03 ft	
Aft dome height	8.22 ft	
Tank surface area (total)	5526.9 ft2	
Tank volume (total)	28178.5 ft3	
Tank length	83.84 ft	

LOX Main Tank Data

Tank structural unit weight	0.33 lb/ft2
Tank insulation unit weight	0.26 lb/ft2
Cryo insulation thickness	0.13 ft
Tank ullage volume/total vol.	0.0425
LOX density	71.2 lb/ft3
Tank dome height/radius	0.707
Aft LH2 tank dome to LOX dome	3.00 ft
Fore diameter	17.65 ft
Fore dome height	8.24 ft
Aft diameter	14.46 ft
Aft dome height	5.11 ft
Tank surface area (total)	986.88 ft2
Tank volume (total)	3466.5 ft3
Tank length	21.31 ft

Tailcone/Base Data

Base diam/LH2 tank max diam	0.5
Tailcone struct. unit weight	2.21 lb/ft2
Base structural unit weight	1.66 lb/ft2
Base diameter	11.62 ft
Base area	106.06 ft2
Tailcone surface area	2011.73 ft2
Tailcone length	36.27 ft
Aft compartment volume	627.8 ft3

Engine Data

Vehicle shelf T/W	1.27	
Total Engine length	34.17 ft	
Inlet section length	24.77 ft	
AB/Rocket Trans. Mach #	14.60	
Engine T/W (less cowl/inlet)	43.54	
Engine Isp (sea level)	453.7 sec	
Liftoff mixture (LOX/LH2)	6.00	
Ejectors weight %	0.30	
Fan/GG/stowage weight %	0.00	
Cowl wrap angle	180.00 deg	
Cowl struts separation angle	20.00 deg	
Cowl unit weight(non-inlet)	2.21 lb/ft2	
Inlet section unit wgt (isp)	2.76 lb/ft2	
Inlet height	3.00 ft	
		Eng. Inlet 18.46
Engine inlet ref. area	166.14 ft2	
Cowl surface area	1456.63 ft2	
Cowl leading edge length	48.75 ft	
Max. inlet hgt. (shock on lip)	3.00 ft	

TPS Data

Nose cap active cooling weight	158.00 lb
Active cooling weight/length	2.70 lb/ft
Active cooling weight/area	2.50 lb/ft2
Tailcone active cooled length	2.00 ft
ACC area/body area	0.34
ACC area/wing&tail area	0.17
ACC unit weight	2.00 lb/ft2
Superalloy area/body area	0.30
Supraly. area/wing&tail area	0.00
Superalloy unit weight	1.00 lb/ft2
Titanium area/body area	0.00
Titanium standoff unit weight	0.61 lb/ft2
Body & cowl passive TPS area	8536.3 ft2
Wing (top&btm) wetted area	1521.03 ft2
Tail wetted area (both)	252.36 ft2
Nozzle ext active TPS area	144.04 ft2

Wing/Tail Data

Wing leading edge sweep	78.69 deg
Wing Aspect ratio	1.80
Landing weight/Sref	42.000
Landing speed	200 knots
Thes. wing c.p. loc. (%l_ref)	68.6%
Tail area(ea.)/wing ref. area	0.025
Wing thickness ratio	0.04
Cruise norm. force/gross wgt	0.449
Wing Reference area	2523.6 ft2
Wing exposed planform	760.5 ft2
Tail planform area(each)	63.1 ft2
Wingspan	58.24 ft
Wing T.E. to body base length	29.86 ft
Wing exp. leading edge (ea.)	63.20 ft
Span through half-chords	112.33 ft
Theoretical center chord	100.47 ft
Thickness at expos. root chord	2.15 ft
Body diam@exp wing apex	18.66 ft
Landing wing loading	42.0 lb/ft2
Design(max.) wing limit load	498,845 lb

RCS Data

Forward RCS on-orbit ΔV	15 ft/sec
Aft RCS on-orbit ΔV	35 ft/sec
RCS Isp	420.0 sec
RCS mixture ratio (O/F)	4
Forward RCS	
Total forward RCS LH2 prop.	40.63 lb
Forward RCS LH2 tank vol.	9.8 ft3
Forward RCS LH2 tank diam.	2.64 ft
Total forward RCS LOX prop.	162.50 lb
Forward RCS LOX tank vol.	2.4 ft3
Forward RCS LOX tank diam.	1.66 ft
Forward He tank diameter	1.77 ft
Aft RCS	
Total aft RCS LH2 prop.	84.85 lb
Aft RCS LH2 tank vol.	22.5 ft3
Aft RCS LH2 tank diam.	3.50 ft
Total aft RCS LOX prop.	378.41 lb
Aft RCS LOX tank vol.	5.6 ft3
AFT RCS LOX tank diam.	2.28 ft
Aft He tank diameter	2.34 ft

OMS Data

OMS on-orbit ΔV (incl circ.)	825 ft/sec
OMS Isp	462.0 sec
OMS mixture ratio (O/F)	6
Total OMS LH2 prop.	748.52 lb
OMS LH2 tank vol.	177.4 ft3
OMS LH2 tank diam.	6.87 ft
Total OMS LOX prop.	4481.10 lb
OMS LOX tank vol.	66.2 ft3
OMS LOX tank diam.	5.02 ft
Aft He tank diameter	3.03 ft

Vehicle Weight Statement
5 degree cone, VTO RBCC SSTO with engine #10
q = 2000 psf, Mtr =14.6, stag. heat rate = 350 BTU/sqft-sec

	Level 3	Level 2	Level 1	local x c.g.	c.g. moment /i
1.0 Wing Group			4,402		
2.0 Tail Group			825	137.49	113360
3.0 Body Group			32,564	0.00	
4.0 Thermal Protection			11,764	0.00	
5.0 Landing Gear			2,756	0.00	0
6.0 Main Propulsion (less cowl)			16,447 lb	0.00	0
7.0 RCS Propulsion			1,071	0.00	
8.0 OMS Propulsion			1,121	0.00	
9.0 Primary Power			954	0.00	0
10.0 Electrical Conversion & Dist.			3,354	0.00	0
11.0 Hydraulic systems			0	0.00	0
12.0 Surface Control Actuation			519	0.00	0
13.0 Avionics			3,300	21.43	70717
14.0 Environmental control			2,541	0.00	
15.0 Personnel Equipment			802	0.00	
16.0 Dry Weight Margin (10%)			9,158		
				Dry weight c.g. (excl. margin)	
Dry Weight			**91,578**	**121.59 ft**	**61.40%**
17.0 Crew and Gear			1,890	28.09	53096
18.0 Payload Provisions			0	0.00	0
19.0 Cargo (up and down)			10,000	63.78	637768
20.0 Residual Propellents			2,007	0.00	
21.0 OMS/RCS Reserve Propellents			515	0.00	
				Landing weight c.g. (P/L in)	
Landed Weight			**105,989**	**115.10 ft**	**58.12%**
				Landing weight c.g. (P/L out)	
22.0 RCS Entry Propellents (ΔV = 25 fps)			196	121.01 ft	61.10%
				Entry weight c.g. (P/L in)	
Entry Weight			**106,185**	**115.14 ft**	**58.14%**
				Entry weight c.g. (P/L out)	
23.0 RCS/OMS Propellents (on-orbit)			4,949	121.04 ft	61.12%
24.0 Cargo Discharged			0	63.78	0
25.0 Ascent Reserve Propellents			1,750	0.00	
26.0 Inflight Losses and Vents			1,062	99.02	105140
Insertion Weight			**113,946**	Insertion weight c.g. (P/L in)	
				119.13 ft	**60.15%**
27.0 Ascent Propellents			349,996	0.00	
Gross Liftoff Weight			**463,943**	Gross weight c.g. (P/L in)	
				155.68 ft	**78.61%**
28.0 Startup Losses			2,781		
Maximum Pre-launch Weight			**466,724**		

Vehicle Weight Statement
5 degree cone, VTO RBCC SSTO with engine #10
q = 2000 psf, Mfr =14.6, stag. heat rate = 350 BTU/sqft-sec

		Level 3	Level 2	Level 1	local x c.g.	c.g. moment (i
1.0 Wing Group				4,402		
	Exposed wing		3,586		147.71	529708
	Carry through		816		147.71	120481
2.0 Tail Group				825	137.49	113360
3.0 Body Group				32,564	0.00	
	Nosecone		227		4.92	1119
	Crew Cabin		2,058		29.67	61462
	Payload Bay Structure		7,055		0.00	
	Structure	2,575			66.40	170984
	P/L Bay Doors	2,980			66.40	197861
	P/L Accommodations	1,500			63.78	95665
	LH2 Tank		8,623		0.00	
	Tank Structure	7,186			130.25	935924
	Tank Insulation	1,437			130.25	187172
	LOX Tank		1,332		0.00	
	Tank Structure	1,137			183.63	208788
	Tank Insulation	195			183.63	35761
	Aft Body		4,657		0.00	
	Tail cone	4,446			177.88	790832
	Base	211			198.03	41795
	Cowl		8,613		0.00	
	Cowl ring	6,693			144.67	968300
	Cowl struts	1,920			144.67	277790
4.0 Thermal Protection				11,764	0.00	
	Active Cooling		1,127		0.00	
	Nosecap	150			0.50	75
	Cowl leading edge	132			127.59	16794
	Wing leading edges	341			137.49	46922
	Engine nozzle exit	504			162.76	82052
	Advanced Carbon/Carbon		7,045		0.00	0
	Body/cowl	6,437			99.02	637409
	Wing/tails	607			128.72	78164
	Superalloy standoff		3,593		0.00	0
	Body/cowl	3,593			118.82	426880
	Wing/tails	0			134.66	0
	Titanium Standoff		0		0.00	0
	Body/cowl	0			148.52	0
	Wing/tails	0			140.60	0
5.0 Landing Gear				2,756	0.00	0
	Nosegear		413		63.78	26363
	Main gear		2,342		154.92	362884
6.0 Main Propulsion (less cowl)				16,447 lb	0.00	0
	RBCC Engines		13,533		0.00	0
	Ejector rockets (incl. pumps)	5,278			138.98	733473
	Diff./Comb./Noz. (w/ cooling	8,255			144.67	1194239
	Fan/gas generator/storage	0			138.98	0
	Presaurization and feed systems		2,247		169.97	381962
	Purge Systems		668		171.47	114469
7.0 RCS Propulsion				1,071	0.00	
	Foreward RCS		270		0.00	
	Thrusters (15 pressure fed)	80			4.92	392
	Prop. tanks/empty(195 psia)	30			9.84	299
	He pressnt. tank(3000 psia)	93			7.38	686
	He pressurant	8			7.38	60
	Lines,manifolds,valves,etc.	59			4.92	290
	Aft RCS		801		0.00	
	Thrusters (22 pressure fed)	284			195.03	55370
	Prop. tanks/empty(195 psia)	71			190.78	13530
	He pressnt. tank(3000 psia)	217			190.78	41362
	He pressurant	19			190.78	3594
	Lines,manifolds,valves,etc.	210			190.78	40060
8.0 OMS Propulsion				1,121	0.00	
	Engines (4 pump fed)		302		198.03	59739
	Prop. tanks/empty(25 psia)		79		188.96	14917
	He presnt. tank(3000 psia)		470		188.96	88879
	He pressurant (for low pressure tanks)		41		188.96	7689
	Lines,manifolds,valves,etc.		229		188.96	43322
9.0 Primary Power				954	0.00	0
	Fuel cells		396		86.13	34109
	Reactant dewers		531		86.13	45711
	Batteries		27		171.47	4598
10.0 Electrical Conversion & Dist.				3,354	0.00	0
	Power conversion and distribution		1,875		171.47	321512
	EMA controllers		168		165.15	27776
	Circuitry & wiring		1,256		66.01	82897
	EMA cabling		55		168.31	9327
11.0 Hydraulic systems				0	0.00	0
12.0 Surface Control Actuation				519	0.00	0
	Elevon EMAs		428		165.15	70716

	Verticals EMAs		91		165.15	15011
13.0 Avionics				3,300	21.43	70717
14.0 Environmental control				2,541	0.00	
	Personnel systems		141		28.09	3961
	Equipment cooling		729		28.09	20480
	Heat transport loop		996		41.42	41261
	Heat rejection system		675		0.00	0
	Radiators	512			63.78	32654
	Flash evaporators	163			63.78	10396
15.0 Personnel Equipment				802	0.00	
	Food, water, waste manag.		502		28.09	14103
	Seats, etc.		300		23.65	7095
16.0 Dry Weight Margin (10%)				9,158		
					Dry weight c.g.	(excl. margin)
Dry Weight				**91,578**	**121.59 ft**	**61.40%**
17.0 Crew and Gear				1,890	28.09	53096
18.0 Payload Provisions				0	0.00	0
19.0 Cargo (up and down)				10,000	63.78	637768
20.0 Residual Propellents				2,007	0.00	
	OMS/RCS residuals		257		0.00	
	Fore LH2 RCS residuals	2			9.84	17
	Fore LOX RCS residuals	7			9.84	70
	Aft LH2 RCS residuals	4			190.78	787
	Aft LOX RCS residuals	16			190.78	3147
	LH2 OMS residuals	33			188.96	6150
	LOX OMS residuals	195			188.96	36898
	Main Propellent residuals		1,750		0.00	
	LH2 residuals	590			133.17	78538
	LOX residuals	1,160			183.63	213054
21.0 OMS/RCS Reserve Propellents				515	0.00	
	RCS reserves		59		0.00	
	Fore LH2 reserves	4			9.84	35
	Fore LOX reserves	14			9.84	139
	Aft LH2 reserves	8			190.78	1574
	Aft LOX reserves	33			190.78	6294
	OMS reserves		456		0.00	0
	LH2 reserves	65			188.96	12299
	LOX reserves	391			188.96	73795
					Landing weight c.g.	(P/L in)
Landed Weight				**105,889**	**115.10 ft**	**58.12%**
					Landing weight c.g.	(P/L out)
22.0 RCS Entry Propellents (ΔV = 25 fps)				196	121.01 ft	61.10%
	Forward RCS Propellents		59		0.00	
	LH2	12			9.84	116
	LOX	47			9.84	463
	Aft RCS Propellents		137		0.00	0
	LH2	27			190.78	5236
	LOX	110			190.78	20945
					Entry weight c.g.	(P/L in)
Entry Weight				**106,185**	**115.14 ft**	**58.14%**
					Entry weight c.g.	(P/L out)
23.0 RCS/OMS Propellents (on-orbit)				4,949	121.04 ft	61.12%
	Forward RCS Propellents		118		0.00	
	LH2	24			9.84	232
	LOX	94			9.84	928
	Aft RCS Propellents		275		0.00	0
	LH2	55			190.78	10499
	LOX	220			190.78	41996
	OMS Propellents		4,556		0.00	0
	LH2	651			188.96	122992
	LOX	3,905			188.96	737954
24.0 Cargo Discharged				0	63.78	0
25.0 Ascent Reserve Propellents				1,750	0.00	
	LH2 reserves		590		133.17	78538
	LOX reserves		1,160		183.63	213054
26.0 Inflight Losses and Vents				1,062	99.02	105140
Insertion Weight				**113,946**	Insertion weight c.g.	(P/L in)
					119.13 ft	**60.15%**
27.0 Ascent Propellents				349,996	0.00	
	LH2 ascent		117,949		133.17	15707553
	LOX ascent		232,048		183.63	42610770
Gross Liftoff Weight				**463,943**	Gross weight c.g.	(P/L in)
					155.68 ft	**78.61%**
28.0 Startup Losses				2,781		
	LH2 startup		397			
	LOX startup		2,384			
Maximum Pre-launch Weight				**466,724**		

			Engine 10 (No Fan)				
mp (lbm/s)	147.52	131.13	Engine Performance				
A max inlet	18.46						
A max exit	36.14		Primary area ratio	18		eta Ustar	0.980
Astar ejt/A max inlet	0.35		Primary Ae (ft2)	2.06		eta primary	0.975
Max inlet height (ft)	3.9		Primary Pc (psi)	2000		eta mixer	0.900
Max. Mach number	14.6		Primary ho (BTU/lbm)	5550		eta combustor	0.950
Astar ejector	5.91		Primary Ustar (fps)	13340		eta nozzle	0.980
A4 (ft2)	16.05						
A4/A3	2.00		Inlet length (ft)	24.77			
A3 (ft2)	8.03		Total engine length (ft)	34.17			
Fuel Ho (BTU/lbm)	50000						
Cone Half angle	5		**Weight (no inlet)(lb)**	**1503.58**			
			Engine T/W (SLS)	**43.54**			
Altitude (ft)	0		Ejector% Weight	0.39			
Pa (psi)	14.7		Fan % Weight	0.00			
Tinf (°R)	519						
Minf	Uinf (fps)	Thrust (lb)	Isp (sec)	Toinf (°R)	hoinf (BTU/lbm	Poinf (psi)	Approx Beta (deg
0.00	0.00	65,467	423.71	519.00	124.56	14.70	0.00
0.25	279.16	64,002	413.88	525.49	126.12	15.35	0.00
0.50	558.31	64,161	413.73	544.95	130.79	17.44	0.00
0.75	837.47	66,258	424.90	577.39	138.57	21.35	0.00
1.00	1116.62	71,002	451.00	622.80	149.47	27.83	0.00
1.25	1395.78	79,685	498.14	681.19	163.49	38.08	0.00
1.50	1674.93	95,247	580.02	752.55	180.61	53.96	42.34
1.75	1954.09	120,581	703.79	836.89	200.85	78.26	35.40